Functional screening on patient-derived organoids identifies a therapeutic bispecific antibody that triggers EGFR degradation in LGR5^{+} tumor cells

Bram Herpers[1], Berina Eppink[2], Mark I. James[3], Carme Cortina[3,4], Adrià Cañellas[3,4] , Sylvia F. Boj[5], Xavier Hernando-Momblona[3,4], Dominik Glodzik[6], Rob C. Roovers[2], Marc van de Wetering[7,8,9], Carina Bartelink Clements[2], Vanessa Zondag van der Zande[2], Jara García Mateos[1], Kuan Yan[1] , Lucia Salinaro[1], Abdul Basmeleh[2], Szabolcs Fatrai[2], David Maussang[2], Jeroen J Lammerts van Bueren[2], Irene Chicote[10], Garazi Serna[10], Laia Cabellos[10,11], Lorena Ramírez[10,11], Paolo Nuciforo[10] , Ramon Salazar[12], Cristina Santos[12], Alberto Villanueva[13,14], Camille Stephan-Otto-Attolini[3], Elena Sancho[3,4], Hector G. Palmer[10,11,4], Josep Tabernero[10,11,4], Michael R. Stratton[6], John de Kruif[2], Ton Logtenberg[2], Hans Clevers[7,8,9], Leo S. Price[1], Robert Vries[5], Eduard Batlle[3,4,15]* & Mark Throsby[2]*

1. Ocello B.V., Leiden, The Netherlands.
2. Merus N.V., Utrecht, The Netherlands.
3. Institute for Research in Biomedicine (IRB Barcelona), Barcelona Institute of Science and Technology, Barcelona, Spain.
4. CIBERONC, Madrid, Spain
5. Hubrecht Organoid Technology (HUB), Utrecht, the Netherlands
6. Wellcome Sanger Institute, Hinxton, Cambridgeshire, UK
7. Princess Maxima Center for Pediatric Oncology, Utrecht, The Netherlands.
8. Hubrecht Institute, Royal Netherlands Academy of Arts and Sciences (KNAW) and University Medical Center Utrecht, Utrecht, the Netherlands
9. Oncode Institute, Hubrecht Institute, Utrecht, the Netherlands
10. Vall d'Hebron Institute of Oncology (VHIO). Barcelona, Spain.
11. Medical Oncology Department. Vall d'Hebron University Hospital (HUVH).
12. Department of Medical Oncology, Catalan Institute of Oncology (ICO), Oncobell Program, Bellvitge Biomedical Research Institute (IDIBELL)-CIBERONC, L'Hospitalet de Llobregat, Barcelona, Spain
13. Chemoresistance and Predictive Factors Group, Program Against Cancer Therapeutic Resistance (ProCURE), Catalan Institute of Oncology (ICO), Oncobell Program, Bellvitge Biomedical Research Institute (IDIBELL), L'Hospitalet del Llobregat, Barcelona, Spain.
14. Xenopat S.L., Parc Cientific de Barcelona (PCB), Barcelona, Spain.
15. Catalan Institution for Research and Advanced Studies (ICREA), Barcelona, Spain.

* Correspondence should be addressed to Mark Throsby (M.Throsby@merus.nl) and Eduard Batlle (eduard.batlle@irbbarcelona.org)

SUMMARY

Patient-derived organoids (PDOs) have demonstrated predictive value in prospective clinical trials supporting selection of personalized treatments. Because PDOs retain the organization and physiological functions of their source tissue, PDO biobanks could also be an ideal substrate to screen for novel therapeutic interventions. Here we describe a large-scale functional screen of dual targeting bispecific antibodies (bAbs) on a colorectal cancer (CRC) PDO biobank to target their dependency on cancer stem cells. A novel drug discovery pipeline was assembled where therapeutic bAb panels generated against WNT and receptor tyrosine kinases (RTK) targets were functionally evaluated by high content imaging to capture the complexity of PDO responses across a wide range of different CRCs and paired normal colonic mucosa samples. Our strategy resulted in the generation of MCLA-158, a bAb that specifically triggers EGFR degradation in LGR5+ cancer stem cells but shows minimal toxicity towards normal LGR5+ colon stem cells. MCLA-158 exhibits unique therapeutic properties such as potent growth inhibition of KRAS mutant CRCs, blockade of metastasis initiation and suppression of tumor outgrowth in preclinical models of different cancer types.

INTRODUCTION

Colorectal cancers (CRCs) are formed by amalgams of cells that exhibit different phenotypes and capabilities. It is widely established that only a subset of tumor cells present in CRCs, the so-called cancer stem cells (CSCs), exhibits long-term tumorigenic potential whereas the tumor bulk is relatively short-lived and poorly tumorigenic. This distinctive property has been linked to expression of a genetic program in CSCs reminiscent of that present in healthy colonic stem cells[1,2]. CSCs are characterized by elevated levels of WNT pathway components including LGR5, ZNFR3 and RNF43, all of which are part of the WNT-receptor complex[1,3–8]. However, whereas the WNT receptor transduces downstream signals and sustains self-renewal in healthy colon stem cells, it is dispensable in most CRCs as a result of constitutive activation of WNT signaling due to inactivation of the APC tumor suppressor gene or mutations in other downstream components of the pathway[9–11].

Growth and survival of CRC cells depend on mitogenic signals triggered by receptor tyrosine kinases (RTKs) of the EGFR family[12]. In about 50% of cases this dependency is partially compensated by activating mutations in the RAS oncogene family (principally KRAS) that result in constitutive activation of the pathway[9,13]. Therapeutic agents targeting RTK signaling such as cetuximab, a monoclonal antibody (mAb) against EGFR, are broadly used in the clinical setting to treat patients with RAS wild-type metastatic CRC[14,15]. However, current anti-EGFR therapies have limitations. Only a subset of CRC patients derive meaningful therapeutic benefit[14,16,17], in some cases due to acquired mechanisms of resistance during treatment. In addition, patients develop significant adverse effects[18,19].

Here, we developed a therapeutic strategy based on blocking proliferation of CSCs in CRC by leveraging the dual targeting capabilities of bAbs. A fundamental technological advance applied in this study is the use of CRC patient-derived organoids (PDO) biobanks to functionally screen and discover novel drug candidates. PDOs recreate the cellular heterogeneity and organization of CRCs[20–22] including dependency on the self-renewal and proliferative properties of cancer stem cells[3,5,6]. By generating a large PDO biobank we were able to screen therapeutic bAb candidates against CRCs of multiple genotypes and phenotypes, and to assess their activity in matched normal colon mucosa organoids. Through this approach, we selected MCLA-158, an LGR5xEGFR bAb with potent and selective growth inhibitory activity *in vitro* and *in vivo* against both wild type and oncogenic KRAS mutant CRCs.

RESULTS

Generation of a large diverse library of common light chain bispecific antibodies targeting mitogenic signals in cancer stem cells

Both healthy colon stem cells and CRC stem cells are characterized by high expression levels of components of the WNT signaling receptor complex including LGR4, LGR5, RNF43 and ZNRF3[1,3,5–8]. There are however only few reported examples of antibodies generated against the ectodomains of these proteins, and their cell surface expression has been difficult to detect reliably. Phage libraries generated from immunized humanized transgenic mice (MeMo®) and synthetic libraries were screened to generate large panels of bAbs against these CSC surface markers and against EGFR using the strategy described in Figure 1. The generation of the HER3 panel is described elsewhere[23]. Close to 400 target clones were selected from MeMo® mice (101 against WNT signaling components targets and 81 against EGFR) and synthetic libraries (189 against WNT signaling and 26 against EGFR) (Fig. 1). Each WNT clone was expressed in bispecific IgG format paired with a non-binding arm to measure monovalent target interaction, whereas the EGFR clones were produced in bivalent antibody format. Characterization of these IgG crude productions demonstrated that clones with good affinity, stability and ligand blocking activity could be isolated from both library formats against all targets (Supplementary Table 1). At the end of the selection and production process, the WNTxRTK panel contained more than 500 bAbs that derived from combining 54 WNT Fab arms (plus a control Fab against the tetanus toxoid, TT Fab) with 4 EGFR and 4 HER3 Fab arms (Fig. 1).

Establishment and characterization of a living biobank of CRC patient-derived organoids

We established a living biobank of CRC patient-derived organoids (PDOs) from fresh surgical specimens as we previously described[21]. The key clinical-pathological features of CRCs from which we expanded PDOs are detailed in Supplementary Table 2. To capture as many genotypes and phenotypes as possible, we did not preselect samples based on any criteria. We derived and stocked PDOs from 61 primary CRCs and 11 CRC liver metastases from a total of 99 tumor samples corresponding to 68 patients treated at two different hospitals (University Medical Center Utrecht and Meander Medisch Centrum). The success rate of tumor PDO generation was 72.7%, similar to that reported for previous PDO biobanks[21,22,24,25]. For 31 patients, we also established PDOs from tumor-adjacent healthy mucosa.

Figure 2a and Extended Data Figure 1a summarize the mutations in components of the 4 main CRC driver pathways (WNT, RTK/RAS, TP53 and TGF-β) in each PDO line according to

exome sequencing results. The complete catalog of genetic alterations present in PDOs is included in Supplementary Table 2. Chromosome amplifications frequently present in CRC such as 20q, 13, 8q, and 7, and chromosome losses such as 18, 15, 17p, 14, 8p, 4, and 5 were also highly represented in the PDO biobank (Extended Data Fig. 1b). The most abundant mutational signature in the PDOs was signature 1, which corresponds to deamination of cytosine at CpG dinucleotides leading to T>G mutations[26] (Extended Data Fig. 1e). In addition, 6 PDOs were hypermutated, as shown by a very high frequency of single base substitutions and small indels (Extended Data Fig. 1c,d), which coincided with an elevated frequency of mutational signature 6 owing to DNA mismatch repair deficiency[26] (Extended Data Fig. 1e). Overall, these analyses illustrate the wide spectrum of genetic alterations captured in the PDO biobank, which is largely consistent with that reported for the CRC dataset of The Cancer Genome Atlas (TCGA)[9] (Extended Data Fig. 1).

PDO dependency on RTK mitogenic signals

Epidermal growth factor (EGF) is a non-redundant mitogen for both normal and tumor stem cells in the colon, and it is included in the standard PDO culture medium[21,22]. Removal of EGF slowed down the growth of the majority of PDOs, although the extent of this effect varied greatly amongst them (Fig. 2b). Heregulin (HRG) is an EGF-like soluble secreted growth factor that binds HER3, a membrane receptor with a nonfunctional kinase domain that relies on heterodimerization. Although HRG is not an essential stem cell factor[21,22], by substituting EGF for HRG we identified a subset of PDOs that can utilize HER3 mitogenic signals for expansion (Fig. 2b).

The above experiments revealed that a substantial fraction of PDOs bearing activating mutations in EGFR downstream pathway components – including many with canonical KRAS activating mutations – exhibited lower growth rates in the absence of EGF and HRG (Fig. 2b). We corroborated this observation by culturing a subset of KRAS wild-type and mutant PDOs over a wide range of EGF concentrations (Fig. 2c-f). As an example, C55T carried a KRAS-G12V mutation yet, similar to some KRAS wild-type PDOs such as C20T (Fig. 2e,f), it became growth arrested at low EGF concentrations (Fig. 2c,d). C37T carried a KRAS-G12D mutation and exhibited a milder response to low EGF concentrations than C55T (Fig. 2c,d) but comparable to that of some KRAS wild-type PDOs such as C39T (Fig. 2e,f). These findings indicate that mutations in EGFR pathway components do not confer complete EGFR signaling independence to CRCs, and confirm previous observations made in other CRC organoid biobanks on the requirement of EGF for the expansion of KRAS mutant PDOs[22]. Our results also underscore the power of organoids to predict EGFR responses.

High-content image-based screening of RTK responses in PDOs

CRC PDOs are formed by heterogenous cell types that encompass CSCs and their progeny, and adopt complex 3D organizations. To be able to capture changes triggered by drug–target interactions in these models, we utilized a high-content image-based screening method. We found that in addition to modulating the size of the organoids, EGF and HRG signaling caused profound modifications in PDO morphology, possibly owing to changes in tumor cell differentiation and polarity. Figure 3a illustrates this effect on two representative and previously characterized PDOs[21]. In response to EGF, P18T grew into large extending structures with a collapsed central branching lumen but developed spherical and swollen lumens in response to HRG. In contrast, P14T PDOs displayed a single round lumen when cultured with HRG but formed multiple lumens in response to EGF (Fig. 3a). Changes in organoid morphology were measured by image-based segmentation using a widefield high-content imaging system. The number of lumens, lumen area, and organoid area discriminated well between P14T and P18T PDOs cultured without RTK-stimulating factors or cultured in either EGF or HRG-supplemented medium (Fig. 3a). Similarly, EGFR and HER3 blocking antibodies caused specific alterations in PDO morphology in a dose-dependent manner that could be distinguished using morphological parameters (example in Fig. 3b). Based on these observations, we calculated a multiparametric score from multiple morphological measurements of PDOs that was more robust than any single feature in discriminating RTK-induced responses (see Methods for details).

Bispecific antibody screen

We chose P14T and P18T as models to perform the primary bAb screen. These two organoids are KRAS wild type, depend on RTK signaling (Fig. 3a,b) and are models for CRCs that carry mutations that constitutively activate the WNT pathway[21]. It is however well established that 10-15% of all CRCs depend on WNT receptor-mediated signaling[21,27–29]. This CRC subset could benefit from therapeutic antibodies that block the function of WNT receptor components. To capture this response, we also included P19Tb, which only expands in medium supplemented with WNT3a[21]. The panel of >500 WNTxRTK bAbs was screened in duplicate at high (H=10 µg/mL) and low (L=2 µg/mL) antibody concentrations in the presence of EGF, HRG or WNT3a. We leveraged the high-content screening system described above to calculate multiparametric scores for each PDO and antibody treatment as a surrogates of potential therapeutic responses.

Results from the primary screen are shown in Figure 3c. The Z'-factor was 0.33 (SD=0.22, n=8) implying an adequate window for measuring effects triggered by antibodies on PDOs

(see Methods). Bispecific antibodies combining the EGFR-targeting arm Fab232 with a subset of LGR4, RNF43, ZNFR3 and more prominently with LGR5 targeting arms modified P14T and P18T growth patterns cultured in EGF-dependent growth conditions as shown by changes in the multiparametric score (left red box in Fig. 3c). Likewise, the HER3-targeting arm Fab264 combined with LGR4, RNF43, ZNFR3 or LGR5 targeting arms triggered responses of these two PDOs in medium supplemented with HRG (right red box in Fig. 3c). However, none of the antibodies modified significantly the growth features of P19Tb in WNT3a supplemented medium (Fig. 3c) implying lack of WNT signaling inhibitory activity in the bAb panel.

We selected the 28 bAbs that most robustly modified CRC organoid growth patterns in the primary screen; 14 contained the EGFR Fab232 antibody arm coupled to distinct arms against WNT pathway components, and the other 14 were based on the Fab264 HER3 targeting arm combined with WNT targeting arms. The activity of these antibodies was subsequently characterized on an extended panel of 22 CRC PDOs and one normal mucosa organoid model (C51N) (Fig. 3d,e). This secondary screen not only confirmed the activity of several EGFR or HER3-based bispecific antibodies in multiple PDO lines, but also revealed two unexpected activities in a subset of bAbs. First, the Fab232 EGFR arm coupled to a control TT arm exerted almost no effect on PDO growth, yet its activity was largely potentiated in combination with several LGR5 arms (Fig. 3d). This synergism was however not observed in the HER3-based antibodies, which exhibited equivalent growth inhibitory activity in combination with the TT, LGR5 or other WNT targeting arms (Fig. 3e). Second, several bispecific antibodies inhibited the growth of PDOs bearing activating KRAS mutations (Fig. 3d,e).

The antibody that showed growth inhibitory activity in the largest fraction of PDOs combined the Fab232 EGFR arm with the Fab072 LGR5 arm (Fig. 3d, arrow). This bAb reduced the growth rate of 52% of the CRC organoid models including many KRAS mutant PDOs. We named this bispecific antibody MCLA-158.

Molecular characterization of MCLA-158

MCLA-158 is a native bispecific IgG that binds both EGFR and LGR5 (Fig. 4a). It contains two CH3-engineered heavy chains that enforce heterodimerization through the inclusion of charged residues in the CH3 interface – dubbed DEKK[30] – and a kappa light chain in germline configuration (Fig. 4a). Biophysical analysis of MCLA-158 produced by transient transfection and subsequently purified by protein A and gel filtration resulted in essentially pure bAb, as demonstrated using mass spectrometry and analytic cation exchange. The main product-related contaminants were trace amounts of half bodies resulting from un-dimerized heavy

chains (Fig. 4b), homodimers of heavy chains containing the DE mutation pair (Fig. 4b) and charged variants of the bAb production in line with that observed in parental mAbs (Fig. 4c).

To calculate the affinity of MCLA-158 for LGR5 and EGFR, we performed Scatchard assays using DLD1 CRC cells and CHO cells engineered to express either EGFR or LGR5. The affinity for both targets was in the picomolar range: 0.22 nM for the anti-EGFR arm and 0.86nM for the anti-LGR5 arm (Supplementary Table 3). To characterize the binding epitopes recognized by the bAb, shotgun mutagenesis analysis was applied[31]. Mutant libraries of recombinant EGFR and LGR5 expressed on cells were constructed and MCLA-158 biding was analyzed by fluorescence-activated cell sorting (FACS). Alanine substitutions in residues I462, G465, K489, I491, N493 and C499 were shown to reduce binding activity of MCLA-158 to EGFR (Extended Data Fig. 2a). These residues map to domain III of EGFR (Fig. 4d, blue surface) and overlap with the surface bound by EGF (Fig 4d, in yellow) implying that binding of MCLA-158 in this region inhibits EGF interaction with its receptor[32]. Indeed, this was confirmed in an EGF-driven cell death assay[33] using the EGFR binding Fab (Fab232) of MCLA-158 reformatted as a bivalent IgG (Fig. 4e). The degree of inhibition in this assay was similar to that of cetuximab (Fig. 4e).

Mutagenesis analysis of MCLA-158 binding to LGR5 identified D43, G44, M46, F67, R90 and F91 as important contact residues (Extended Data Fig. 2b). These residues (blue surface in Fig. 4f) map to the N-CAP (orange) and first leucine-rich repeat (LRR1) domain (dark teal), in a region proximate to but non-overlapping the RSPO binding region (yellow surface)[34], which is consistent with the anti-LGR5 Fab domain of MCLA-158 having no effect on R-SPO binding. Indeed, binding of the LGR5 arm of MCLA-158 reformatted as a bivalent IgG (Fab072) to LGR5-overexpressing CHO cells was only weakly inhibited by high RSPO concentrations (Fig. 4g). This is in contrast to the activity of two RSPO1-blocking antibodies OMP88R20 and bivalent Fab049 IgG (Fig. 4g), the latter also generated in this study (Supplementary Table 1).

The LGR5 arm of MCLA-158 recognizes stem-like tumor cells

We next studied the capacity of the LGR5 arm included in MCLA-158 (Fab072) to recognize endogenous LGR5 levels at the cell surface. In dissociated P18T organoids, a mono-specific Fab072 IgG identified a subset of cells that expressed elevated LGR5 mRNA levels, shown by FACS followed by RT-qPCR analysis (Extended Data Fig. 2c,d). In P18T-derived tumor xenografts, about 10-20% of all dissociated epithelial cells (Epcam+) were strongly labeled by the Fab072 monospecific antibody (Fig. 4h). These Fab072+ tumor cells expressed elevated mRNA levels of LGR5 and of other intestinal stem cell-specific genes such as SMOC2 or ASCL2, whereas Fab072- cells had upregulated markers of intestinal differentiation including

KRT20 and SLC26A3[5,35] (Fig. 4i). Global gene expression profiles of these two cell populations confirmed that Fab072+ tumor cells were largely enriched in the signature gene set of LGR5+ intestinal stem cells whereas the intestinal differentiation gene program characterized the Fab072- cell population (Fig. 4j). Flow cytometry analysis on a subset of PDO biobank specimens confirmed LGR5 expression on the surface of a large proportion of models (Extended Data Fig. 2e). Therefore, MCLA-158 combines an EGFR antagonistic arm with a high-affinity, non-ligand-competing anti-LGR5 arm that binds to LGR5+ stem cell-like cells in CRCs.

Therapeutic activity of MCLA-158 compared to cetuximab

Treatment with EGFR-targeting mAbs has become the standard of care for patients with RAS wild-type metastatic CRC. Cetuximab (Erbitux), the most widely prescribed EGFR-blocking mAb, was used as a reference to compare the activity of MCLA-158. Experiments using the P18T PDO to model responses of RAS wild-type CRC demonstrated that MCLA-158 exerted a strikingly robust growth inhibitory activity compared to cetuximab (Fig. 5). Non-linear regression analysis estimated a 30-fold difference in IC50 between the two antibody treatments (mean [95%CI] 0.36 µg/mL [0.20-0.65] versus 10.5 µg/mL [7.1-15.7]) (Fig. 5a). The enhanced effect of MCLA-158 was accompanied by a large reduction in the number of Ki67-high cells in PDOs (Fig. 5b, Extended Data Fig. 3a) and cell cycle analysis confirmed that MCLA-158 induced a more pronounced G1 arrest than cetuximab, equivalent to that triggered by removal of EGF from the medium (Fig. 5c and Extended Data Fig. 3b). MCLA-158 also elevated the apoptosis index as measured by the number of cells with a condensed nucleus (Extended Data Fig. 3c). Of note, these effects were not observed when the EGFR arm of MCLA-158 (Fab232) was coupled to the TT control arm (Fig. 5b,c and Extended Data Fig. 3a-c). Consistent with these findings, high concentration MCLA-158-treated CRC organoids displayed delayed kinetics of recovery after the withdrawal of antibody treatment compared to cetuximab (Extended Data Fig. 3d).

Organoid initiating capacity has been extensively used as functional readout of normal and cancer stem cell activity[1,36–38]. At high doses (10 µg/mL), both antibodies decreased organoid size (Fig. 5d) yet MCLA-158 was particularly efficient at preventing organoid initiation compared to cetuximab (Fig. 5e). To further assess the specificity of MCLA-158 towards LGR5+ cancer stem cells, we knockdown LGR5 levels in P18T PDOs using an shRNA vector (Fig. 5f-i and Extended Data Fig. 3e). Downregulation of LGR5 did not cause significant changes in expression of stem cell/WNT target genes (Fig. 5f) owing to constitutive activation of beta-catenin/TCF transcription due to inactivation of APC in this PDO. Furthermore, P18T PDOs with downregulated LGR5 levels showed no significant changes in growth kinetics

compared to PDOs expressing a control shRNA (Fig. 5g), implying that, as in the case of normal crypt stem cells[34], LGR5 function is dispensable for cancer stem cell expansion. However, LGR5 knockdown conferred a large degree of insensitivity to MCLA-158 (Fig. 5h,i), further confirming specific targeting of the LGR5+ cell population.

We next compared *in vivo* anti-tumor activity of MCLA-158 versus cetuximab on subcutaneous xenografts generated by the inoculation of P18T organoids (Fig. 5j and Extended Data Fig. 4a,b). 3-4 weeks after tumor implantation, mice bearing xenografts with similar average volumes were randomized into treatment groups. MCLA-158 caused a significant reduction in the average tumor volume compared to both PBS (vehicle) and cetuximab regimes from day 2 onwards ($P<0.01$ for all time points, Fig. 5j and Extended Data Fig. 4a,b). Of note, cetuximab and PBS-treated mice showed comparable growth kinetics over the observation period as measured by tumor volume and survival (Extended Data Fig. 4a,b). Histological inspection revealed reduced cellularity and a prominent decrease in the number of Ki67+ cells in MCLA-158-treated P18T xenografts (Fig. 5k). MCLA-158 also showed superior growth inhibitory capacity relative to cetuximab in subcutaneous xenografts generated from inoculation of C31M, a PDO bearing a KRAS G12D mutation (Extended Data Fig. 4c). These experiments successfully translated the enhanced therapeutic activity of MCLA-158 compared to cetuximab observed ex vivo in PDO models to a conventional *in vivo* PDX setting.

Broad activity of MCLA-158 against LGR5$^+$ KRAS wild-type and mutant PDOs and PDXs

We next compared the activity of the two antibodies at high concentration (10 μg/mL) over a PDO panel. MCLA-158 reduced growth rates by more than 50% in 11 out of 21 organoids tested, including two metastasis-derived PDOs (C0M and C31M), and outperformed the growth inhibitory capacity of cetuximab in the majority of these CRC models (Fig. 6a). Of note, the different therapeutic potency of the two antibodies was particularly evident in a subset of PDOs bearing KRAS activating mutations (C0M, C55T, C27T, C31M and C25T; Fig 6a). Further supporting these observations, we measured large differences (8 to 125-fold) in IC50 between cetuximab and MCLA-158 in both KRAS wild-type and mutant PDOs (Fig. 6b) and this differential effect was even more pronounced in culture conditions with elevated EGF concentrations (Supplementary Table 4). PDOs that responded to MCLA-158 contained higher percentages of LGR5+ cells than non-responder PDOs (Fig. 6c and Supplementary Table 5). Moreover, stratification of PDOs according to high versus low % of LGR5+ cells (defined as above or below average) predicted growth inhibition by MCLA-158 (Fig. 6d and Supplementary Table 5).

To extend our observation beyond the CRC PDO biobank, we selected 24 PDX models that co-express elevated LGR5 and EGFR mRNA levels according to RNA sequencing data. MCLA-158 demonstrated significant anti-tumor activity in the majority of PDX models of CRC (3 out 5; individual growth kinetics in Extended Data Fig. 5), esophageal squamous cell carcinoma (4 out of 6), gastric adenocarcinoma (6 out of 8), and squamous head and neck cancers (2 out of 5), both in a KRAS WT and KRAS mutant setting (Fig. 6e).

Limited responses of normal colonic stem cells to MCLA-158

EGF is a mitogen for healthy colonic stem cells[39] and treatment with EGFR pathway inhibitors causes gastrointestinal toxicity in a subset of patients[40]. The detrimental effect of EGFR inhibitory antibodies was evident in two out of five normal mucosa PDOs included in our biobank (C71N and C57N; Fig. 6b). However, the response triggered by MCLA-158 in these two normal mucosa-derived PDOs was substantially weaker than that of cetuximab (Fig. 6b). An advantage of the PDO-based screening system described herein is the possibility of testing antibody responses on pairs of normal–tumor organoids derived from the same patient. Figure 6f shows a dose-response curve of C55T PDO, which was generated from a KRAS-G12V mutant CRC, versus C55N, a normal PDO expanded from adjacent healthy mucosa. At 1 µg/mL, MCLA-158 exerted a robust (maximal) tumor growth inhibitory effect without affecting the expansion of normal mucosa-derived PDO culture. In contrast, cetuximab only reduced tumor growth at concentrations approximately 100-fold higher than those required for MCLA-158, and at such high doses the growth inhibitory response triggered on C55N was equivalent to that of C55T (Fig. 6f). Therefore, MCLA-158 beneficially distinguished between tumor and healthy tissue and exerted a potent anti-tumor response, whereas cetuximab did neither in these models. Of note, C55N PDO exhibited substantially reduced LGR5 cell surface expression and contained many fewer LGR5+ cells compared to its tumoral counterpart C55T (Fig. 6g-i). This finding, together with our observations that downregulation of LGR5 levels inhibits MCLA-158 activity (Fig. 5h,i), supports the notion that specific targeting of CRC by MCLA-158 is due to higher LGR5 expression in tumor compared to healthy colonic stem cells.

MCLA-158 inhibits metastasis formation

In experimental models of advanced CRC, LGR5+ tumor cells are required for metastasis formation[3]. This finding prompted us to test the effects of MCLA-158 on orthotopic xenografts (PDXs) (Fig. 6j,k and Extended Data Fig. 4d-f). For these experiments we used PDXs that were not derived from PDOs but generated by direct implantation of patient tumor cells into the cecum of immunodeficient mice. The three different PDX models used for these experiments were selected because they carried KRAS activating mutations (Supplementary

Table 2), generated metastases, and expressed detectable LGR5 mRNA levels. After PDX growth at the primary site was evident, mice were randomized into treatment arms. Effects on primary CRC growth (Fig. 6j) and the formation of metastases (Fig. 6k and Extended Data Fig. 4d,e) were assessed at experimental end-points. Mice bearing model LM-CRCX3 were treated with an identical regime of either cetuximab or MCLA-158 whereas models M001 and M005 were treated only with MCLA-158. As shown in Figure 6j, MCLA-158 exhibited superior therapeutic capacity to cetuximab in terms of reducing the size of the primary CRC generated by LM-CRCX3. MCLA-158 also completely prevented development of local and distant metastases, whereas cetuximab exerted no effect on the disseminated disease (Fig. 6k and Extended Data Fig. 4d). In the M001 and M005 models, not only did MCLA-158 treatment cause a significant reduction of primary CRC growth (Fig. 6j), it robustly blocked the formation of metastasis (Fig 6k, Extended Data Fig. 4e,f). Two mice bearing M001 CRCs developed peritoneal metastases despite MCLA-158 treatment (Fig. 6j and Extended Data Fig. 4e). However, there were no major differences in LGR5 mRNA levels between MCLA-158-resistant metastases and those arising in vehicle-treated mice (Extended Data Fig. 4g). Therefore, in a small fraction of cases, LGR5+ metastatic cells can apparently bypass MCLA-158 inhibitory effects.

Transcriptional response to MCLA-158 treatment

MCLA-158 binds to LGR5 thus raising the possibility that besides blocking EGFR signaling, it may affect the WNT signaling pathway. We however showed that MCLA-158 does not block R-SPO binding to LGR5 (Fig. 4g). To exclude the possibility of non-conventional modulation of WNT signaling by MCLA-158, we investigated this issue further by performing RNA sequencing of P18T and C55T exposed to MCLA-158 or cetuximab (Fig. 7a-d and Extended Data Fig. 6). This experiment revealed that expression of the WNT target gene, LGR5+ ISC, and Paneth cell signatures were upregulated rather than inhibited by MCLA-158 (Fig. 7a,b). Cetuximab also induced upregulation of WNT, ISC and Paneth cell signatures implying that these transcriptional effects are direct consequence of EGFR inhibition (Fig. 7a,b). These findings are consistent with a recent study demonstrating that cetuximab treatment enforces an ISC and Paneth cell-like phenotype in CRC[41].

MYC is a direct beta-catenin/TCF target gene[42] and plays a causal role in the expansion of CRC stem cells due to WNT activating mutations[43,44]. Despite increased WNT/ISC gene levels upon MCLA-158 and cetuximab treatment, the expression of MYC was downregulated (Fig 7c,d). MCLA-158 was particularly efficient at suppressing MYC expression compared to cetuximab (Fig 7c), and this differential effect was even more evident in C55T KRAS mutant

PDO (Fig 7d). We further investigated global differences in response triggered by both antibodies through GSEA (Extended Data Fig. 6). The biological responses of P18T to high-dose MCLA-158 and cetuximab treatment (10 μg/mL) were largely overlapping (Extended Data Fig. 6a). In contrast, changes in gene expression provoked by low dose MCLA-158 (1 μg/mL) were of much higher magnitude and significance than those of cetuximab, and involved not only downregulation of MYC target genes but also suppression of the mTOR biosynthesis pathway and the mitogenic program (Extended Data Fig. 6b). This differential response was marked in the C55T KRAS mutant PDO line, which remained largely unresponsive to low dose cetuximab (Extended Data Fig. 6d). From these results, we conclude that both antibodies elicit qualitatively similar transcriptional changes yet MCLA-158 exerts a much more potent response than cetuximab.

MCLA-158 induces EGFR internalization and degradation

Our data demonstrate that MCLA-158 does not impair WNT signaling whereas the EGFR arm of MCLA-158 inhibits EGFR with an IC50 similar to that of cetuximab (Fig. 4e). Furthermore, the EGFR arm of MCLA-158 triggered weak responses on PDOs when combined with a control Fab arm (Fig. 3d and Fig. 5b,c). To address the mechanistic basis for the enhanced therapeutic properties of MCLA-158, we investigated whether its activity was correlated with binding to EGFR, binding to LGR5 or the combination of both over a range of antibody concentrations (Fig. 7e). For these experiments we used as models PDOs derived from primary CRCs (P18T and C55T), metastasis (C1M) and normal mucosa (C55N) (Fig. 7e). In all cases, the LGR5 arm (Fab072) combined with the EGFR arm (Fab232) in the same antibody exerted profound synergetic growth inhibitory effects on CRC PDOs compared to the individual arms combined with the TT control arm (Fig. 7e). Therefore, physical linkage of the EGFR and the LGR5 arms in full-length bispecific IgG format is strongly associated with synergistic inhibition of CRC organoid growth.

We next studied EGFR distribution in PDOs upon antibody treatment (Fig. 7f). Addition of cetuximab did not modify EGFR localization, which remained basolateral for the duration of the treatment. EGFR co-localized with cetuximab in the basolateral membrane (Fig. 7f, white arrows). In contrast, 60 minutes after the addition of MCLA-158, EGFR displayed a punctuated cytoplasmic distribution, which overlapped with the localization of MCLA-158 (Fig. 7f, white arrowheads), implying that both receptor and antibody were rapidly internalized. Treatment of PDOs with LGR5xTT and EGFRxTT bAbs demonstrated that the cytoplasmic localization of MCLA-158 occurred as a consequence of binding to LGR5, a constitutively internalizing cell surface protein[45], yet was independent of EGFR binding (Extended Data Fig. 7a). Of note,

MCLA-158 was not internalized by normal colon organoids and remained basolateral for the duration of treatment (Extended Data Fig. 7b). Similarly, there was no EGFR internalization in C47T (Extended Data Fig. 7b), a PDO model that contain no LGR5-positive cells (Supplementary Table 5). We also noticed that EGFR staining intensity was strongly reduced after 24h whereas MCLA-158 remained in the cytoplasm (Fig. 7f, open arrowheads). Western blot analysis of PDO P18T lysates confirmed a time-dependent decrease in total EGFR levels under MCLA-158 treatment, beginning at 6 hours and continuing to decrease at 72 hours (Fig. 7g). After washing out MCLA-158, EGFR levels continued to be downregulated during at least another 72 hours (Fig. 7h). In contrast, EGFR levels upon cetuximab treatment remained unchanged throughout the treatment (Fig. 7g). LGR5 knockdown prevented MCLA-158-induced EGFR degradation (Fig. 7i). Downregulation of EGFR by MCLA-158 also occurred in the KRAS mutant C55T PDO whereas this effect was attenuated in normal mucosa-derived organoids (Extended Data Fig. 7c). We conclude that, unlike cetuximab, MCLA-158 triggers EGFR internalization and degradation in a LGR5-dependent manner.

DISCUSSION

PDOs predict drug and radiation responses in colorectal cancer patients[46–49]. Ongoing efforts are now focused on the implementation of PDOs as tools to inform personalized treatments in the clinical setting. Here we describe the first use of PDO biobanks in a drug discovery pipeline. Our approach has several important advantages over traditional pharmaceutical strategies. First, we demonstrate that PDO biobanks permit the unbiased functional testing of large panels of drug candidates across a relevant cross section of patient genotypes and phenotypes at the first stage of the discovery pipeline. This approach avoids making mechanistic assumptions upfront and bypasses the common reliance on model systems such as cell lines, which may at best only partially reflect the pathophysiology of a disease state. Although we derived PDOs from the majority of CRC patients, 27 samples (18%) failed to expand. A reason for failure could be that growth conditions for these particular CRCs were suboptimal. Although not used herein, an optimized PDO growth medium that includes a distinct set of growth factors and the use of low O_2 culture conditions have been shown to enable the expansion of near 100% of samples[22]. The application of PDO biobanks could help in selection of drug candidates that target a group of patients from a large population. In this regard, we illustrated the versality of PDOs by showing that they can be used to select bAbs that target HER3 upon adaptation to HRG-supplemented medium. Although we did not progress on the characterization of the anti-HER3 bAbs, this case is of particularly interest because HER3 expression is elevated in a CRC subset displaying poor prognosis[50,51]. A second advantage of our approach is that PDOs are better surrogates of tumor biology than cell lines as they recapitulate the heterogeneity, organization, and vulnerabilities of the tumor of origin[21,22,52]. These advantages are illustrated

by the discovery that a large fraction of CRCs carrying a KRAS activating mutation still display EGF dependency[22]. Cell lines selected to expand in standard culture conditions had failed to reveal this feature. Third, the use of normal–tumor PDO pairs from the same patients facilitates the screening of drugs that exert tumor-specific responses and helps to identify drugs that may exhibit toxicities against the normal tissue cells, facilitating the early selection of drug candidates with a large therapeutic index and more favorable safety profiles. The unique properties of MCLA-158 would have not been elucidated via reliance on simple model systems such as cell lines, which further substantiates the advantages offered by this novel approach.

We focused on dual targeting bAbs as a therapeutic modality because they facilitate the pharmaceutical intervention of pathways in specific cell populations[23] which was relevant for our goal of targeting the dependency of CRCs on CSCs. Cetuximab and panitumumab are mAbs that bind EGFR and prevent ligand-dependent downstream signaling. Both antibodies have been approved for the treatment of RAS wild-type metastatic CRC. These anti-EGFR mAbs exhibited certain clinical benefit in randomized phase 3 clinical studies for this indication [14,15]. Cetuximab has also been approved in advanced head and neck squamous cell carcinoma yet it shows limited efficacy in this setting[53]. Several lines of evidence suggest that EGFR inhibitors with greater potency could provide increased benefit to patients. The majority (~70%) of RAS wildtype metastatic CRC patients do not derive benefit from cetuximab or panitumumab, yet a far greater proportion of these tumors are sensitive to EGFR inhibition in preclinical settings[13,54–56]. Consistent with our results, this dependency is in some cases observed even in the context of acquired mutations in RAS genes[55]. Finally, investigation of EGFR mAb cocktails with preclinical potency greater than cetuximab have shown clinical responses in patients that progressed on EGFR mAb treatment[57] and this activity is mechanistically associated with EGFR receptor internalization and degradation[57–59]. However, the use of more potent EGFR-inhibiting treatments is also associated with significantly increased on-target off-tumor toxicities, in particular skin rash, hypomagnesemia and diarrhea, that limit the dose and duration of treatment with these drugs and thus ultimately limit their effectiveness.

MCLA-158 is significantly more active on organoids derived from CRCs than on organoids derived from normal tissue. Our data supports that this differential effect is facilitated by the elevated expression of LGR5 in CRC due to constitutive activation of the WNT pathway. In addition, MCLA-158 potency was significantly greater than the combination of the parental bivalent monospecific mAbs against LGR5 and EGFR or cetuximab. These results illustrate the unique properties of MCLA-158. Mechanistically, we provide evidence that the increased potency is due to LGR5-dependent internalization of EGFR, which ultimately leads to its degradation. Dysregulation of the WNT pathway is a cardinal event in the growth and

metastasic dissemination of CRC. Upregulation of the WNT target gene LGR5 is detected in the majority of CRCs, its expression is particularly elevated in CSCs[1,3–8,60], and it correlates with lymph node metastases[61,62]. Indeed, LGR5+ cells are required for metastatic outgrowth in preclinical CRC models[3]. Our data indicate that MCLA-158 effectively targets the highly mitotic LGR5^{+} CSC population that supports organoid growth and that initiates primary and metastatic tumors. Moreover, MCLA-158 shows *in vivo* anti-tumor activity in preclinical models of other cancer types characterized by LGR5 expression such as esophageal squamous cell carcinoma, gastric carcinoma and head & neck squamous cell carcinoma. MCLA-158 combines the potency exhibited by mAb cocktails resulting in EGFR degradation with selectivity for malignant cells driven by WNT dysregulation. We anticipate that this combined effect will result in an enhanced therapeutic window; that is, superior anti-tumor activity without the on-target toxicities associated with EGFR antibodies and small molecule inhibitors. An ADCC-enhanced development candidate of MCLA-158 is currently undergoing clinical evaluation in different solid tumor patient populations.

ACKNOWLEDGMENTS

We would like to thank all patients for donating materials to the organoid biobank and all employees of U-PORT UMC Utrecht, as well as Onno Kranenburg at UMCU, and Els Wink-van Gestel and Noortje van Scharrenburg at Meander Medisch Centrum for their assistance with patient inclusion and tissue acquisition. We would like to thank Joyce Blokker, Ricardo Korporaal and Tamana Mehraban for their contributions to building the CRC organoid biobank. Thanks also go to Rachel Fong from Integral Molecular for performing the alanine scanning; Linda Kaldenberg for graphically displaying the structural models; Hans van der Maaden and Willem Bartelink for technical assistance; Marta Sevillano, Antonio Berenguer and IRB facilities for excellent support with flow cytometry, functional genomics and histopathology. This study was funded by the European Union under the Seventh Framework Programme (FP7-2007-2013) (SUPPRESSTEM - Grant agreement No. 601876). IRB Barcelona is the recipient of a Severo Ochoa Award of Excellence from the Spanish Ministry of Economy and Competitiveness (MINECO), and EB receives support from AGAUR 2017-SGR-698 (Generalitat de Catalunya). A.V was supported by grant from the Spanish Ministry of Economy and Competitiveness - Instituto de Salud Carlos III FEDER (PI19/01320). AC held an FPU predoctoral fellowship from MINECO.

COMPETING INTEREST

SFB and RV are employed by the Foundation Hubrecht Organoid Technology (HUB), which holds the exclusive license to the Organoid Technology. RV and HC are inventors on patents for Organoid Technology. BE, RR, CBC, VZvZ, AB, SF, JLvB, JK, TL and MT are employees of Merus N.V. BH, JGM, KY and LP are employees of Crown Bioscience Netherlands B.V. MT, JK, TL, HC, RV, EB and BH are inventors on intellectual property related to this work. JT and HC are paid advisors to Merus N.V.

AUTHORS CONTRIBUTIONS

MT, EB, TL, HC, and RV conceived and designed the study. BH, JGM, KY, LP performed antibody screens and characterized mechanisms of action. BE, RR, CBC, VZvZ, AB, SF, JK, TL and MT generated the bispecific antibody panel. MJ, AC, CC, SF, JLvB, XH-M, ES and EB characterized the MCLA-158 mode of action and performed xenograft experiments. DG and MS performed genomic analyses of PDOs. CS-OA performed statistical analysis. LC, LR and PN performed ISH for LGR5. SB, MvW, RV and HS generated the organoid biobank. HP, JT, IC, GS, RS, CS and AV performed and analyzed the effects on orthotopic PDXs. EB and MT coordinated the study and wrote the manuscript.

FIGURE LEGENDS

Figure 1. bAb panel generation

Schematic diagram depicting bAb panel generation and selection procedures indicating the numbers of materials generated at each step.

Figure 2. PDO biobank and EGF dependency

a. Summary of genetic alterations in main driver pathways (y-axis) across the PDO panel (x-axis). The organoid models were ordered by their APC and TP53 mutation status. **b.** Organoid size was compared between PDOs cultured with either EGF (5ng/mL) or HRG (5ng/mL) and the absence of growth factors over a culture period of 7 days. % indicates change relative to absence of EGF. "--" indicates that no data was collected. Each data point is average of n=4 independent cultures. **c**. Dose-response curves to EGF in KRAS mutant PDOs. Organoid size was measured at day 7 and referred as % of maximum. Each data point is average +/- SD of n=4 independent cultures. **d**. Examples of KRAS mutant PDOs cultured without EGF or with EGF (5 ng/mL). DNA is labeled in blue using Hoechst, and actin in red using phalloidin. The pictures are taken from day 7 cultures. **e**. Dose-response curves to EGF in KRAS wild-type PDOs. Each data point is average +/- SD of n=4 independent cultures. **f**. Examples of KRAS wild-type PDOs cultured without EGF or with EGF (5 ng/mL).

Figure 3. Functional bAb screening on PDOs

a. Characterization of the morphological change of P18T and P14T in response to 5ng/mL EGF or 5ng/mL HRG. Pictures illustrate morphology adopted in different conditions and the graph depicts measurements of lumen counts, lumen area and organoid area. Each data point represents a well-average of ~100 organoids. **b.** Effects of either EGFR or HER3 blocking antibodies on P14T cultured with EGF, HRG or no growth factors. Graph depicts measurement of lumen complexity versus width on different treatments. The size of each data point indicates antibody doses (from smallest to largest: 1, 2.5, 10, and 25μg/mL). Each data point represents the average measurement of all PDOs growing in one culture well. Note that antibody-mediated growth inhibition in EGF-stimulated growth conditions has different morphological effects than in HRG-stimulated growth conditions, indicating the requirement of a multiparametric score. **c.** Primary bAb panel screen. Changes in multiparametric scores triggered by different bAbs on P14T, P18T and P19b PDOs cultured with EGF, HRG or WNT3a. % indicates change relative to absence of growth factor. Red boxes indicate the antibodies considered for secondary screening. L4 indicates LGR4 Fab arm, L5 is LGR5, RN is RNF43, ZN is ZNFR3, and TT is Tetanus Toxoid (control Fab). Each data point is average of n=2 independent culture wells. **d.** Secondary screen of bAbs containing EGFR Fab arms on

PDOs supplemented with EGF. Red intensity indicates % of growth inhibition in each PDO calculated as multiparametric score. Bottom panel indicates % of PDOs that showed responses to each antibody. KRAS mutation status is shown in the right. Arrow points to MCLA-158. Each data point is average of n=2 independent wells. **e.** Secondary screen of bAbs containing HER3 Fab arms on PDOs supplemented with HRG. Each data point is average of n=2 independent wells.

Figure 4. Characterization of MCLA-158

a. Schematic depiction of MCLA-158 showing monovalent affinities of the EGFR (Fab232) and LGR5 (Fab072) Fab arms. **b**. nMS spectrogram of a representative bench scale production of MCLA-158 to assess mass heterogeneity; magnified insets below show trace amounts of half-body fragments (pink) or DEDE homodimer (blue). **c.** CIEX chromatogram (upper panel) and IEF gel (lower panel) of same MCLA-158 production as (b.) to assess charge heterogeneity; 1=MCLA-158, 2=Fab070 IgG, 3=Fab072 IgG, 4=Fab232 IgG, 5=Fab266 IgG (TT irrelevant control). **d.** EGFR structure showing the four domains colored in shades of teal, critical binding residues for MCLA-158 denoted in blue, binding surface of EGF highlighted in yellow. **e.** Percentage inhibition of EGF-driven A431 cell apoptosis measured in a dose titration of Fab232 mAb, cetuximab or negative control TT (irrelevant control IgG). Each data point is mean +/- SD of n=2 wells. **f.** LGR5 structure showing the LRR in shades of teal, N-Cap region in orange, critical binding residues for MCLA-158 denoted in blue, binding surface of RSPO-1 highlighted in yellow. **g.** Percentage of normalized binding of Fab072, Fab049 or OMP88R20 to LGR5-positive CHO-K1 cells in FACS in the presence of an increasing dose of ligand RSPO1. The MFI signal obtained at a certain ligand concentration was normalized to that obtained in the absence of ligand (set at 100%) and all values are plotted relative to the signal obtained at uninhibited binding. Each data point is mean +/- SD of n=3. **h.** Flow cytometry histograms of representative P18T xenografts stained with Fab072 monospecific antibody or TT irrelevant control IgG. Alive (DAPI-) epithelial (Epcam+) tumor cells are shown. Gates used to isolate Fab072+ and Fab072- cells for subsequent experiments are indicated. **i.** RT-qPCR analysis of stem cell (LGR5, SMOC2, ASCL2, OLFM4), proliferation (MYC, KI67) and differentiation (CDKN1A, KRT20, SLC26A3) marker genes on Fab072+ and Fab072- tumor cells isolated by FACS from dissociated P18T-derived xenografts (n= 3 technical replicates of 1 representative xenograft). **j.** Gene Set Enrichment Analyses (GSEA) of the transcriptomes of Fab072+ and Fab072- cells purified from P18T-derived xenograft. Fab072+ and Fab072- cells were isolated from 2 xenografts and profiled. Enrichment of signatures of normal mouse LGR5+ crypt cells[63] and human normal colon crypt proliferation[1] or differentiation signatures[1] are shown.

Figure 5. Targeting of LGR5+ cells by MCLA-158.

a.Dose-response curves of PDO P18T to cetuximab and MCLA-158. Each data point is mean +/- SD of n=3 independent wells for cetuximab, n=6 for MCLA-158. Estimated IC50s are indicated. **b.** P18T cultures were treated with 2μg/mL of the indicated antibodies and the fraction of Ki67-high tumor cells was assessed by image-based quantification (see methods). Each dot indicates average fraction of Ki67-high cells in an independent well. Mean. Two-sided Wald test of a linear model. **c.** Quantification of number of cells in S phase in P18T PDOs. Cultures were treated with 2μg/mL of the indicated antibodies. n=2 independent wells per condition. Mean +/- SD. Two-tailed t-test. **d.** P18T Organoid size (diameter in pixels) 4 days after treatment with the indicated antibodies at a concentration of 20μg/mL. Each dot is an independent culture well (n=16 for control and cetuximab and 14 for MCLA-158). Bars comprise min and max values. Antibodies were added the day of plating cells. Mann Whitney two-tailed test. **e.** Number of organoids counted after 5 days of treatment with the indicated antibodies at a concentration of 20μg/mL. Each dot is an independent culture well (n=16 for control and cetuximab and 14 for MCLA-158). Bars comprise min and max values. The same number of single cells were plated, and antibodies were added the day of plating. Mann Whitney two-tailed test**. f.** Expression levels of the indicated genes assessed by RT-qPCR in parental non-infected, shRNA control or shLGR5 P18T PDOs. n=3 technical replicates. Bars are SEM. T test. **g.** Relative organoid growth normalized to day 1. n=5 independent wells. Bars are SD. T test. * and ** corresponds to non-infected vs. shLgr5. **h.** % seeded cells that gave raise to organoids after 16 days in culture. Antibodies were added on the day of plating at a concentration of 1 μg/mL and refreshed every 2 days. Each dot is an independent culture well (n=4-5). Bars are SD. T test. **i.** P18T Organoid size (diameter in pixels) 16 days after treatment with the indicated antibodies at a concentration of 1 μg/mL. Each dot is an independent culture well (n=4-5). Bars are SD. Antibodies were added the day of plating cells and refreshed every 2 days. Each dot is an independent culture well (n=5). Control antibody is TT. Bars are SD. T test. **j.** Mice bearing PDO P18T-derived subcutaneous xenografts were treated with indicated antibodies or PBS. Relative tumor volumes relative to day 1 of treatment are shown. Absolute tumor volumes are shown in Extended Data Fig. 4b. Each data point is mean +/- SEM. * $p<0.01$ for cetuximab versus MCLA-158 and # $p<0.01$ for vehicle versus MCLA-158 by two-tailed t-test. **k.** Representative images of P18T-derived PDX stained for Ki67.

Figure 6. MCLA-158 compared to cetuximab.

a. Effects of antibodies on PDO size are represented as % of inhibition compared with untreated. Antibodies were added at 10μg/mL and EGF at 2.5ng/mL. Numbers indicate average of 4 independent wells. **b.** Estimated IC50 values from non-linear regression models

of the effects of cetuximab or MCLA-158 on CRC and normal mucosa PDO growth in 2.5 ng/mL EGF. **c.** % of LGR5+ cells by flow cytometry in MCLA-158-responder versus no responder PDOs (see Supplementary Table 5 for details). Wilcoxon test. **d.** % of growth inhibition in PDOs with % LGR5+ cells above (high) or below (low) average (see Supplementary Table 5). Wilcoxon test. **e.** Volume of individual CRC, esophageal, gastric, and head and neck PDX xenografts treated either with vehicle (control) or MCLA-158 (25 mg/kg/week for 6 weeks). Asterisks indicate results of unpaired t-tests (*= p>0.05; **= p>0.01; ***= P>0.001; ns = not significant). Mutations in EGFR pathway components are indicated. **f.** Dose-response curves to cetuximab and MCLA-158 of PDOs C55T and C55N in 2.5 ng/mL EGF. Each data point is average +/- SEM. n=6 independent cultures. **g.** LGR5 surface levels in the indicated PDOs measured using a LGR5(Fab072)xTT antibody. Staining of TTxTT antibody on C55T was used as a negative control. Frequency plot was normalized to the mode and shows a representative experiment. Bar indicate the gate used to quantify LGR5+ cells. **h.** LGR5 surface expression levels expressed as mean fluorescence intensity. n=2 independent experiments. **i.** % of LGR5+ cells in C55N and C55T. n=2 independent experiments. **j.** Size or weight of the caecum-bearing orthotopic PDXs. Three KRAS mutant PDXs derived from different patients – LM-CRCX3, M001 and M005 – were evaluated. Each dot is a mouse. Mann Whitney test. **k.** Number of mice that developed metastasis for the experiment shown in panel h**.** Fisher exact test. Quantifications of site-specific metastasis are shown in Extended Data Fig. 4d-f.

Figure 7. Internalization and degradation of EGFR by MCLA-158 treatment.

a.b. Expression levels of the indicated gene expression signatures as determined by RNA sequencing (z scores) of P18T (a) or C55T (b) treated with a low (1 μg/mL) or high (10 μg/mL) dose of control IgG, cetuximab or MCLA-158 during 48 hours. Each dot is an independent PDO culture. Wilcoxon test. **c,d.** As in panels a,b but showing MYC RNA levels. **e.** Dose-response curves for treatment with bAbs containing different Fab combinations of CRC-derived PDOs (P18T, C55T and C1M) and normal mucosa (C51N and C55N). Each data point is average +/- SD of n=4 independent wells. **f.** Representative confocal images of P18T treated with either MCLA-158 or cetuximab at 1μg/mL. EGFR or MCLA-158 localization was detected by immunofluorescence. Arrows indicate co-localization of EGFR (green) and cetuximab (red) at basolateral membranes. Arrowheads indicate co-localization of MCLA-158 (red) and EGFR (green) in intracellular structures in the cytoplasm. Bar is 50μm. **g.** Virtual image of a capillary western blot measuring EGFR levels on P18T protein extracts. Antibodies were added at 1μg/mL for the indicated timepoints. **h.** P18T cultures were treated for 72 hours with MLCA-158 (1 μg/mL) and recovery of EGFR levels assessed by western blot analysis at indicated

736 time points after antibody washout. Actin levels were used to normalize protein loads. **i.** EGFR
737 levels by western blot in the parental, control shRNA or LGR5 shRNA P18T PDOs upon MCLA-
738 158 treatment (1 µg/mL) during 72 hours. Actin levels were used to normalize protein loads.
739

EXTENDED DATA FIGURE LEGENDS

Extended Data Figure 1. Genomic alteration of PDOs.

a. Frequency of mutations in common driver genes among the PDO biobank and the TCGA CRC dataset[9]. **b.** Graphs indicate % of PDOs in the biobank with amplifications, deletions and loss of heterozygosity segments across chromosome regions. Upper side of the graphs correspond to PDO biobank and bottom part to the TCGA CRC dataset[9]. **c.** Number of single base substitutions in each PDO. **d.** Number of small indels in each PDO. **e.** Frequencies of mutational signatures[26] in each PDO.

Extended Data Figure 2. Molecular characterization of MCLA-158.

a. Alanine scanning epitope mapping of MCLA-158 on EGFR. For each clone, the mean binding value with Ab MCLA-158 is plotted as a function of the clone's mean EGFR expression value (gray circles). Critical residues contributing to the binding of MCLA-158 to EGFR are depicted in blue. **b.** Alanine scanning epitope mapping of MCLA-158 on LGR5. For each clone, the mean binding value with Ab MCLA-158 is plotted as a function of the clone's mean LGR5 expression value (gray circles). Critical residues contributing to the binding of MCLA-158 to LGR5 are depicted in blue. **c.** Flow cytometry histograms of representative P18T PDOs stained with Fab072 bivalent antibody or control TT antibody. Gates used to isolate Fab072+ and Fab072- cells for subsequent experiments are indicated. **d.** LGR5 mRNA levels by RT-qPCR on FACS-purified cell populations. Average of n=3 technical replicates of one representative PDO +/- SD. **e.** Flow cytometry analysis of PDO biobank samples using Fab072 or Fab266 (irrelevant TT control) antibodies. Mean fluorescent intensity (MFI) values are shown.

Extended Data Figure 3. Therapeutic effects of MCLA-158.

a. Representative Ki67 IHC staining in P18T samples treated with the indicated antibodies for 48h. Lower panels are magnifications. **b.** Representative cell cycle plots of P18T PDOs treated with the indicated antibodies at a concentration of 2 μg/mL. % of cells in each cell cycle phase are indicated. **c.** Nucleus size in PDO P18T cultures treated with indicated antibodies. Each dot indicates average nucleus area (pixels) of all organoids in an independent slice. Two-sided Wald test of a linear model. **d.** P18T cultures were treated with the indicated antibodies for 4 days at a concentration of 20 μg/mL and then antibodies were washed away (arrow). Organoid size was monitored and y-axis shows growth relative to the day the treatment started. Each data point is mean +/- standard error (n=3 independent wells). *** P<0.001 by two-tailed t-test **e.** MCLA-158+ cell distributions analyzed by flow cytometry in parental non-infected, shControl

and shLGR5 P18T PDO culture. As a negative control we stained with TT-TT Ab. Cell frequencies were normalized to the mode of every sample.

Extended Data Figure 4. Effects of MCLA-158 in PDX and orthotopic xenografts.
a. Kaplan-Meier plot displaying mice survival for the experiment shown in Fig. 5j. Mice were sacrificed when either the tumors exceeded 300 mm^3 or they became ulcerated. P value between MCLA-158 and cetuxmab. Mantel-Cox test. **b.** Volume of individual P18T xenografts in experiment shown in Fig. 5j. **c.** Mice bearing PDO C31M-derived subcutaneous xenografts were treated with indicated antibodies or PBS. Tumor volumes relative to day 1 of treatment are shown. Each data point is mean +/- SEM. * p values for vehicle versus MCLA-158 and # for cetuximab versus MCLA-158 by two-tailed t-test. */# p<0.05, **/## p<0.01, ***/### p<0.001. **d-f.** Organ-specific metastases for the experiment shown in Fig. 6j,k. **g.** LGR5 mRNA (density) analyzed in tissue sections by RNAscope on peritoneal metastases found in M001 model.

Extended Data Figure 5. Subcutaneous CRC PDX growth corresponding to experiment in Figure 6e. Panels show growth of individual mice.

Extended Data Figure 6. Gene set enrichment analyses (GSEA) of P18T and C55T treated with either MCLA-158 or cetuximab. Indicated PDOs were treated with high (10 μg/mL) or low (1 μg/mL) concentration for 48 hours. 'True' indicates a false discovery rate (FDR) <0.05. Only genesets within Broad Hallmarks category that were significant for at least one antibody are shown.

Extended Data Figure 7. Localization of MCLA-158 in normal colon mucosa and CRC-derived organoids.
a. Representative confocal images of P18T and C0M PDOs treated with MCLA-158, or with EGFR (Fab232) or LGR5 (Fab072) combined with a control TT arm. PDOs were treated for 24 hours. Antibody localization was detected by immunofluorescence. Arrows indicate localization of antibodies (green) at basolateral membranes. Arrowheads indicate localization of antibodies in the cytoplasm. Red staining is actin labeled with phalloidin. Nuclei (blue) are stained with Hoechst. **b.** Representative confocal images of normal colon mucosa (C82N and C110N) and CRC (C55T and C47T) PDOs treated with MCLA-158 for 24 hours. Antibodies were added at 1μg/mL. MCLA-158 (red) and EGFR (green) localization was detected by immunofluorescence. Arrows indicate localization of MCLA-158 at basolateral membranes. Arrowheads indicate localization of MCLA-158 in intracellular structures in the cytoplasm. **c.** Virtual image of a capillary western blot measuring EGFR levels on P18T, C55T or C82N

811 (normal mucosa PDO) protein extracts. Antibodies were added at 1 μg/mL for the indicated
812 timepoints.

MATERIALS AND METHODS

Immunization of MeMo® mice

MeMo® mice were immunized with expression constructs encoding full length human LGR4 and LGR5 (pVax1_hLGR4-FLAG-HA and pVax1_hLGR5-FLAG-HA), with the extracellular domain of LGR4 or LGR5 (pVax1_hLGR4(ECD)-GPA33-FLAG and pVax1_hLGR5(ECD)-GPA33-FLAG) or with recombinant proteins rhLGR4-Fc, rhLGR5-Fc, rhZNRF3-Fc, rhRNF43-Fc or rhEGFR-Fc (RND systems), or with a combination of protein and cells. 12 to 16-week-old MeMo® mice were immunized using protein antigens and/or DNA encoding the antigens in vector pVAX. 6 to 36 mice were immunized per antigen. Dependent on the target, one or multiple immunization routes were used, sometimes combining different protein antigen formats.

In protein immunizations, mice received 40 µg protein in adjuvant (Gerbu Biotechnic, Heidelberg, Germany or TitermaxGold adjuvant (TMG, Sigma Aldrich, T2684)) subcutaneously in the left groin at day 0 followed by 20 µg protein in adjuvant at days 14 and 28. When required, additional boosts were performed using 20 µg of antigen in PBS at days 42, 49, 63, and 70. Two mice immunized with rhEGFR-Fc also received a boost with A431 cells (DSMZ ACC 91). Serum samples were collected at day 21, 35, 56, 77 and analyzed in FACS using transfected cells expressing the human protein. Mice with a positive serum titer then received three boosts on three consecutive days. One day after the final boost, mice were sacrificed, bled for serum, and spleens and left inguinal lymph nodes were collected. Materials from individual mice were kept separate.

One day prior to DNA immunization, the left hind leg of the MeMo® mice was treated with hair removal cream (Veet). Mice were immunized by DNA tattoo on the left hind leg using an Amieamed Revive medical micropigmentation device (MT.Derm GmbH, Germany) and 10 µl of a 2 mg/mL DNA solution. From day zero, the mice received three DNA tattoos given at 3-day intervals (at days 0, 3 and 6). The first and second boosts consisted of two DNA tattoos with a 3-day interval at days 14 and 17 and at days 28 and 31. Subsequent boosts, when required, were given as a single DNA tattoo at days 42, 49, 63, 70, 84, and 91. Serum samples were collected at days 21, 35, 56, 77, and 98 and analyzed in FACS using transfected cells expressing the human protein. Mice with a positive serum titer received one additional boost and three days after this final immunization, mice were sacrificed, bled for serum and left inguinal lymph nodes were collected. Materials from individual mice were kept separate.

Testing EGF blocking capacity of EGFR arms

A biotin-EGF-based competition assay was performed using serum. Goat anti-human IgG-Fc (Bethyl Laboratories cat# #A80-104A; 5 µg/mL) was coated overnight. Wells of the ELISA plates were washed 3x (PBS-0.02% v/v Tween 20) and blocked (PBS (pH 7.2), 5% BSA) for 1 hour at RT. rhEGFR-Fc at 5 µg/mL (RND systems cat# 344-ER) was captured for 1 hour at RT and plates washed again 3x. 1.5 nM biotinylated EGF (Invitrogen cat# 3477) in blocking buffer with or without different dilutions of sera were added to the plates and incubated for 1 hour at RT, after which plates were washed again 3x. HRP-streptavidin (BD cat# 554066) was added to the plates for 1 hour at RT, washed again and visualized by TMB/H_2SO_4 staining. Quantification was performed by means of OD450nm measurement.

Antibody library construction and panning

From successfully immunized mice, the lymph nodes were used for the construction of 'immune' phage antibody repertoires. RNA was extracted from the lymphoid tissue using Trizol Reagent LS (Invitrogen) and 1µg of total RNA was used in a room temperature reaction using an IgG-CH1 specific primer. The resulting cDNA was then used to amplify the polyclonal pool of VH-encoding cDNA using in-house developed VH-specific primers. PCR products were purified, digested with SfiI and XhoI, and ligated into Fab phagemid MV1043 that already contained the IGKV1-39 common light chain (cLC). Libraries were rescued using helper phage VCS-M13. All phage libraries contained $>10^6$ transformants and had an insert frequency of > 80%. Materials from individual mice were kept separate throughout this procedure.

Phage libraries were rescued according to standard procedures, and phage were selected for two rounds of selection in the case of in-house generated synthetic repertoires, and a single round in the case of the immune phage antibody repertoires. Briefly, Fc- or HIS-tagged fusion protein and cells expressing the target antigens were used for panning in a single selection round. Approximately 1000 individual colonies resulting from the selections on each antigen were picked, rescued and screened for binding to antigen-positive and antigen-negative cells in FACS. Clones that bound specifically to the target antigen of both species were identified and sequenced to establish VH gene sequence. The VH sequence was aligned to the VH of all other clones that met these criteria. Clones were grouped into 'superclusters' – defined as a group of clones sharing the same VH V-gene usage and having at least 70% sequence identity in HCDR3 and the same HCDR3 length – and into 'clusters' that use the same VH gene and 100% identical HCDR3. One or two clones from each cluster were used to prepare a streak and pick one clone to confirm binding and sequence data and for storage.

Generation of Fabs and bispecific antibodies

VH regions of cLC Fabs resulting from these selections were recloned into a WT IgG1 vector or into vectors for expression of bAbs: the KK vector (T366K, L351K) and DE vector (L351D, L368E). WT IgG1 constructs were expressed individually; bispecific IgGs were prepared by mixing equal amounts of DNA of KK and DE vectors. Expression was done in Freestyle 293-F cells (Invitrogen, Carlsbad, US) after transfection using polyethylenimine (PEI, Polysciences Inc., Warrington, US) according to the manufacturer's recommendations. IgGs were purified over protein A, buffer exchanged to PBS, and quantified using Octet (Fortébio, Menlo Park, US). Larger batches of protein were purified over protein A and gel filtration. Purified IgGs were stored in PBS at 4°C.

IgGs (both mono- and bispecific) were analyzed for binding in flow cytometry and ELISA. Briefly, for flow cytometry cells were incubated with 5µg/mL of IgG for 1 hour on ice. Cells were washed twice with ice-cold PBS-1% BSA and IgG detected by incubation with a fluorescent-labeled anti-human IgG antibody for 30 minutes on ice. Cells were washed again, resuspended in PBS-1% BSA and measured in a FACSCanto cytometer (Becton Dickinson, San Jose, USA).

For ELISA, antigens were coated overnight to MAXISORP™ ELISA plates. Wells of the ELISA plates were blocked (PBS (pH 7.2), 5% BSA) for 1 hour and incubated with selected antibodies (5µg/mL diluted in PBS-5% BSA) for 1 hour at 25°C. The ELISA plates were washed 3 times (PBS-0.05% v/v Tween 20) and bound IgG was detected with 1:2000 diluted HRP-conjugate (Goat anti-human IgG, Becton Dickinson). The plates were then washed again and visualized by TMB/H_2SO_4 staining. Quantification was performed by means of OD450nm measurement.

EGFR domain mutations and antibody competition assays

Phage mini preps of Fab clones belonging to the different superclusters were tested for binding to CHO cell clones stably expressing either wtEGFR or EGFR-variant III in FACS, as described above.

Anti-EGFR Fabs (as Fabs expressed on phage) were tested for binding to EGFR in the presence of an excess of control, literature-derived IgG, namely ICR10 (Abcam cat# ab231; domain I), EGFR.1 (Thermo Scientific cat# MS-311-P; domain II), Matuzumab (made in house; domain III), or cetuximab (Merck clinical batch; domain III) as described in Cochran et al.[64]

Serum stability binding assays

In order to get an indication of the stability of the bispecific IgGs, all IgGs were incubated at 40°C for a week in serum-containing medium (DMEM high glucose (Gibco, cat. nr. 41966-029) supplemented with 9% fetal bovine serum (Thermo Scientific Cat. nr. SV30180)) and were then tested for binding in a binding ELISA (essentially as described above). This ELISA consisted of coating 2µg/mL antigen (rhLGR4-Fc, rhLGR5-Fc, rhZNRF3-Fc or rhRNF43-Fc), using 100µl of 5µg/mL IgG and blocking in 5% BSA in PBS. In this assay, the binding to antigen of the same IgG (in serum containing medium) kept at 2-8°C (refrigerator) was compared to that of IgG kept at 40°C. The percentage loss of binding after 1 week incubation at 40°C was calculated.

Affinity determinations

MCLA-158 was radiolabeled with ^{125}I using IODO-GEN according to the protocol described by van Uhm et al.[65] The immuno-reactivity of the antibody after radiolabeling was investigated with the method described by Lindmo et al[66]. Steady state cell affinity measurements of ^{125}I-MCLA-158 were performed with CHO cells expressing either EGFR or LRG5 to investigate the affinity towards EGFR and LGR5 respectively. In addition, measurements were performed with DLD1 cells expressing EGFR and LGR5 to determine the apparent affinity for cells expressing both targets. The assay used a constant concentration of target (cells) and the amount of radio ligand was titrated without violating the assumptions behind affinity measurements at steady state conditions. Non-specific binding was assessed by the presence of 100-fold molar excess of unlabeled MCLA-158 in a parallel series. The assay was repeated twice and the estimated K_D value was reported as the mean of three independent experiments. Estimation of the K_D values was performed using GraphPad Prism v. 6.0h and the non-linear regression equation “One-Site -- Total and Non-specific binding” with the constraint that KD values must be greater than 0.

Native MS

nMS was performed according to de Nardis et al.[30]

CIEX

Cation exchange HPLC was performed to assess the charge heterogeneity and retention time of the IgGs. The experiments were performed at ambient temperature on a Dionex HPLC system equipped with an SP STAT 7 µm column and a UV-vis detector. 10 µg of sample was injected in each run. A gradient of 25 mM phosphate buffer pH 6.0 with NaCl concentrations increasing from 0 to 1 M was applied to separate the antibodies. The data were analyzed using Chromeleon software.

IEF

FocusGels with pI range 6-11 (Web Scientific, cat# 1006-03) were run on a GE Healthcare Multiphor II electrophoresis unit at 10°C. 10 µg of untreated sample was loaded to the sample next to a high pI range marker (GE Healthcare, cat# 17047301V). The electrophoresis program consisted of three phases: initial focusing for 10 minutes at 500 V followed by 90 minutes at 1,500 V and finally a focusing phase at 2,000 V for 10 minutes. Subsequently, the gel was fixed and stained using colloidal coomassie dye (Pierce, cat# 24590).

Shotgun mutagenesis

The epitopes on EGFR and LGR5 recognized by MCLA-158 were determined by shotgun mutagenesis analysis as previously described[31]. Two mutation libraries were made from the two antigens: one library encompassed amino acids 300-520 (ligand binding domain L2 or domain III) of human EGFR (GenBank reference sequence NP_005219.2) and the other encompassed amino acids 22-560 (N-terminal domain until the first transmembrane helix) of human LGR5 (GenBank reference sequence AAH96324.1). The LGR5 expression construct was truncated at amino acid 834 to increase cell surface expression of the receptor. In-house developed antibodies targeting a different epitope were used as control antibodies for the expression of the mutants. An amino acid residue was considered as a critical residue if the binding activity or reactivity of MCLA-158 was reduced by more than 75%, as compared to the unmodified amino acid sequence.

A431 apoptosis inhibition assay

In order to test the capacity of the Fab232 mAb to block EGF-mediated signaling, a cell-based assay was used to measure its ability to prevent EGF-induced apoptotic cell death of A431 cells[33]. A431 cells were plated at 1500 cells/well in 96-well tissue culture plates and grown overnight. The next day, antibody was added at the indicated concentrations together with 62.5ng/mL (10nM) of recombinant, human EGF (R&D Systems, cat. nr. 236-EG) and cells were grown for three days. After three days, the number of metabolically active cells was determined by addition of alamar blue (Invitrogen, cat. nr. DAL1100) and measurement of the fluorescence at 590nm emission with 560nm excitation. Fab232 mAb was tested for its EGF-blocking effects in this assay compared with cetuximab and TT irrelevant control IgG (Fab267).

RSPO blocking assay

For assessing the capacity to block RSPO1, a FACS assay was used. Binding of antibody (Fab072 and Fab049 at 100ng/mL; OMP88R20 (Oncomed, described in patent number US-8628774-B2) at 50ng/mL) to LGR5-positive CHO-K1 cells was assessed in FACS analysis in the presence of increasing concentrations of the ligand RSPO1 (ranging from 0.05 µg/mL to

19 μg/mL; R&D Systems, cat. nr. 4645-RF/CF). The MFI signal obtained at a certain ligand concentration was normalized to that obtained in the absence of ligand (set at 100%).

Preparation of protein lysates and measurement of total protein concentration

Lysates were prepared by adding 250 µl Tris Lysis buffer (Meso Scale Discovery, Rockville, USA) including phosphatase and protease inhibitor (all from Sigma, Germany) to the organoid pellet and vortexing for 1 min followed by 45 min incubation on ice. Lysates were centrifuged for 10 min at 13,000 x g and the supernatants were aliquoted and stored at -80°C. In order to determine the protein concentrations of lysates, a BCA assay (Thermo Fisher Scientific) was performed according to the Pierce™ BCA Protein Assay Kit (method range 0.13 – 2.0 mg/mL).

Western blot analysis: Simple Western™ Size (SWS) Assay

The Simple Western™ Size assays were run on the Peggy Sue instrument (Protein Simple, USA). Simple Western™ Size assays were performed according to the Protein Simple user manual. In brief, samples were diluted with 0.1x Sample buffer and 5x Fluorescent Master-Mix to a final concentration of 2 mg/mL. A431 cells treated with 0.2 mg/mL EGF were used as positive controls; MCF-7 cell lysate was used as negative control. EGFR antibody (EGF Receptor (D38B1) XP® Rabbit mAb, Cell Signaling Technology #4267) was used at 1:25 dilution. The evaluation of the data was performed using the Compass Software 3.1.7. Peaks were assigned according to their expected molecular size. The quantified data of the detected proteins were reported as area under the curve (AUC). Results are shown as virtual western blot image.

Human material for organoid cultures

The collection of patient data and tissues for the generation and distribution of organoids was performed according to the guidelines of the European Network of Research Ethics Committees (EUREC) following European, national, and local laws. The Biobank Research Ethics Committee of the UMC Utrecht (TCBio) approved the biobanking protocol under which this research was performed (12-093 HUB-Cancer). All donors participating in this study signed informed consent. Patients were identified by their treating physician/specialist in the hospital and selected from those undergoing resection of the tumor. Patients received a letter with the information at least 2 days prior to their visit to the hospital. Furthermore, the biobank study coordinator in the hospital visited the patient and explained the research project and answered any questions related to the project. In addition, the patients were informed that they could retract permission at all times, without having to provide a reason for doing so. Available organoids can be requested at info@hub4organoids.eu. P18T, P19bT and P14T PDOs have been previously described[21].

Colorectal cancer (CRC) organoid culture

CRC organoids were produced as described[21] as working cell banks, and shipped for screening assays on dry ice as frozen vials at a density of 1,500,000 cells per 1mL freezing medium (Fetal Bovine Serum containing 10% DMSO as a cryoprotectant). Cryo-tubes were stored at -80°C for use within 3 months or at -150°C for long-term storage. For 31 patients we established PDOs from paired tumor and normal mucosa samples.

We did not preselect samples based on any criteria. We derived and stocked PDOs from 61 primary CRCs and 11 CRC liver metastases from a total of 99 tumor samples corresponding to 68 patients treated at two different hospitals (University Medical Center Utrecht (UMCU) and Meander Medisch Centrum). For 31 patients, we also established PDOs from adjacent normal mucosal tissue. We failed to establish 27 samples: 9 samples were contaminated; in 14 tumor samples organoids were not obtained after seeding cells owing either to reduced amount of tumor cells in the surgical sample, inefficient dissociation or because suboptimal growth conditions; and PDOs from 4 samples could not be propagated in the long term.

PDO culture media

Tumoroid Expansion Medium was produced by enriching 500mL Advanced DMEM (Thermo Fisher 12491-023) with 5mL 100x Penicillin-Streptomycin (Thermo Fisher 15140-122), 5mL 100x Glutamax (Thermo Fisher 35050-038) and 5mL 1M Hepes (Thermo Fisher 15630-056). To 70mL of the enriched Advanced DMEM, 20mL R-spondin 1 conditioned medium and 10mL of Noggin-conditioned medium[21] was added to prepare 100mL Tumoroid Expansion Medium which was additionally supplemented with 2mL 50x B27 supplement (Thermo Fisher 17504-044), 1mL 1M Nicotinamide (Sigma-Aldrich N0636), 250µl 500mM N-Acetyl Cysteine (Sigma-Aldrich A9165), 10µl 5mM A83-01 (TGFβ inhibitor, Tocris 2939) and 33µl 30mM SB202190 (p38 inhibitor, Sigma Aldrich S7067). The Tumoroid Expansion Medium was further supplemented with 100µl 10mM Y27632 (Rho kinase inhibitor, Abmole CETUXIMAB-27632 dihydrochloride) upon fresh seeding of colon tumoroids in the presence of human EGF (Peprotech AF-100-15) or human NRG-1/HRG (ImmunoTools 11343047). EGF and HRG are growth factors that stimulate organoid expansion, and the concentration that is used determines the sensitivity of the screening assay. EGF was added at 2.5ng/mL, 5ng/mL or 10ng/mL during screening, or at 10ng/mL or 50ng/mL during expansion. HRG was used at 5ng/mL. Wild-type Organoid Expansion Medium is equivalent to the Tumoroid Expansion Medium, with one replacement: the 70mL enriched Advanced DMEM is replaced by a combination of 20mL enriched Advanced DMEM and 50mL Wnt3A-conditioned medium[21]. Normal tissue-derived colon organoids and colon tumoroids with wild type APC are WNT-dependent and therefore require the presence of WNT for expansion.

Sequencing of PDO biobank

Pairs of DNA derived from colorectal organoids and blood from the same patients were shipped to the Sanger Institute for sequencing. Each DNA sample, from tumor and normal separately, was sent for exome sequencing on the HISEQ 2000 sequencer. After mapping the sequencing reads to the reference genome, we obtained an estimate of sequencing coverage of the exome of 147X, with standard deviation of 56X. In order to obtain reliable copy-number profiles, each DNA sample was also genotyped using the Affymetrix SNP6 array. Prior to that the samples were confirmed to originate from the same patient by genotyping a small number of polymorphisms, where only two pairs were inconsistent and rejected.

Analysis of genetic alterations of PDOs

Whole exome sequencing from the DNA samples was processed using the algorithms developed or customized at the Sanger Institute. Resulting BAM files were aligned to the reference human genome (GRCh37) using Burrows-Wheeler Aligner, BWA (v0.5.9). Briefly, CaVEMan (Cancer Variants Through Expectation Maximization: http://cancerit.github.io/CaVEMan/) was used for calling somatic substitutions. Indels in the tumor and normal genomes were called using a modified Pindel version 2.0 (http://cancerit.github.io/cgpPindel/) on the NCBI37 genome build[67].

Data were analyzed and visualized using custom scripts written in R. In particular, we implemented a set of rules for identifying driver mutations among the somatic mutations. A list of 726 genes causally implicated in cancer had been retrieved from the Cosmic Cancer Gene census (http://cancer.sanger.ac.uk/census/), and we reported some of the mutations affecting these genes. For cancer genes classified as recessive (tumor suppressors), we reported all nonsense, frameshift, essential splice site and stop-lost mutations, as well as missense and in-frame mutations at positions previously reported in the Cosmic database from other cancer studies. For dominant cancer genes, we reported missense or in-frame indels previously reported in other studies. We used the Cosmic database (http://cancer.sanger.ac.uk/cosmic) to ensure that the missense or in-frame mutations we classified as putative drivers had been reported in other studies and therefore are recurrent.

Furthermore, we implemented rules that prioritized some of the copy number changes to be putative driver events. As a first step, we identified a set of regions in individual samples as amplicons (total copy number >= 5 if ploidy lower than 2.7, otherwise total copy number >= 9) or homozygous deletions (total copy number = 0). We then intersected those with regions of

common copy number alterations in the TCGA study[9], and reported those amplicons and homozygous deletions regions including genes previously implicated in colorectal cancer.

Preparation of PDOs for antibody screen

Frozen PDOs were thawed rapidly in a water bath at 37°C and collected in 5mL enriched Advanced DMEM. The organoids were pelleted by 5-minute centrifugation at 1000rpm at 4°C. The supernatant was removed, and the organoids taken up in Tumoroid Expansion Medium without growth factors. This organoid suspension was mixed with Cultrex Reduced Growth Factor Basement Membrane Extract, Type 2 (BME2), PathClear (Amsbio 3533-010-02). The final Cultrex gel percentage was 60% and the number of cells per mL was 100,000.

To expand colon tumoroids, 24-well or 6-well plates (Greiner Bio-One) were used and per well, either 3 or 10 drops of 15µl gel/organoid suspension was spotted at regular distances. Tumoroid Expansion Medium (0.5mL or 2mL) containing 10ng/mL to 50ng/mL EGF was added after a 30 minute gelation period at 37°C. At day 1 of seeding, the Tumoroid Expansion Medium contained 10µM Y27632. Medium replacements during expansion were with EGF-containing Tumoroid Expansion Medium devoid of Y27632.

To perform screens, clear-bottom 384-well plates (µclear, Greiner Bio-One 781091) were used. Per well, 15µl of the gel/organoid mix was dispensed using a CyBio Felix automated liquid handling robot (Analytik Jena, Jena, Germany). Upon 30 minutes gelation at 37°C, 45µl Tumoroid Expansion Medium (or Organoid Expansion Medium where applicable) was added on top of the gel in each well. The medium was supplemented with or without growth factors, and antibodies and compounds were mixed with the medium in v-bottom 96-well plates before applying to the 384-well plates with solidified gel.

Antibody screen

Reference antibodies, negative control antibodies, single arm HER3 or EGFR-targeting antibodies and HER3/EGFR antibodies (on dry ice) were shipped and stored at 4°C for screening. Bispecific and monospecific antibodies were delivered in deep-well 96-well plates that were sealed and shipped at 4°C. The antibodies were manually transferred to four v-bottom 96-well plates (Greiner Bio-One 736-0118) in randomized locations ranging from well B02 to well G11 (inner 60 wells). Reference antibodies were added to the plates at random locations as well, at equal concentration. These antibody master plates were used to prepare 1:10 dilution plates in PBS. The master plates and dilution plates were stored sealed at 4°C.

For validation of screening results, a lead panel of bispecific IgGs at a concentration of 0.5mg/mL were shipped in screw-capped microvials, to allow easy randomization of the antibodies in screening plates and to prevent cross-contamination and evaporation. Prior to each experimental run, the bispecific IgGs were placed in one v-bottom 96-well plate (inner 60 wells) along with reference antibodies at 0.1mg/mL by diluting them in PBS. This plate was diluted once more 1:5 in PBS to achieve a second master plate containing antibodies at 20µg/mL. Dilutions and plate exposures were performed using the CyBio Felix liquid handler (Analytik Jena, Jena, Germany).

The high-dose and low-dose v-bottom 96-well antibody master plates were diluted 1:10 in culture medium before exposure. The antibody concentrations applied in the primary screen were 10µg/mL and 1µg/mL, or 40µg/mL and 4µg/mL; and in the validation screen the antibody doses were 10µg/mL and 2µg/mL. The antibodies were added to the organoids 30 minutes after seeding.

For primary and secondary screens, all models were initiated at the same seeding density in the same culture medium. For most models the endpoint (day of fixation) was day 9, but in some PDOs with high growth rates, day 7 or 8 was chosen to prevent overgrowth of the control wells.

High content imaging

To prepare the exposed tumoroid plates for imaging, the samples were fixed and stained to visualize the nuclei and the actin cytoskeleton as previously described[68]. Imaging of the plates (Fig. 2b-f; 3a-e; 5a, 5f-h, 6a) was performed using an ImageXpress Micro XLS system (Molecular Devices, Wokingham, UK) as previously described[69]. Briefly, z-stacks of each well in a 384-well plate were captured using a 4x objective lens, with a z-step size of 50µm. The number of sections per well ranged from 20 sections to 24 sections, to cover the entire depth range of the gel in each well. Confocal images were captured using an ImageXpress Micro Confocal (Molecular Devices) (Fig.7f, Extended Data Fig. a,b) or a Nikon Ti A1 confocal laser microscope (Sup. Fig. 7a,b) using a 20x 0.75NA objective, and processed in ImageJ. For antibody localization studies, the organoids were incubated for the indicated times with 1µg/mL antibody prior to fixation in 4% PFA. Upon washing in TBP (0.1% Triton X100 (Sigma-Aldrich) + 0.5% BSA (Sigma-Aldrich) in PBS) the antibodies were detected with a goat-anti-human-Cy5 secondary antibody (1:2000; Thermo Fisher Scientific) before washing in TBP, and fixation and staining for the nuclei and actin cytoskeleton. Endogenous EGFR levels were detected using the mouse monoclonal antibody MA5-13319 (1:40; Thermo Fisher Scientific)

followed by a goat-anti-mouse-Alexa488 secondary antibody (1:2000; Thermo Fisher Scientific).

Image analysis

Captured images were stored on a central data server, accessible by the OcellO Ominer® image analysis platform integrated into the KNIME Analytics Platform (http://knime.com/) which allows direct parallel analysis of the 3D image stacks by its distributed computational design[68,69]. The software analyzes the structure of the objects (nuclei and cytoskeleton) detected in each well, and their relative positions. Upon analysis, quality control of the output was performed to check the quality of the organoid cultures, the raw images and the segmentation of objects. The per-object measurements of nucleus shape and number, lumen shape and number, and organoid shape and number were subsequently aggregated per well and the data coupled to the plate layout information (cell line, growth factor condition, treatment, etc.). The data were then checked for consistency within control treatments, absence of edge effects, consistency between replicates and the Z'-factor between positive and negative controls. Next, the data were z-score normalized and inspected using TIBCO Spotfire® to purge additional outliers. 500 different morphological features were collected from the per-object measurements; the data was then analyzed and an optimal subset of 3 to 20 features were selected based on their ability to distinguish the reference treatment effect from the negative control morphology. The distance between the reference and the negative controls was calculated as a Euclidian distance measurement and scaled between zero and one to calculate the normalized multiparametric response. This unified score of morphology change was used to discriminate hits in the compound screens across all organoid models. The individual selected feature measurements, together with corroboration with the images were used to substantiate and verify the effects of the hit compound treatments on the organoids.

Calculation of the Z'-factor

The Z'-factor is a statistical measure for quality of a high throughput screening assay[70] and indicates the separation window between positive (no growth factor) and negative controls (EGF, HRG or WNT3A). The Z'-factor is defined as $Z' = 1 - \frac{3*(\text{SD of positive control} + \text{SD of negative control})}{|\text{mean of negative control} - \text{mean of positive control}|}$. Z'-values smaller than 0 indicate that there is too much overlap between negative and positive controls, values between 0 and 0.5 indicate a useful but moderate screening window, and values between 0.5 and 1.0 indicate an excellent assay with a strong separation between positive and negative controls.

FACS staining using Fab072 antibodies in PDOs

The day prior to analysis, the organoids were disaggregated into single cells. After 12 hours the cells were isolated from the Reduced Growth Factor Basement Membrane Matrix, Type 2 (BME2) using cell recovery solution. After 1 hour on ice, the cells were centrifuged, and washed once in 10 mL of PBS containing 0.5% BSA and 0.5 mM EDTA (staining buffer). A maximum of 100,000 cells/100 µL of antibody was used, and cells were labeled using a primary antibody diluted to 10 µg/mL. The cells were incubated on ice for 45 minutes, with regular inversion of the tubes to ensure homogeneous staining. The cells were washed and incubated with anti-human IgG antibody conjugated to R-PE (Invitrogen, H10104) diluted 1:400 for 20 minutes on ice. After subsequent washing, the cells were re-suspended in staining buffer containing 0.1 µM DAPI (Sigma-Aldrich) to identify dead cells and were then immediately analyzed in BD FACSAria.

FACS staining using Fab072 antibody in xenografts

P18T-derived subcutaneous tumor xenografts were minced into small pieces using a blade and incubated for 30 minutes at 37ºC with HBSS and 166U/mL of Collagenase IV (Sigma ref: C5138-1G). After incubation, samples were pipetted up and down and subsequently filtered through 70µm and 40 µm mesh filters. Cells were spun down (5 min at 1500 rpm) and the pellet was resuspended with 2 mL of ammonium chloride and incubated at RT for 3 min to lyse the red blood cells. After lysis, HBSS was added and the cells were spun down again. Finally, the cell pellet was resuspended in 5mL staining buffer. Cells were Fc blocked with CD16/32 (mouse, Tonbo Biosciences, 70-0161-U500) for 10 min at 4ºC, stained with EPCAM-PeCy7 (human, eBioScience, 25-9326-42) and 5 µg/mL Fab072 monospecific antibody or negative control TT primary antibodies for 40 min at 4ºC and then with 1:400 donkey anti-human IgG Alexa Fluor-647 secondary antibody (Jackson Immunoresearch, 709-605-149) for 30 min at 4ºC. Samples were resuspended in 1 µg/mL DAPI in FACS buffer (HBSS- 0.5% BSA- 0.25mM EDTA).

Cell sorting and transcriptomic analysis

Cells were sorted using BD FACSAria. Fab072+ and Fab072- cells from the alive (DAPI negative) and Epcam+ populations were sorted using the gates indicated in the figure 4h. A total of 1000 cells for each cell population were sorted into picoprofiling buffer, and further processed for RNA extraction and cDNA synthesis at IRB genomics facility by picoprofiling[71]. LGR5 expression was assessed using quantitative PCR using TaqMan probes and TaqMan Universal PCR Master Mix (both from Applied Biosystems). RT-qPCR analysis in fig 4i was performed with Taqman assays following the manufacturer's instructions (Applied Biosystems)

with the following probes: LGR5 (Hs_00173664_m1), SMOC2 (Hs_0159663_m1), ASCL2 (Hs_00270888_S1), OLFM4 (Hs_00197437_m1), MYC (Hs_00905030_m1), KI67 (Hs_01032443_m1), CDKN1A (Hs_00355782_m1), KRT20 (Hs_00300643_m1), SLC26A3 (Hs_00995363_m1), and using B2M (Hs_99999907_m1) and PPIA (HS_ 99999904_m1) as normalizers. Transcriptomic profiling of Fab072+ and Fab072- cells from n=2 xenogafts was performed as described elsewhere[5].

Organoid antibody treatments for immunohistochemistry and cell cycle analysis

For antibody treatment experiments, the culture medium contained an EGF concentration of 2.5 ng/mL. After disaggregation of organoids, Tryphan Blue staining (Sigma-Aldrich) was used to determine the number of live cells, and 5000 cells were plated/25 µL of BME2 on a 48-well plate. Each treatment had 8 replicates, and was cultured in 250 µL medium/well. Seven days after seeding single cells, the medium was removed and replaced with medium containing the antibody treatments (2 µg/mL).

Immunohistochemistry of P18T PDOs

48 hours after the addition of the antibodies, culture medium was removed, and BME2 drops on a 48-well plate were fixed in 300µL of formalin for 2 hours at room temperature. BME2 drops were then manually broken using a pipette, pelleted, and placed in fresh formalin. Pellets were left at room temperature overnight before washing in PBS three times. Ki67 staining was performed by the IRB histology facility using an Autostainer Plus (Dako, Agilent). Rabbit polyclonal anti-Ki67 (ab15580, Abcam) was diluted 1:1000 and incubated for 60 mins at room temperature. BrightVision Poly-HRP-Anti Rabbit IgG Biotin-free was used for the secondary antibody (Immunologic, DPVR-110HRP), and was incubated for 30 mins at room temperature. Staining specificity was confirmed through omission of the primary antibody. Representative images were captured using a Nikon Eclipse E600 attached to a Nikon DS-Ri1 camera.

Cell cycle analysis

To assess the effect of the antibodies on cell cycle progression, the organoids were treated for 48 hours with a low dose of antibody (2 µg/mL). EdU was then added to the medium at a final concentration of 10 µM, and incubated for 2 hours. The organoids were then harvested and processed to a single cell suspension. The Click-iT® EdU Alexa Fluor® 647 Flow Cytometry Assay Kit was used according to the manufacturer's protocol. The organoids were counterstained with DAPI (1 µg/mL) for 30 minutes on ice and then analyzed using the Gallios flow cytometry machine.

PDO recovery analysis after Ab treatment

P18T organoids were dissociated into a single cell suspension with Trypsin/EDTA. 5000 cells were plated in 20 µL BME2 drops in 48-well tissue culture plates. For the antibody treatment experiments, the culture medium contained an EGF concentration of 2.5 ng/mL. Organoids were treated either with PBS, cetuximab or MCLA-158 at 20 µg/mL for 4 days. At day 4, antibodies were washed away and replaced with control medium. Each treatment had 3 technical replicates. The plate was scanned using an Olympus ScanR with a 4x light objective at days 0, 4, 8, 10 and 14. The number and size of organoids was quantified using ImageJ. Total area occupied by the organoids in a given well and time point was calculated as a surrogate of organoid growth and normalized to day 0.

Ki67 quantifications in P18T

The staining intensity for Ki67 in each individual nucleus was measured using ImageJ. The activity of Ki67 was divided up into four groups of intensity level. The number of nuclei that fell within a certain staining group was divided by the total to calculate the fraction. The graph in Fig. 5b shows the fraction of nuclei present within the Ki67-high signal group. Four intensity groups were identified on an 8-bit scale (0-255): Low < 35; 35 < Lower middle < 85; 85 < Upper middle < 110; High >110.

RT-qPCR of WNT/stem cell marker genes

For Fig. 5f, organoids were harvested from 70% BME2 drops in PBS and cell pellets were used for RNA extraction using PureLink RNA mini kit (Thermo Fisher, 12183018A) and cDNA retrotranscription (AB, 4368813) according to the manufacturer's instructions. RT-qPCR was performed using 5ng cDNA and SYBR Green master mix reagent (Applied Biosystems, 100029284) or Taqman 2x Universal Master Mix (Thermos Fisher, 4324018) and the following primers (5'-3'): LGR5 (Fwd: TGGAGGAGTTACGTCTTGCG, Rev: AGAGCTTCTGTGGGTACGTG), MYC (Fwd: GTAGTGGAAAACCAGCCTCC, Rev: AGAAGTTCTCCTCCTCGTCG), ASCL2 (Fwd: CATAACTTGAGCTGCTGGAGG, Rev: TGCTCGTGTCCAGATCTTGG), OLFM4 (Fwd: GAGGTTCTGTGTCCCAGTTG, Rev: TCCAAGCGTTCCACTCTGTC), EPHB2 (Fwd: 5'-TCAACAGCCGGACCACTTCT-3', Rv: 5'-GAGGGAGGTCTCATTGACACTG-3'), SMOC2 (Fwd: ACAGTCAGGTCCAGTGTCAC, Rev: TTCATTTACGGAACCCGGGC), AXIN2 (Taqman, HS_00610344_m) which were normalized to B2M (Fwd: GAGGCTATCCAGCGTACTCCA, Rev: CGGCAGGCATACTCATCTTTT) and PPIA (Fwd: CCCACCGTGTTCTTCGACATT, Rev: GGACCCGTATGCTTTAGGATGA).

Effects of MCLA-158 on shLGR5 P18T organoid formation

P18T organoids were infected with shControl (SHC002) or shLgr5 (TRCN0000011586) shRNA Mission Sigma-Aldrich lentiviral constructs. Infected cells were selected and maintained in 0.5 µg/ml puromycin (Invivogen, ant-pr). 1500 cells from 7-day grown organoids were plated in 20µl 90% BME2 drops and medium containing AdvancedDMEM/F12, Hepes, Glutamax, B27, nicotinamide 10mM, N-actelyl-cysteine 1.25mM, Rspondin-1 1µg/ml, EGF 2.5 ng/ml, Noggin 100 ng/ml, SB202190 9 µM, gastrin 20ng/ml and A-83-01 500 nM. P18T cells were treated with 1 µg/ml control TT-TT irrelevant antibody, cetuximab or MCLA-158 from day 0 and medium was changed every other day. Organoid growth was monitored from day 1 after seeding until assay endpoint using an Olympus ScanR microscope, and ImageJ dedicated macros for quantification were used as described previously[5,72]. Organoid forming efficiency was calculated by dividing the number of organoids (>1200 pixel objects) at the end time point by the number of seeded cells detected at day 1 (>60 pixel objects). Organoid size was calculated by measuring the average area in pixels of >1200 pixel objects. Relative organoid growth was calculated by multiplying the organoid forming efficiency by the average organoid area in pixels and it was normalized to the values obtained for day 1.

EGFR levels in shRNA LGR5 P18T PDO.

For experiments shown in Fig. 7h,i, P18T organoids were plated in 70% BME2 drops and treated with 1µg/ml MCLA-158 or irrelevant control antibody (TT-TT, PG1337) for 72h in organoid culture medium, with 2.5 ng/ml EGF. At the start of recovery, wells were washed and medium changed. At different time points medium was collected after antibody withdrawal. Organoids were harvested in cell recovery solution (Corning, 354253) and incubated for 45min on ice and then washed in PBS. Cell pellets were lysed in RIPA buffer with proteinase inhibitors, snap frozen, centrifuged at 4ºC for 15min at 10000rpm and supernatants were transferred to new tubes. Protein concentration was determined with a BCA assay (Thermo Scientific, 23225). 30 µg of protein of each sample were loaded into miniprotean TGX 10% acrylamide gels (Biorad, 4561034) and SDS-PAGE and transfer to PVDF Immobilon membranes (Merk, IPDH00010) was performed. Membranes were blocked in 5% BSA–TBS-Tween 0.2% for 1h. Membranes were cut at the 75KDa size and the >75KDa membrane part was incubated with anti-EGFR antibody (Cell signaling, 4267S) at 1:1000 overnight and then with anti-rabbit-HRP (Amersham, NA934V) 1:5000 for 2h and the <75KDa membrane part was incubated with anti bActin-HRP antibody (abcam, 20272) at 1:2000 for 2h. Membranes were incubated with Super Signal West pico Plus chemiluminescence substrate (Thermo Scientific, 34580) and exposed in the Odyssey Fc LI-COR imaging system.

LGR5 surface levels in normal and tumor PDOs

T x TT and MCLA-158 staining of dissociated PDOs (Extended Data Fig 3e): Non-infected, shControl (Mission Sigma SHC002) and shLgr5 (TRCN0000011586) P18T PDOs were grown in 70% BME and tumor organoid medium consisting of AdvancedDMEM/F-12- 10 mM Hepes - Glutamax - B27 - 10 mM Nicotinamide - 1.25 mM nAcetylcystein - 50 ng/ml EGF - 100 ng/ml Noggin - 1 ug/ml Rspondin-1, 10uM SB202190 - 10 nM gastrin - 500 nM A93-01. Infected cells were maintained in 0.5 ug/ml puromycin (invivogen, ant-pr). 1-week grown PDOs were single-cell dissociated in TryplE Express and plated in 70% BME and tumor organoid medium overnight. The following day, PDOs were harvested in cold PBS. Cells were counted and stained with 5 µg/ml MCLA-158 or TT x TT control antibody in stain buffer (AdvancedDMEM/F12-Hepes-Glutamax, 10% FBS, 0.5% BSA) for 30 min on ice, washed three times and stained with 5µg/ml of secondary antibody Alexa Fluor 647 Goat anti Human igG (Life Technologies, A21445) for 30 min on ice. Samples were washed and resuspended in 1µg/ml DAPI in HBSS- 0.5% BSA and analyzed in BD Diva FACS Aria Fusion. Centrifugation steps were performed at 450g for 5 min at 4ºC.

Treatment of P18T-derived xenografts with antibodies

Mouse experiments were approved by the Animal Care and Use Committee of Barcelona Science Park (CEEA-PCB) and the Catalan government under protocol number DAAM7329. P18T was grown for seven days before disaggregating into a single cell suspension for injection. For all mouse studies female NOD.CB17/AlhnRj-Prkdcscid/Rj mice (Janvier Labs) aged between 6-8 weeks were used. Xenografts were initiated by subcutaneously injecting 100 µL of BME2:PBS (50:50) solution containing 200,000 single P18T cells. Once the tumor volume reached 300 mm^3, mice were sacrificed and tumors harvested. One tumor was manually cut into small pieces approximately 0.5 mm x 0.5 mm x 0.5 mm (width x length x height). The pieces were then placed into four flanks of recipient NOD-SCID mice, using one piece/flank. A trocker was used to implant the pieces into the mice, a device which pushes a tumor piece underneath the skin. Once the tumor volume on a mouse reached an average of 50 mm^3, the mice were randomly assigned to a treatment group. Mice were injected once a week for four weeks with 200 µL of PBS (vehicle), cetuximab, or MCLA-158. Cetuximab and MCLA-158 were injected at a dose of 0.5 mg/mouse, regardless of mouse weight. Tumor volume was calculated using manual calipers with measurements taken thrice a week, using the formula (length x width x height)/2. Mice were sacrificed when either the tumor volume exceeded 300 mm^3, the tumor ulcerated, or on day 28.

MCLA-158 treatment of CRC, gastric, esophageal and head and neck carcinomas PDX models

Models were conducted at the Crown Biosciences facility in Beijing, China and at their facility in San Diego, USA. For these experiments, we selected PDXs belonging to different tumor types that showed elevated EGFR and LGR5 mRNA expression levels according to available RNA sequencing data. Human cancer cells were inoculated subcutaneously in the flank of immunodeficient mice, either BALB/c Nude or NOD/SCID mice depending on the mode (Supplementary Table 2). These tumor grafts were either tumor fragments or a cell suspension that had been harvested from donor mice bearing established primary human tumors. After tumor inoculation, animals were checked daily for morbidity, mortality and clinical signs. When mean tumor size reached 100-150 mm^3, mice were randomized over the treatment arms to receive an intraperitoneal injection of MCLA-158 in PBS. HNSCC: mice were injected with 25 mg/kg/week MCLA-158 depending on their weight, n=4 mice/group. Gastric /oesophageal /CRC: mice were injected with 0,5 mg/week MCLA-158 (about 25 mg/kg) regardless of the weight of the animal, gastric/oesophageal n=4 mice/group; CRC: n=8 mice/group. Mice were treated once a week for 6 weeks, followed by a 3-week observation period. Tumors were measured twice a week using calipers, and tumor volume was calculated by assimilating them to an ellipsoid using the formula: l (length) × w2 (width) × ½. The percentage change in tumor growth from baseline was calculated using the tumor volume data on day 0 and the tumor volume data on the last day at which all mice in both groups were still in the experiment. Statistical significance was determined by one-way ANOVA.

LM-CRCX3 orthotopic CRC model

A small fragment of a unique lung metastasis from a colorectal cancer patient previously treated with fluoropyrimidines-based chemotherapy was obtained with the informed consent of the patient. The tumor has a KRAS mutation (G12D) and it is MSS (with microsatellite stability). Briefly, a tumor sample taken by a pathologist was placed in DMEM supplemented with 10% FCS and penicillin/streptomycin and implanted in two five-week-old male nu/nu Swiss mice (Envigo) weighing 18–22 g. Mice were anesthetized by isoflurane inhalation, and a small fragment of 4 x 4 mm^3 maintaining tridimensional structure was anchored to the serosa of the caecum with a Prolene 7.0 suture. The abdominal incision was closed with 4.0 Vicryl, mice were inspected twice a week and tumor formation checked by palpation. Once the tumor grew, the mouse was sacrificed and the tumor (named LM-CRCX3) was re-implanted in the caecum another three mice to expand and generate enough high-quality tissue for seeding drug assay experiments. A good histology correlation was evidenced between primary and xenografted tumors.

Animals were housed in a sterile environment, in cages with autoclaved bedding, food, and water. Mice were maintained on a daily 12 hours light, 12 hours dark cycle. The Institutional

Ethics Committees approved the study protocol, and the animal experimental design was approved by the IDIBELL animal facility committee (AAALAC Unit1155) under approved procedure 9111. All experiments were performed in accordance with the guideline for Ethical Conduct in the Care and Use of Animals as stated in The International Guiding Principles for Biomedical Research Involving Animals, developed by the Council for International Organizations of Medical Sciences.

20 mice were implanted with LM-CRCX3 at passage #2 and nineteen days later, when homogeneous small masses were detected at palpation, 18 mice were randomized and allocated into three treatment groups (n=6/group): (i) Vehicle (PBS); (ii) cetuximab (0.05 mg/animal in PBS); (iii) MCLA-158 (0.05 mg/animal in PBS). All mice were treated by intraperitoneal injection (i.p.) once per week during four weeks. At sacrifice tumors were collected, photographed and measured. Diaphragm, liver, lung and peritoneal cavity were macroscopically inspected for the presence of metastases, and the different organs collected to detect presence of micrometastases by standard H&E analysis.

M001 and M005 orthotopic CRC models

Colon carcinoma tissues obtained upon surgery were washed 3 times in cold PBS solution and incubated overnight in DMEM/F12 (Gibco) containing a cocktail of antibiotics and antifungals (penicillin (250 U/mL), streptomycin (250 mg/mL), fungizone (10 mg/mL), kanamycin (10 mg/mL), gentamycin (50 mg/mL), and nystatin (5 mg/mL; Sigma-Aldrich)). Isolation of patient-derived cells has been previously described[73]. Enzymatic digestion was performed using collagenase (1.5 mg/mL; Sigma-Aldrich) and DNase I (20 mg/mL; Sigma-Aldrich) in a medium supplemented with a cocktail of antibiotics and antifungals (as described above) during 1 hour at 37°C with intermittent pipetting every 15 minutes to disperse cells. The dissociated sample was then filtered (100 mm pore size) and washed with fresh medium. Red blood cells were lysed by brief exposure to ammonium chloride and the sample was washed again. Purified tumor cells were frozen in liquid nitrogen using the above-mentioned culture medium (DMEM/F12 + complements) and 10% DMSO for long term storage. Thawed cells were rinsed from DMSO and orthotopically injected in NOD-SCID mice as previously reported[73]. In brief, 3 x 10^5 patient-derived tumor cells suspended in 50mL of PBS were injected into the cecum wall of NOD-SCID females (8-10 weeks of age). For these experiments, we selected models derived from two patients that carried activating mutations in KRAS. Additionally, the M005 model carries a non-frameshift deletion in PI3KCA locus predicted as oncogenic. PDX genotypes were characterized by exome sequencing. Main driver mutations are detailed in Supplementary Table 2. Both PDX models M001 and M005 were derived from liver metastases of patients with stage IV advanced CRC. Experiments with mice were

conducted following the European Union's animal care directive (86/609/EEC) and were approved by the Ethical Committee of Animal Experimentation of the Vall d'Hebron Research Institute (VHIR) (ID: 17/15 CEEA and 18/15 CEEA). NOD-SCID mice (NOD.CB17-Prkdcscid/NcrCrl) were purchased from Charles River Laboratories.

Mice were treated MCLA-158 (0.5 mg/animal in PBS intraperitoneally once per week) starting on the day that orthotopic tumor growth was confirmed by microcomputed tomography. Control mice were injected with the corresponding amount of vehicle (PBS). Tumor growth was monitored by microCT imaging during treatment. All mice were sacrificed when more of a third of the cohort showed generals signs of illness. At this endpoint mice were euthanized and complete necropsies were performed. Organs were macroscopically inspected for the presence of metastases. Primary carcinomas in the cecum, liver, lungs and any other visible tissue affected were collected for histological analysis. Standard hematoxylin and eosin (H&E) staining was performed on repeated sections of each tissue to confirm the presence of metastatic lesions.

RNA sequencing after Ab treatment

P18T and C55T organoids were dissociated into single cells and plated in 6-well plates. After plating, organoids were treated with a low (1μg/mL) or high (10 μg /mL) dose of control IgG, cetuximab or MCLA-158 during 48 hours in low EGF conditions (2.5 ng/μl). RNA was isolated from samples using an RNA Mini kit (12183025; Life Technologies). The concentrations of total RNA extractions were quantified with Qubit RNA Hs Assay kit (Invitrogen) and RNA integrity was assessed with the Bioanalyzer 2100 RNA Pico assay (Agilent). mRNA was isolated from 150-200 ng of total RNA using the kit NEBNext Poly(A) mRNA Magnetic Isolation Module (New England Biolabs). NGS libraries for RNA-seq were prepared from the purified mRNA using the NEBNext Ultra II RNA Library Prep Kit for Illumina (New England Biolabs). Twelve cycles of PCR amplification were applied to all libraries. The final libraries were quantified using the Qubit dsDNA HS assay (Invitrogen) and quality controlled with the Bioanalyzer 2100 DNA HS assay (Agilent). An equimolar pool was prepared with the twenty-four libraries and submitted for sequencing to the Centre for Genomic Regulation. A final qPCR quality control was performed before sequencing in two lanes of an Illumina HiSeq2500. Sequencing output was 550 Million 50-bp single-end reads, and at least 20 million of reads were obtained for each library.

Analysis of RNASeq data

Paired end reads were aligned to the hg38 human genome with STAR (version 2.5.2b) and default parameters. Sambamba was used to convert to bam and sort resulting sam files. All subsequent analyses were performed in the R programming environment unless otherwise stated. Count matrices were generated with the Rsubread package using the GENCODE homo sapiens v34.GRCh38.p13 version. Complementary genes annotations were added using biomaRt version GRCh38.p12. Normalization and contrasts were performed using the DESeq2 R package. Biological replicate was included as covariable in the model.

Pathway mean expressions for figures 7a and 7b were computed after adjusting for biological replicate. Boxplot show z-scores of mean expression of genes in pathway for each sample.

Geneset enrichment analyses

Functional enrichment was performed using a rotation-based methodology. The ROAST algorithm as implemented in the R package limma was used to represent the null distribution. The maxmean enrichment statistic under restandardization was considered for competitive testing. P-values were adjusted for multiple testing with the Benjamini-Hochberg algorithm.

Statistical analyses

For continuous outcomes, group differences were assessed using a Mann-Whitney test when no other covariates were involved in the analyses (Fig. 5d, e). When statistical control for confounding variables were required (Fig. 5b, Extended Data Fig. 3c), a two-sided Wald test derived from a linear model was used. When the experiment involved repeated measurements on the same biological samples (Fig. 5j), values were fitted to a mixed-effect model in which biological replicate was modeled as a random effect using the R package *lme4*. Normality and homocedasticity assumptions were assessed graphically and response variables were log-transformed when needed (Fig. 5j). Stripcharts plots were used to represent data values, means and standard errors in their original scale. Association between categorical variables (Fig. 6k) were assessed using an exact Fisher's test. Absolute frequencies were graphically represented with barplots. A 5% threshold was set for statistical significance.

DATA AVAILABILITY

Organoid exome sequencing data will be deposited at EGA and released at the moment of publication. The authors declare that all other data supporting the findings of this study are available within the paper and its Extended Data information files.

REFERENCES

1. Merlos-Suárez, A. *et al.* The Intestinal Stem Cell SignatureIdentifies Colorectal Cancer Stem Cells and Predicts Disease Relapse. *Cell Stem Cell* 1–14 (2011) doi:10.1016/j.stem.2011.02.020.
2. Vermeulen, L. *et al.* Single-cell cloning of colon cancer stem cells reveals a multi-lineage differentiation capacity. *Proc Natl Acad Sci U S A* **105**, 13427–13432 (2008).
3. de Sousa e Melo, F. *et al.* A distinct role for Lgr5+ stem cells in primary and metastatic colon cancer. *Nature* **543**, 676–680 (2017).
4. Schepers, A. G. *et al.* Lineage Tracing Reveals Lgr5+ Stem Cell Activity in Mouse Intestinal Adenomas. *Science (80-.).* **337**, 730–735 (2012).
5. Cortina, C. *et al.* A genome editing approach to study cancer stem cells in human tumors. *EMBO Mol. Med.* **9**, 869–879 (2017).
6. Shimokawa, M. *et al.* Visualization and targeting of LGR5 + human colon cancer stem cells. *Nature* **545**, 187–192 (2017).
7. BK, K. *et al.* Tumour Suppressor RNF43 Is a Stem-Cell E3 Ligase That Induces Endocytosis of Wnt Receptors. *Nature* **488**, (2012).
8. De Lau, W. *et al.* Lgr5 homologues associate with Wnt receptors and mediate R-spondin signalling. *Nature* **476**, 293–297 (2011).
9. Muzny, D. M. *et al.* Comprehensive molecular characterization of human colon and rectal cancer. *Nature* **487**, 330–337 (2012).
10. Dow, L. E. *et al.* Apc Restoration Promotes Cellular Differentiation and Reestablishes Crypt Homeostasis in Colorectal Article Apc Restoration Promotes Cellular Differentiation and Reestablishes Crypt Homeostasis in Colorectal Cancer. *Cell* **161**, 1539–1552 (2015).
11. Buske, P. *et al.* A Comprehensive Model of the Spatio-Temporal Stem Cell and Tissue Organisation in the Intestinal Crypt. *PLoS Comput. Biol.* **7**, e1001045 (2011).
12. Wong, V. W. Y. *et al.* Lrig1 controls intestinal stem-cell homeostasis by negative regulation of ErbB signalling. *Nat. Cell Biol.* **14**, 401–408 (2012).
13. Shaib, W., Mahajan, R. & El-Rayes, B. Markers of resistance to anti-EGFR therapy in colorectal cancer. *J. Gastrointest. Oncol.* **4**, 308–18 (2013).
14. Karapetis, C. S. *et al. K-ras* Mutations and Benefit from Cetuximab in Advanced Colorectal Cancer. *N. Engl. J. Med.* **359**, 1757–1765 (2008).
15. Douillard, J.-Y. *et al.* Panitumumab-FOLFOX4 treatment and RAS mutations in colorectal cancer. *N. Engl. J. Med.* **369**, 1023–34 (2013).
16. Van Cutsem, E. *et al.* Fluorouracil, leucovorin, and irinotecan plus cetuximab treatment and RAS mutations in colorectal cancer. *J. Clin. Oncol.* **33**, 692–700 (2015).
17. Peeters, M. *et al.* Massively parallel tumor multigene sequencing to evaluate response to panitumumab in a randomized phase III study of metastatic colorectal cancer. *Clin. Cancer Res.* **19**, 1902–1912 (2013).
18. Yaeger, R. *et al.* Clinical Sequencing Defines the Genomic Landscape of Metastatic Colorectal Cancer cancers Article Clinical Sequencing Defines the Genomic Landscape of Metastatic Colorectal Cancer. *Cancer Cell* **33**, 125-136.e3 (2018).
19. Montagut, C. *et al.* Identification of a mutation in the extracellular domain of the Epidermal Growth Factor Receptor conferring cetuximab resistance in colorectal cancer. *Nat. Med.* **18**, 221–223 (2012).
20. Sato, T. *et al.* Long-term expansion of epithelial organoids from human colon, adenoma, adenocarcinoma, and Barrett's epithelium. *Gastroenterology* **141**, 1762–72 (2011).
21. van de Wetering, M. *et al.* Prospective Derivation of a Living Organoid Biobank of Colorectal Cancer Patients. *Cell* **161**, 933–945 (2015).
22. Fujii, M. *et al.* A Colorectal Tumor Organoid Library Demonstrates Progressive Loss of Niche Factor Requirements during Tumorigenesis. *Cell Stem Cell* **18**, 827–838 (2016).
23. CAW, G. *et al.* Unbiased Combinatorial Screening Identifies a Bispecific IgG1 That

Potently Inhibits HER3 Signaling via HER2-Guided Ligand Blockade. *Cancer Cell* **33**, (2018).
24. N, S. *et al.* A Living Biobank of Breast Cancer Organoids Captures Disease Heterogeneity. *Cell* **172**, (2018).
25. SF, B. *et al.* Organoid Models of Human and Mouse Ductal Pancreatic Cancer. *Cell* **160**, (2015).
26. Alexandrov, L. B. *et al.* Signatures of mutational processes in human cancer. *Nature* **500**, 415–21 (2013).
27. S, S. *et al.* Recurrent R-spondin Fusions in Colon Cancer. *Nature* **488**, (2012).
28. Giannakis, M. *et al.* RNF43 is frequently mutated in colorectal and endometrial cancers. *Nat. Genet.* **46**, 1264–1266 (2014).
29. G, P. *et al.* Loss of AXIN1 Drives Acquired Resistance to WNT Pathway Blockade in Colorectal Cancer Cells Carrying RSPO3 Fusions. *EMBO Mol. Med.* **9**, (2017).
30. De Nardis, C. *et al.* A new approach for generating bispecific antibodies based on a common light chain format and the stable architecture of human immunoglobulin G1. *J. Biol. Chem.* **292**, 14706–14717 (2017).
31. Davidson, E. & Doranz, B. J. A high-throughput shotgun mutagenesis approach to mapping B-cell antibody epitopes. *Immunology* **143**, 13–20 (2014).
32. Koefoed, K. *et al.* Rational identification of an optimal antibody mixture for targeting the epidermal growth factor receptor. *MAbs* **3**, 584–95 (2011).
33. Gulli, L. F., Palmer, K. C., Chen, Y. Q. & Reddy, K. B. Epidermal growth factor-induced apoptosis in A431 cells can be reversed by reducing the tyrosine kinase activity. *Cell Growth Differ.* **7**, 173–8 (1996).
34. De Lau, W. *et al.* Lgr5 homologues associate with Wnt receptors and mediate R-spondin signalling. *Nature* **476**, 293–297 (2011).
35. Dalerba, P. *et al.* Single-cell dissection of transcriptional heterogeneity in human colon tumors. *Nat. Biotechnol.* **29**, 1120–7 (2011).
36. Sato, T. *et al.* Single Lgr5 stem cells build crypt-villus structures in vitro without a mesenchymal niche. *Nature* **459**, 262–265 (2009).
37. Vermeulen, L. *et al.* Wnt activity defines colon cancer stem cells and is regulated by the microenvironment. *Nat Cell Biol* **12**, 468–476 (2010).
38. Todaro, M. *et al.* CD44v6 is a marker of constitutive and reprogrammed cancer stem cells driving colon cancer metastasis. *Cell Stem Cell* **14**, 342–56 (2014).
39. Jung, P. *et al.* Isolation and in vitro expansion of human colonic stem cells. *Nat. Med.* 1225–1227 (2011) doi:10.1038/nm.2470.
40. RD, H., S, S., MJ, S., G, D. & H, P. Management of Adverse Events During Treatment of Gastrointestinal Cancers With Epidermal Growth Factor Inhibitors. *Crit. Rev. Oncol. Hematol.* **114**, (2017).
41. Lupo, B. *et al.* Colorectal cancer residual disease at maximal response to EGFR blockade displays a druggable Paneth cell–like phenotype. *Sci. Transl. Med.* **12**, (2020).
42. He, T. C. *et al.* Identification of c-MYC as a target of the APC pathway. *Science (80-.).* **281**, 1509–1512 (1998).
43. van de Wetering, M. *et al.* The beta-catenin/TCF-4 complex imposes a crypt progenitor phenotype on colorectal cancer cells. *Cell* **111**, 241–250 (2002).
44. Sansom, O. J. *et al.* Myc deletion rescues Apc deficiency in the small intestine. *Nature* **446**, 676–679 (2007).
45. Snyder, J. C., Rochelle, L. K., Lyerly, H. K., Caron, M. G. & Barak, L. S. Constitutive internalization of the leucine-rich G protein-coupled receptor-5 (LGR5) to the trans-Golgi network. *J. Biol. Chem.* **288**, 10286–97 (2013).
46. Vlachogiannis, G. *et al.* Patient-derived organoids model treatment response of metastatic gastrointestinal cancers. *Science* **359**, 920–926 (2018).
47. Y, Y. *et al.* Patient-Derived Organoids Predict Chemoradiation Responses of Locally Advanced Rectal Cancer. *Cell Stem Cell* **26**, (2020).
48. Ganesh, K. *et al.* A rectal cancer organoid platform to study individual responses to

chemoradiation. *Nat. Med.* **25**, 1607–1614 (2019).
49. Ooft, S. N. *et al.* Patient-derived organoids can predict response to chemotherapy in metastatic colorectal cancer patients. *Sci. Transl. Med.* **11**, (2019).
50. Yan, Q. *et al.* Association between the overexpression of Her3 and clinical pathology and prognosis of colorectal cancer: A meta-analysis. *Medicine (United States)* vol. 97 (2018).
51. Lédel, F., Hallström, M., Ragnhammar, P., Öhrling, K. & Edler, D. HER3 expression in patients with primary colorectal cancer and corresponding lymph node metastases related to clinical outcome. *Eur. J. Cancer* **50**, 656–662 (2014).
52. Drost, J. & Clevers, H. Organoids in cancer research. *Nat. Rev. Cancer* **18**, 407–418 (2018).
53. Vermorken, J. B. *et al.* Platinum-based chemotherapy plus cetuximab in head and neck cancer. *N. Engl. J. Med.* **359**, 1116–1127 (2008).
54. Woolston, A. *et al.* Genomic and Transcriptomic Determinants of Therapy Resistance and Immune Landscape Evolution during Anti-EGFR Treatment in Colorectal Cancer. *Cancer Cell* **36**, 35-50.e9 (2019).
55. Misale, S. *et al.* Emergence of KRAS mutations and acquired resistance to anti-EGFR therapy in colorectal cancer. *Nature* **486**, 532–6 (2012).
56. Hobor, S. *et al.* TGFα and amphiregulin paracrine network promotes resistance to EGFR blockade in colorectal cancer cells. *Clin. Cancer Res.* **20**, 6429–38 (2014).
57. Dienstmann, R. *et al.* Safety and Activity of the First-in-Class Sym004 Anti-EGFR Antibody Mixture in Patients with Refractory Colorectal Cancer. *Cancer Discov.* **5**, 598–609 (2015).
58. Kearns, J. D. *et al.* Enhanced Targeting of the EGFR Network with MM-151, an Oligoclonal Anti-EGFR Antibody Therapeutic. *Mol. Cancer Ther.* **14**, 1625–36 (2015).
59. Spangler, J. B. *et al.* Combination antibody treatment down-regulates epidermal growth factor receptor by inhibiting endosomal recycling. *Proc. Natl. Acad. Sci. U. S. A.* **107**, 13252–7 (2010).
60. Malliri, A. *et al.* The rac activator Tiam1 is a Wnt-responsive gene that modifies intestinal tumor development. *J. Biol. Chem.* **281**, 543–8 (2006).
61. Baker, A.-M., Graham, T. A., Elia, G., Wright, N. A. & Rodriguez-Justo, M. Characterization of LGR5 stem cells in colorectal adenomas and carcinomas. *Sci. Rep.* **5**, 8654 (2015).
62. Uchida, H. *et al.* Overexpression of leucine-rich repeat-containing G protein-coupled receptor 5 in colorectal cancer. *Cancer Sci.* **101**, 1731–1737 (2010).
63. Muñoz, J. *et al.* The Lgr5 intestinal stem cell signature: robust expression of proposed quiescent '+4' cell markers. *EMBO J.* **31**, 3079–91 (2012).
64. Cochran, J. R., Kim, Y.-S., Olsen, M. J., Bhandari, R. & Wittrup, K. D. Domain-level antibody epitope mapping through yeast surface display of epidermal growth factor receptor fragments. *J. Immunol. Methods* **287**, 147–58 (2004).
65. van Uhm, J. I. *et al.* The ultimate radiochemical nightmare: upon radio-iodination of Botulinum neurotoxin A, the introduced iodine atom itself seems to be fatal for the bioactivity of this macromolecule. *EJNMMI Res.* **5**, 5 (2015).
66. Lindmo, T., Boven, E., Cuttitta, F., Fedorko, J. & Bunn, P. A. Determination of the immunoreactive fraction of radiolabeled monoclonal antibodies by linear extrapolation to binding at infinite antigen excess. *J. Immunol. Methods* **72**, 77–89 (1984).
67. Raine, K. M. *et al.* cgpPindel: Identifying Somatically Acquired Insertion and Deletion Events from Paired End Sequencing. *Curr. Protoc. Bioinforma.* **52**, 15.7.1-15.7.12 (2015).
68. Z, D. *et al.* Ultra high content image analysis and phenotype profiling of 3D cultured micro-tissues. *PLoS One* **9**, e109688–e109688 (2014).
69. AM, S. *et al.* Identification of Anti-Tumour Biologics Using Primary Tumour Models, 3-D Phenotypic Screening and Image-Based Multi-Parametric Profiling. *Mol. Cancer* **14**, (2015).
70. Birmingham, A. *et al.* Statistical methods for analysis of high-throughput RNA

interference screens. *Nature Methods* vol. 6 569–575 (2009).
71. Gonzalez-Roca, E. *et al.* Accurate expression profiling of very small cell populations. *PLoS One* **5**, e14418 (2010).
72. Morral, C. *et al.* Zonation of Ribosomal DNA Transcription Defines a Stem Cell Hierarchy in Colorectal Cancer. *Cell Stem Cell* **26**, 845-861.e12 (2020).
73. Rashidi, B. *et al.* An orthotopic mouse model of remetastasis of human colon cancer liver metastasis. *Clin. Cancer Res.* **6**, 2556–61 (2000).

Figure 1

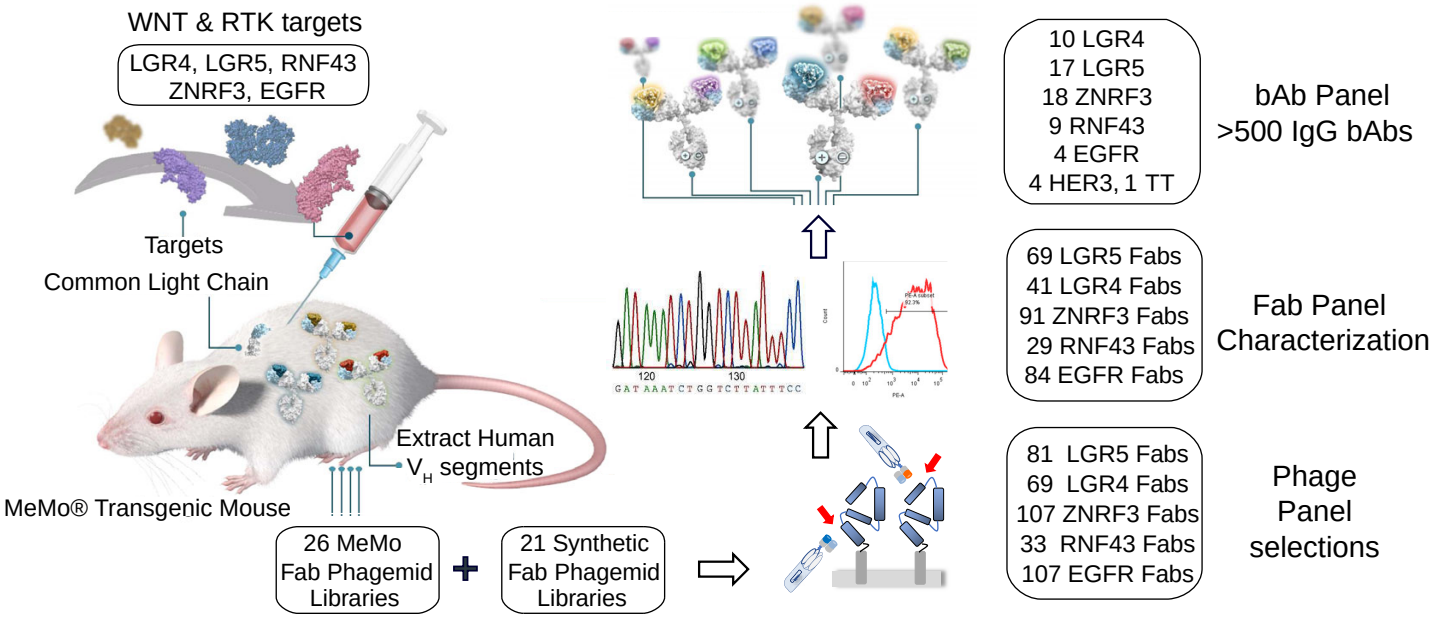
WNT & RTK targets
LGR4, LGR5, RNF43
ZNRF3, EGFR
Targets
Common Light Chain
Extract Human
V_H segments
MeMo® Transgenic Mouse
26 MeMo
Fab Phagemid
Libraries
21 Synthetic
Fab Phagemid
Libraries
10 LGR4
17 LGR5
18 ZNRF3
9 RNF43
4 EGFR
4 HER3, 1 TT
bAb Panel
>500 IgG bAbs
69 LGR5 Fabs
41 LGR4 Fabs
91 ZNRF3 Fabs
29 RNF43 Fabs
84 EGFR Fabs
Fab Panel
Characterization
81 LGR5 Fabs
69 LGR4 Fabs
107 ZNRF3 Fabs
33 RNF43 Fabs
107 EGFR Fabs
Phage
Panel
selections

Figure 2

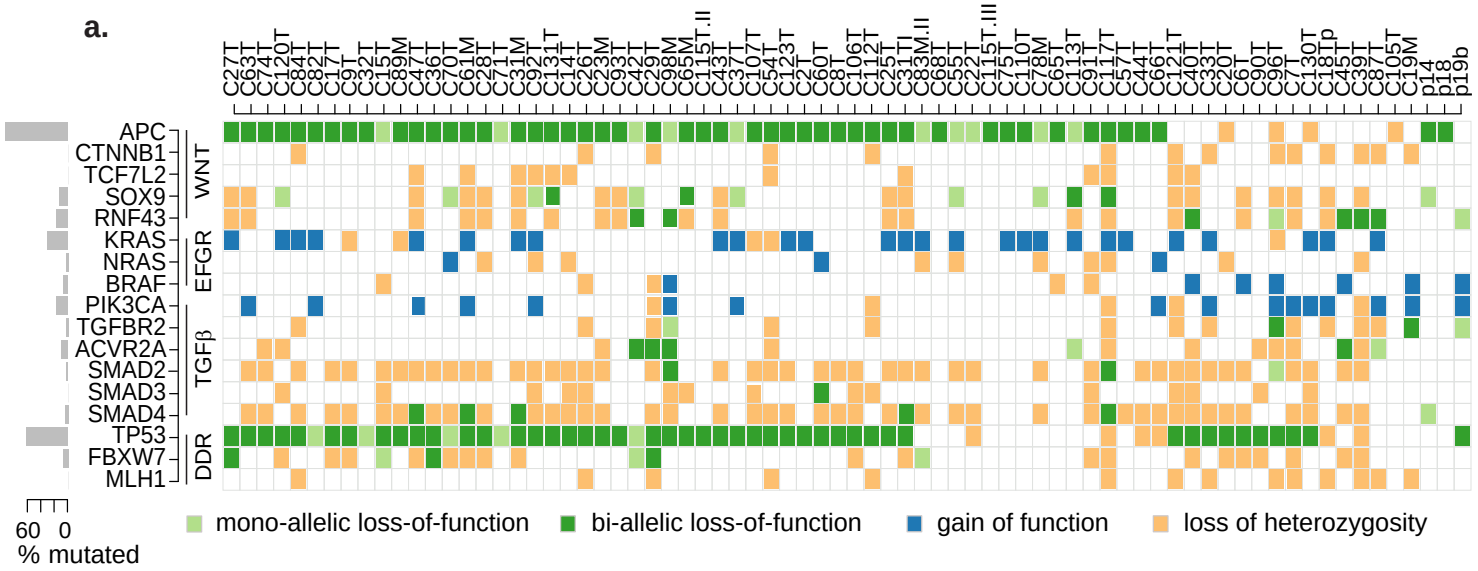
a.
C27T C63T C74T C120T C84T C82T C17T C9T C32T C15T C89M C47T C36T C70T C61M C28T C71T C31M C92T C131T C14T C26T C23M C93T C42T C29T C98M C65M C115T.II C43T C37T C107T C54T C123T C2T C20T C8T C106T C112T C25T C31T.I C83M.II C68T C55T C22T C225T.III C75T C110T C78M C65T.I C91T C113T C117T C57T C44T C66T C121T C40T C33T C20T C6T C90T C96T C7T C130T C18Tp C45T C39T C87T C105T C19M p14 p18 p19b
APC
CTNNB1
TCF7L2
SOX9
RNF43
KRAS
NRAS
BRAF
PIK3CA
TGFBR2
ACVR2A
SMAD2
SMAD3
SMAD4
TP53
FBXW7
MLH1
WNT
EFGR
TGFβ
DDR
60 0
% mutated
mono-allelic loss-of-function
bi-allelic loss-of-function
gain of function
loss of heterozygosity

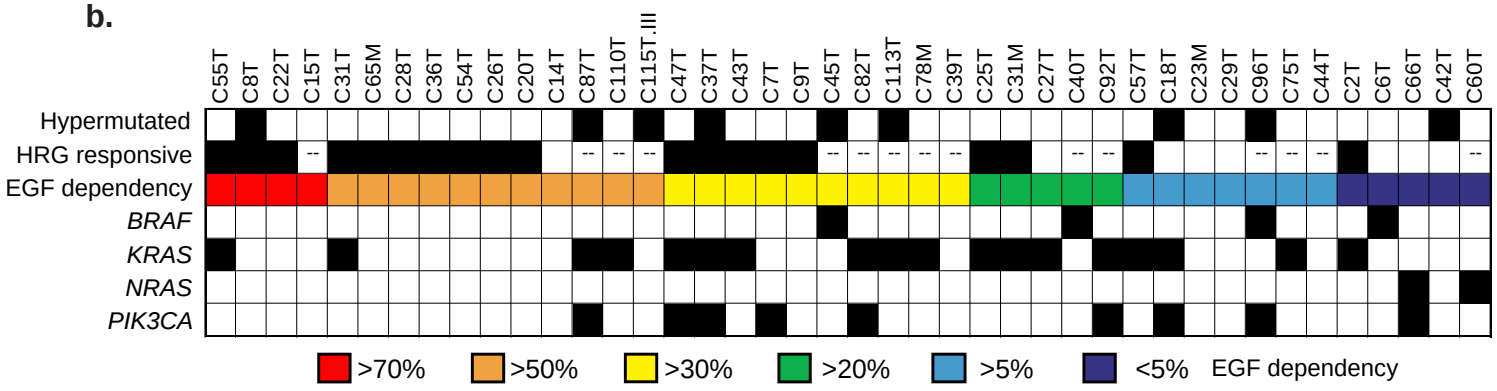
b.
C55T C8T C22T C15T C31T C65M C28T C36T C54T C26T C20T C14T C87T C110T C115T.III C47T C37T C43T C7T C9T C45T C82T C113T C78M C39T C25T C31M C27T C40T C92T C57T C18T C23M C29T C96T C75T C44T C2T C6T C66T C42T C60T
Hypermutated
HRG responsive
EGF dependency
BRAF
KRAS
NRAS
PIK3CA
>70%
>50%
>30%
>20%
>5%
<5%
EGF dependency

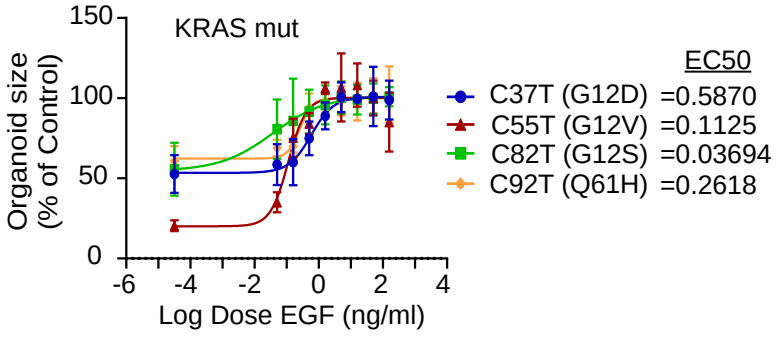
c.
KRAS mut
Organoid size (% of Control)
Log Dose EGF (ng/ml)
EC50
C37T (G12D) =0.5870
C55T (G12V) =0.1125
C82T (G12S) =0.03694
C92T (Q61H) =0.2618

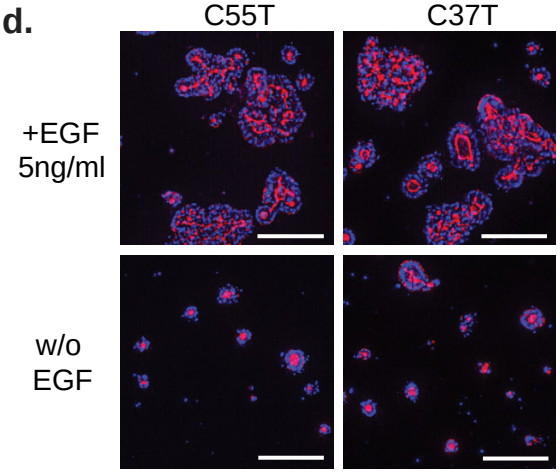
d.
C55T
C37T
+EGF 5ng/ml
w/o EGF

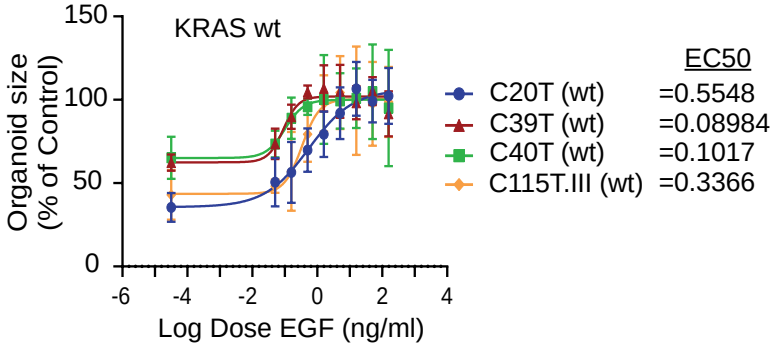
e.
KRAS wt
Organoid size (% of Control)
Log Dose EGF (ng/ml)
EC50
C20T (wt) =0.5548
C39T (wt) =0.08984
C40T (wt) =0.1017
C115T.III (wt) =0.3366

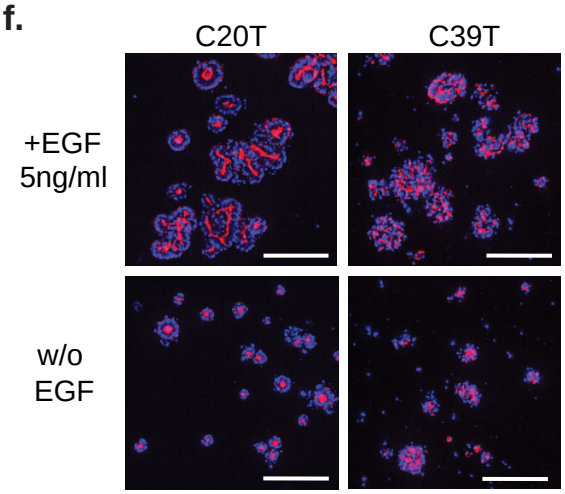
f.
C20T
C39T
+EGF 5ng/ml
w/o EGF

Figure 3

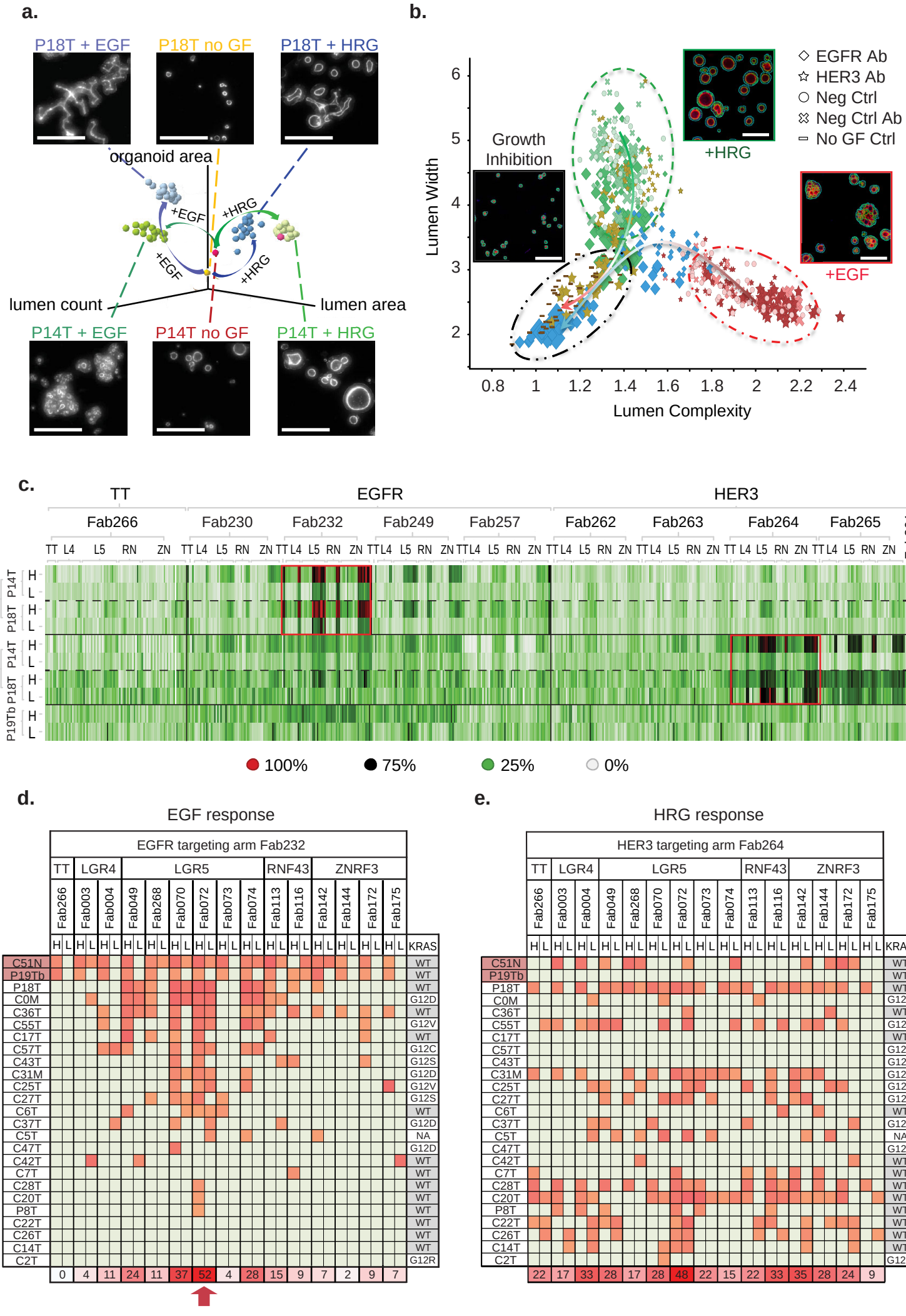
a.
P18T + EGF
P18T no GF
P18T + HRG
organoid area
+EGF
+HRG
+EGF
+HRG
lumen count
lumen area
P14T + EGF
P14T no GF
P14T + HRG
b.
EGFR Ab
HER3 Ab
Neg Ctrl
Neg Ctrl Ab
No GF Ctrl
Growth Inhibition
+HRG
+EGF
Lumen Width
Lumen Complexity
c.
TT
EGFR
HER3
Fab266
Fab230
Fab232
Fab249
Fab257
Fab262
Fab263
Fab264
Fab265
Fab264
EGF
HRG
WNT3a
P14T
P18T
P19Tb
100%
75%
25%
0%
d.
EGF response
EGFR targeting arm Fab232
TT
LGR4
LGR5
RNF43
ZNRF3
KRAS
24 CRC patient organoids
e.
HRG response
HER3 targeting arm Fab264

Figure 4

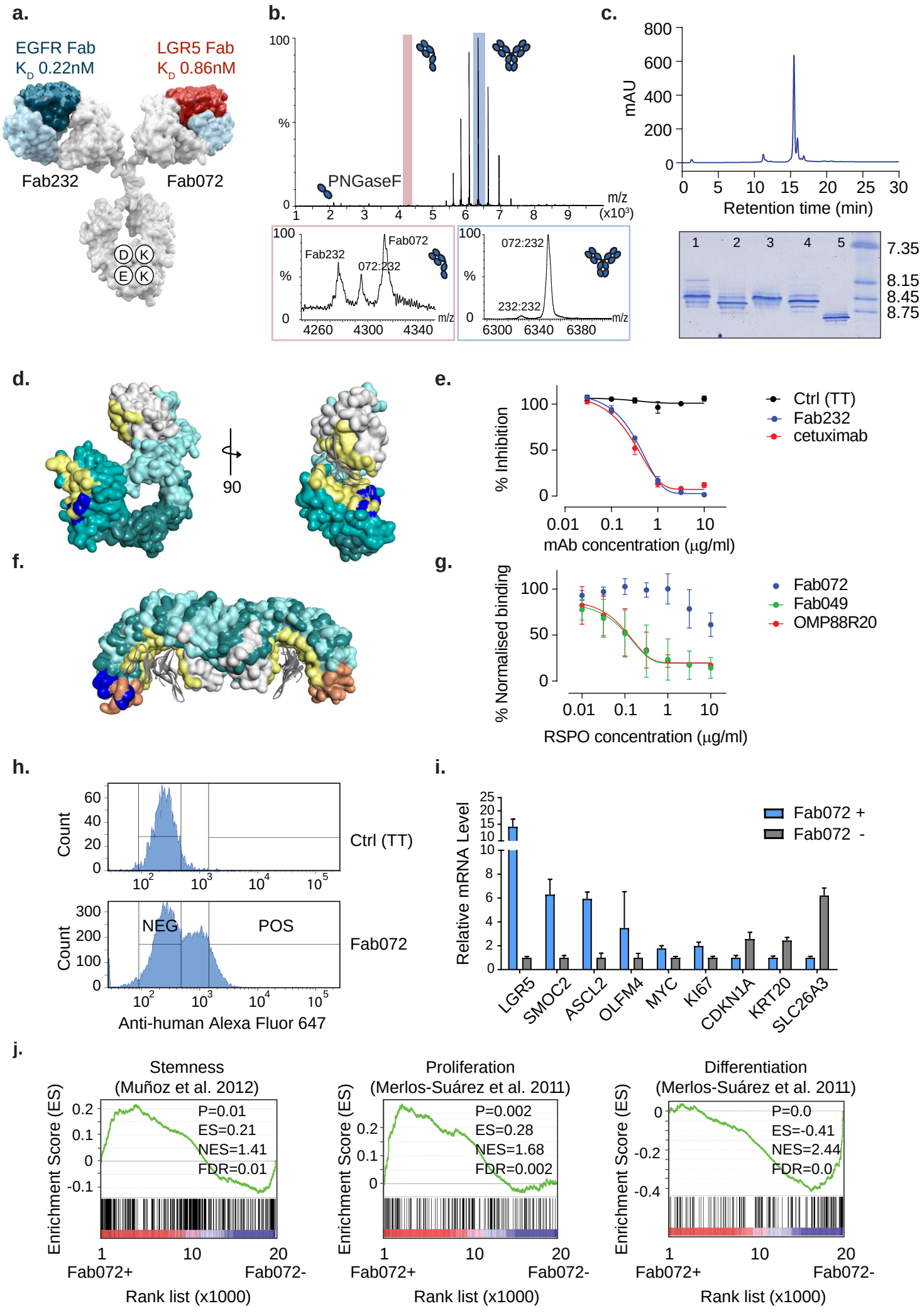
a.
EGFR Fab
K_D 0.22nM
LGR5 Fab
K_D 0.86nM
Fab232
Fab072
D K
E K
b.
PNGaseF
m/z
(x10³)
Fab232
Fab072
072:232
232:232
c.
mAU
Retention time (min)
1 2 3 4 5
7.35
8.15
8.45
8.75
d.
90
e.
% Inhibition
mAb concentration (μg/ml)
Ctrl (TT)
Fab232
cetuximab
f.
g.
% Normalised binding
RSPO concentration (μg/ml)
Fab072
Fab049
OMP88R20
h.
Count
Ctrl (TT)
NEG
POS
Fab072
Anti-human Alexa Fluor 647
i.
Relative mRNA Level
Fab072 +
Fab072 -
LGR5
SMOC2
ASCL2
OLFM4
MYC
KI67
CDKN1A
KRT20
SLC26A3
j.
Stemness
(Muñoz et al. 2012)
P=0.01
ES=0.21
NES=1.41
FDR=0.01
Proliferation
(Merlos-Suárez et al. 2011)
P=0.002
ES=0.28
NES=1.68
FDR=0.002
Differentiation
(Merlos-Suárez et al. 2011)
P=0.0
ES=-0.41
NES=2.44
FDR=0.0
Enrichment Score (ES)
Fab072+
Fab072-
Rank list (x1000)

Figure 5

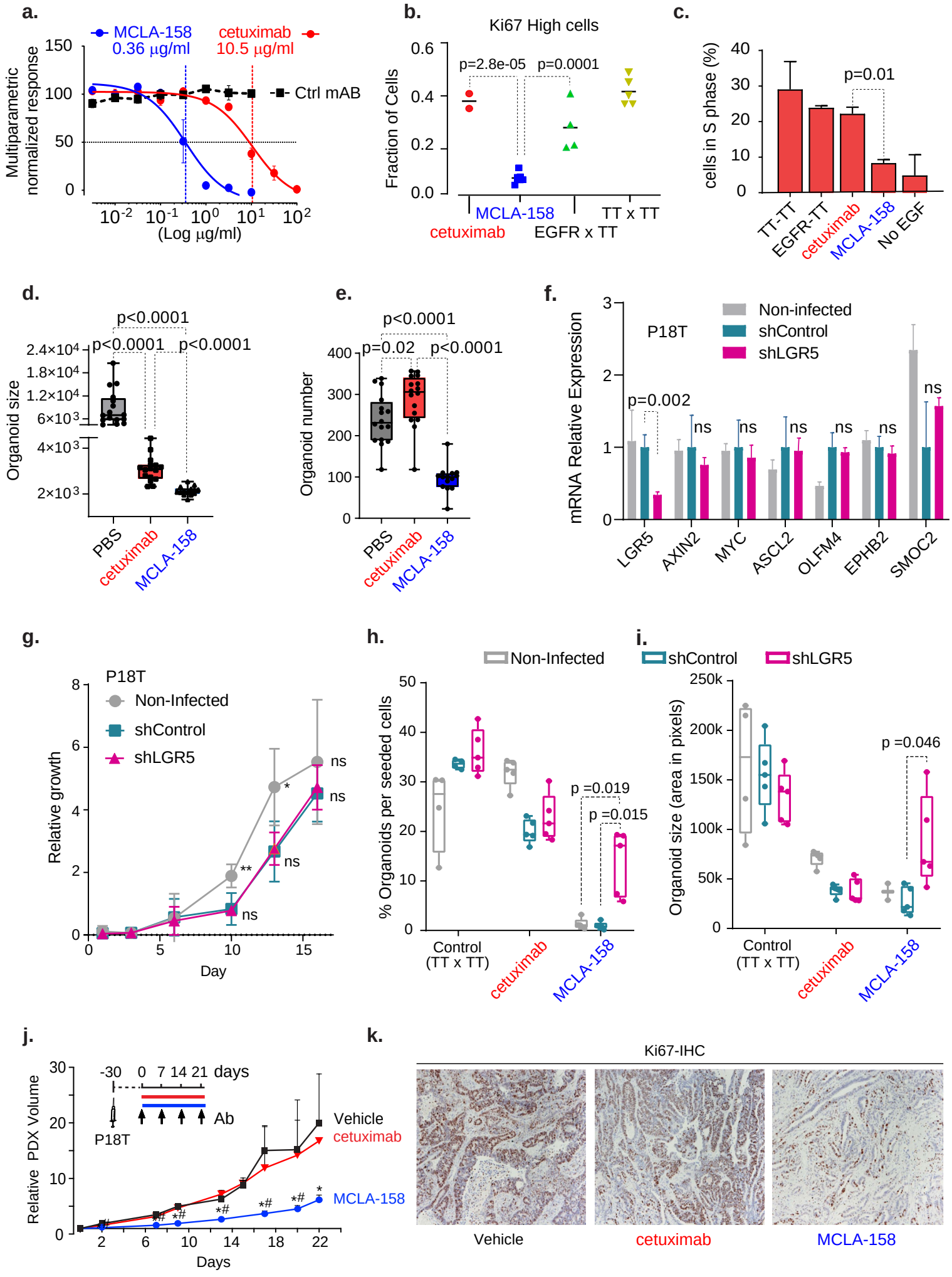
a.
MCLA-158 0.36 µg/ml
cetuximab 10.5 µg/ml
Ctrl mAB
Multiparametric normalized response
(Log µg/ml)
b.
Ki67 High cells
p=2.8e-05
p=0.0001
Fraction of Cells
MCLA-158
cetuximab
TT x TT
EGFR x TT
c.
cells in S phase (%)
p=0.01
TT-TT
EGFR-TT
cetuximab
MCLA-158
No EGF
d.
p<0.0001
p<0.0001
p<0.0001
Organoid size
PBS
cetuximab
MCLA-158
e.
p<0.0001
p=0.02
p<0.0001
Organoid number
PBS
cetuximab
MCLA-158
f.
P18T
Non-infected
shControl
shLGR5
mRNA Relative Expression
p=0.002
ns
LGR5
AXIN2
MYC
ASCL2
OLFM4
EPHB2
SMOC2
g.
P18T
Non-Infected
shControl
shLGR5
Relative growth
Day
h.
Non-Infected
shControl
shLGR5
% Organoids per seeded cells
p =0.019
p =0.015
Control (TT x TT)
cetuximab
MCLA-158
i.
shControl
shLGR5
Organoid size (area in pixels)
p =0.046
Control (TT x TT)
cetuximab
MCLA-158
j.
-30 0 7 14 21 days
P18T
Ab
Vehicle
cetuximab
MCLA-158
Relative PDX Volume
Days
k.
Ki67-IHC
Vehicle
cetuximab
MCLA-158

Figure 6

a.

Model	P18T	C0M	C17T	C55T	C27T	C31M	C25T	C28T	P19Tb	C20T	P14T	C8T	C26T	C6T	C22T	C14T	C7T	C2T	C42T	C37T	C5T
MCLA-158 % inhibition	95	89	80	81	77	72	64	61	58	56	54	49	47	47	33	33	31	10	<1	<1	<1
cetuximab % inhibition	57	65	39	41	<1	11	15	47	30	32	36	4	70	28	47	44	18	14	<1	<1	25
KRAS	WT	G12D	WT	G12V	G12S	G12D	G12V	WT	WT	WT	WT	WT	WT	WT	WT	WT	WT	G12R	WT	G12D	NA

b.

Name	Organoid type	Driver mutations	IC50 (μg/ml)	
			cetuximab	MCLA158
C7N	Normal	NA	>10	>10
C51N	Normal	NA	>10	>10
C71N	Normal	NA	1.37	3.09
C57N	Normal	NA	1.08	4.52
C55N	Normal	NA	>10	>10
C55T	Tumoroid	APC, KRAS (G12V)	>10	0.08
C57T	Tumoroid	APC, KRAS (G12C)	>10	1.25
C0M	Tumoroid	APC, KRAS(G12D)	>10	0.39
C1M	Tumoroid	NA	>10	0.25
C65M	Tumoroid	APC, TP53, SOX9	>10	0.99
P18T	Tumoroid	APC	5.17	0.25

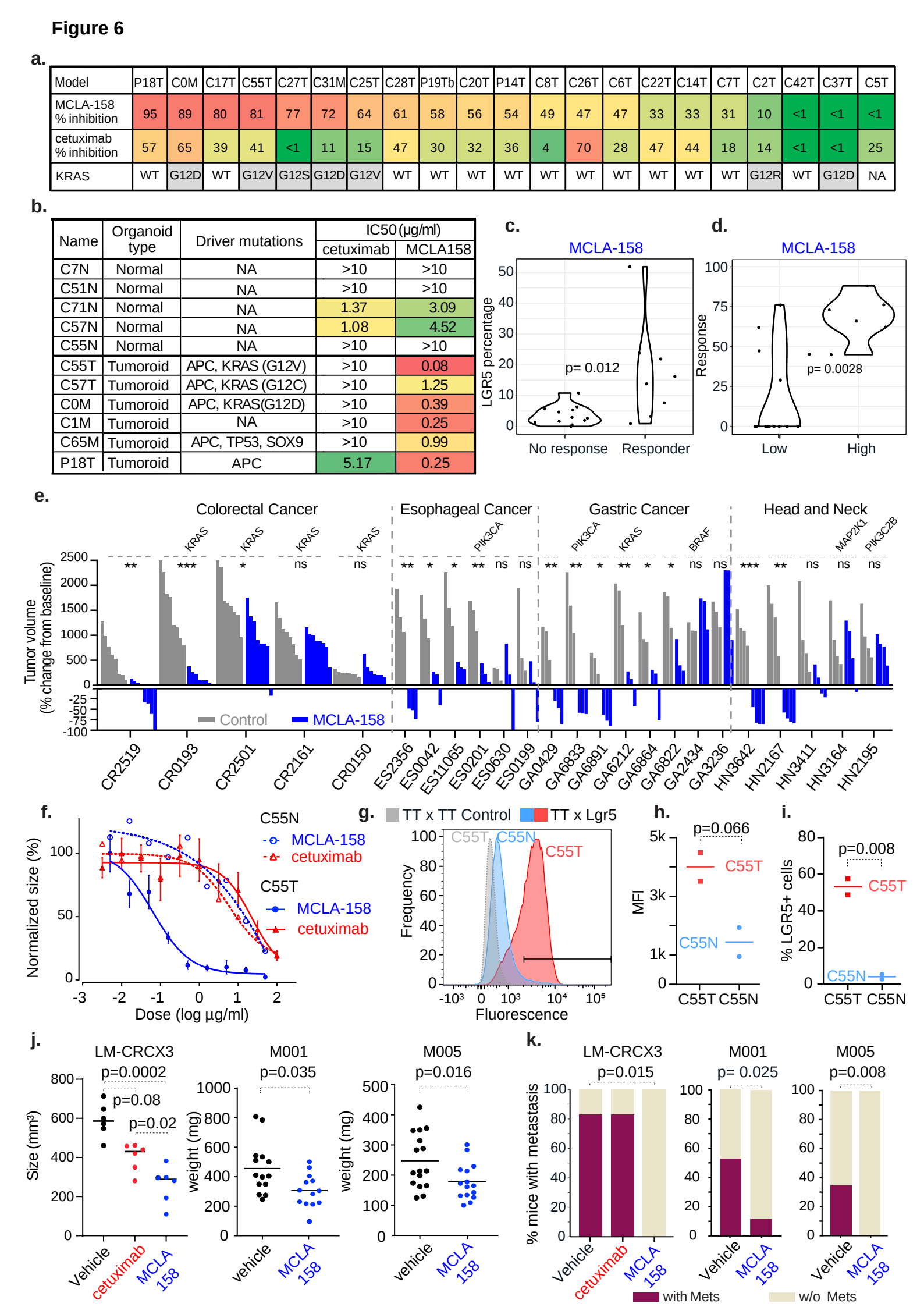

Figure 7

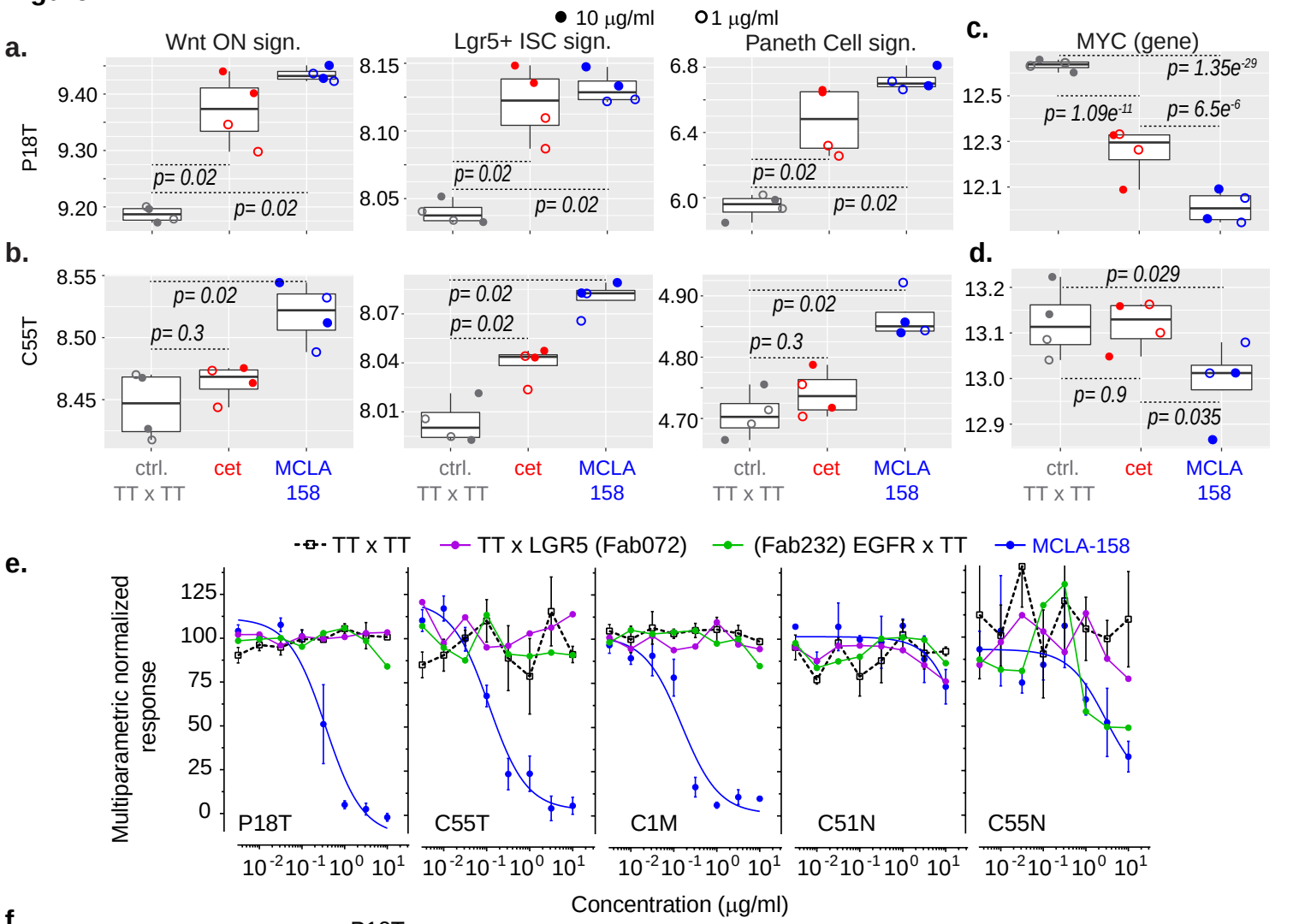
a.
b.
c.
d.
10 µg/ml
1 µg/ml
Wnt ON sign.
Lgr5+ ISC sign.
Paneth Cell sign.
MYC (gene)
P18T
C55T
p= 0.02
p= 0.3
p= 1.35e-29
p= 1.09e-11
p= 6.5e-6
p= 0.029
p= 0.9
p= 0.035
ctrl.
TT x TT
cet
MCLA 158

e.
TT x TT
TT x LGR5 (Fab072)
(Fab232) EGFR x TT
MCLA-158
Multiparametric normalized response
P18T
C55T
C1M
C51N
C55N
Concentration (µg/ml)

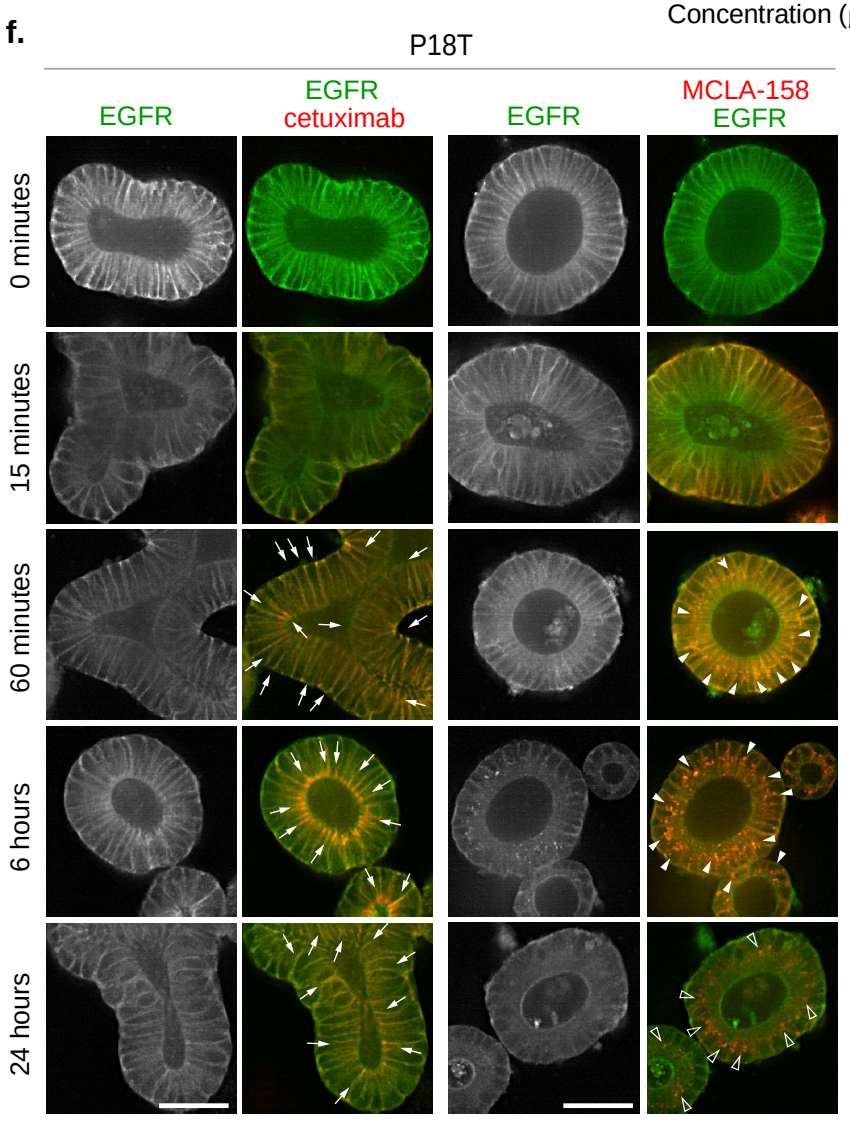
f.
P18T
EGFR
EGFR cetuximab
EGFR
MCLA-158 EGFR
0 minutes
15 minutes
60 minutes
6 hours
24 hours

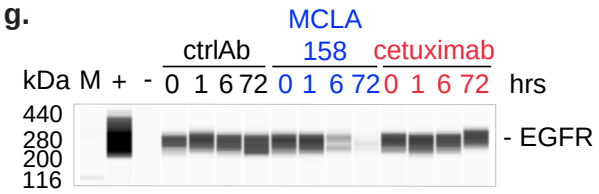
g.
MCLA
ctrlAb
158
cetuximab
kDa M + -
0 1 6 72 0 1 6 72 0 1 6 72 hrs
440
280
200
116
- EGFR

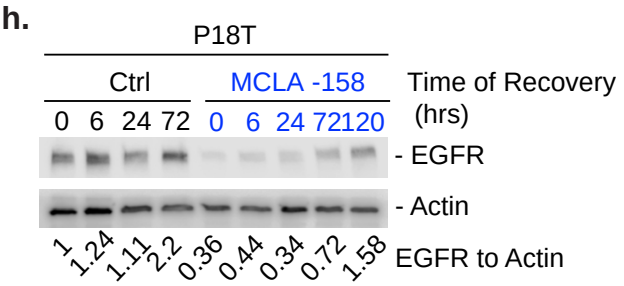
h.
P18T
Ctrl
MCLA -158
Time of Recovery (hrs)
0 6 24 72 0 6 24 72 120
- EGFR
- Actin
1 1.24 1.11 2.2 0.36 0.44 0.34 0.72 1.58
EGFR to Actin

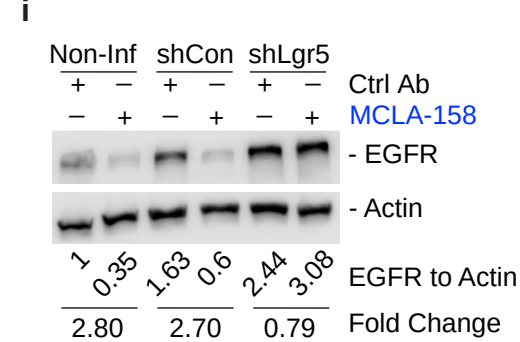
i
Non-Inf
shCon
shLgr5
Ctrl Ab
MCLA-158
- EGFR
- Actin
1 0.35 1.63 0.6 2.44 3.08
EGFR to Actin
2.80 2.70 0.79
Fold Change

Extended Data Figure 1

a.

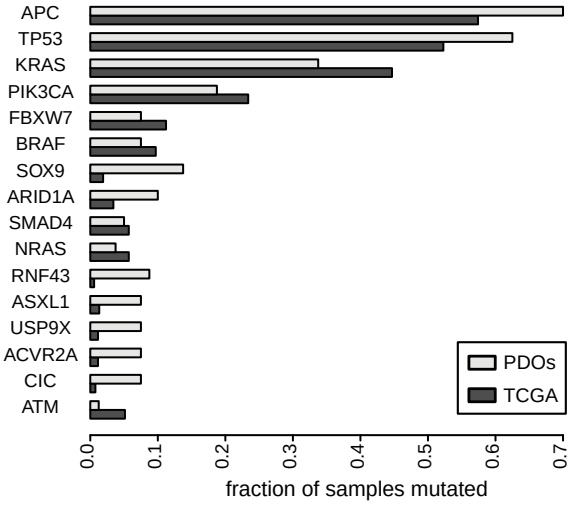

b.

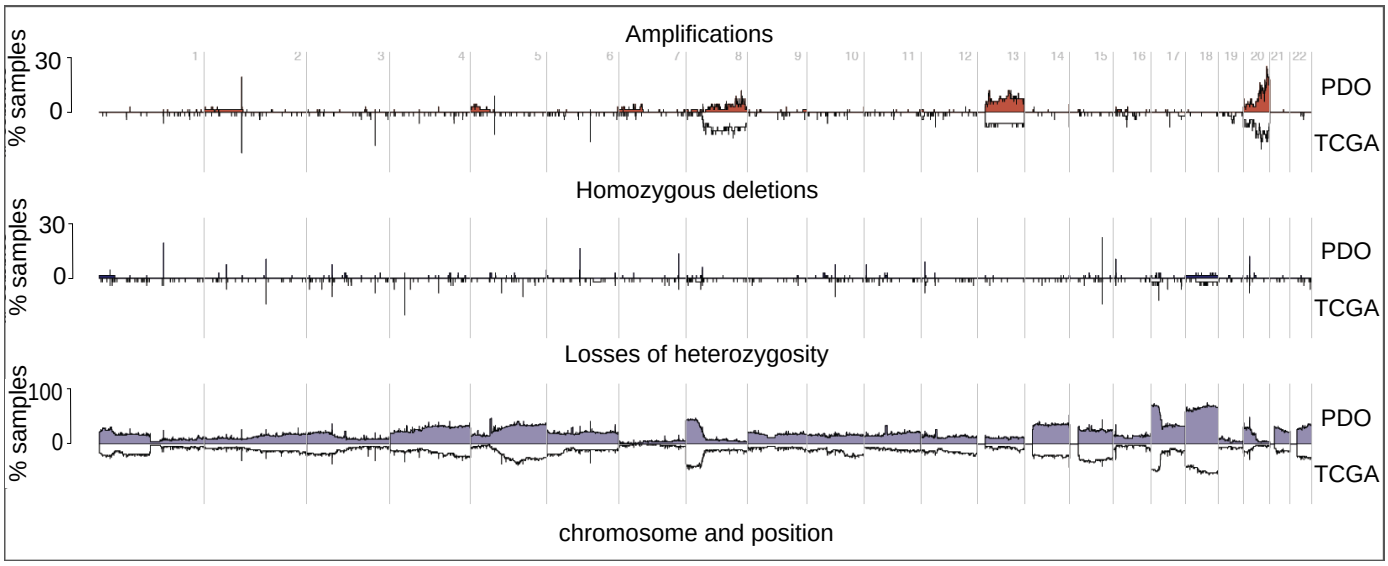

c.

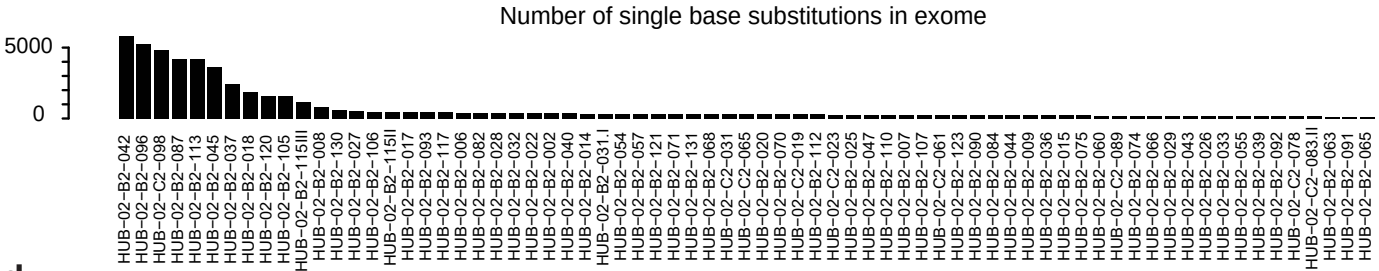

d.

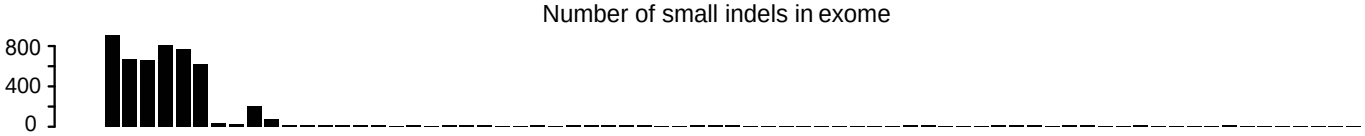

e.

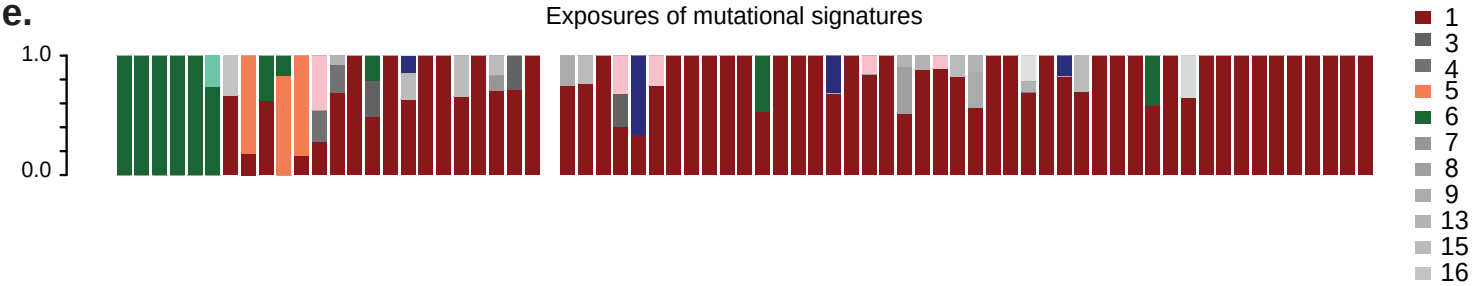

Extended Data Figure 2

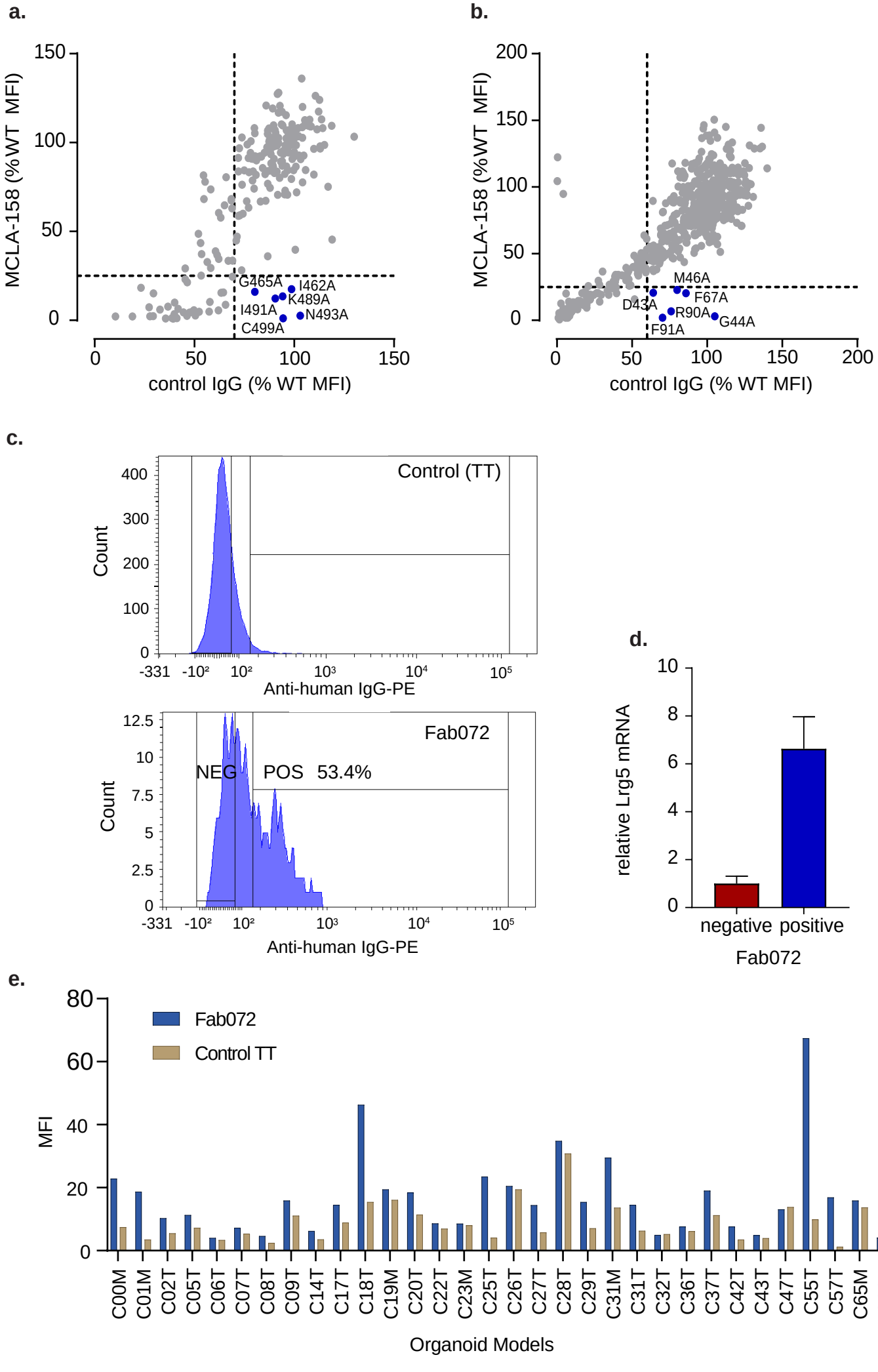

Extended Data Figure 3

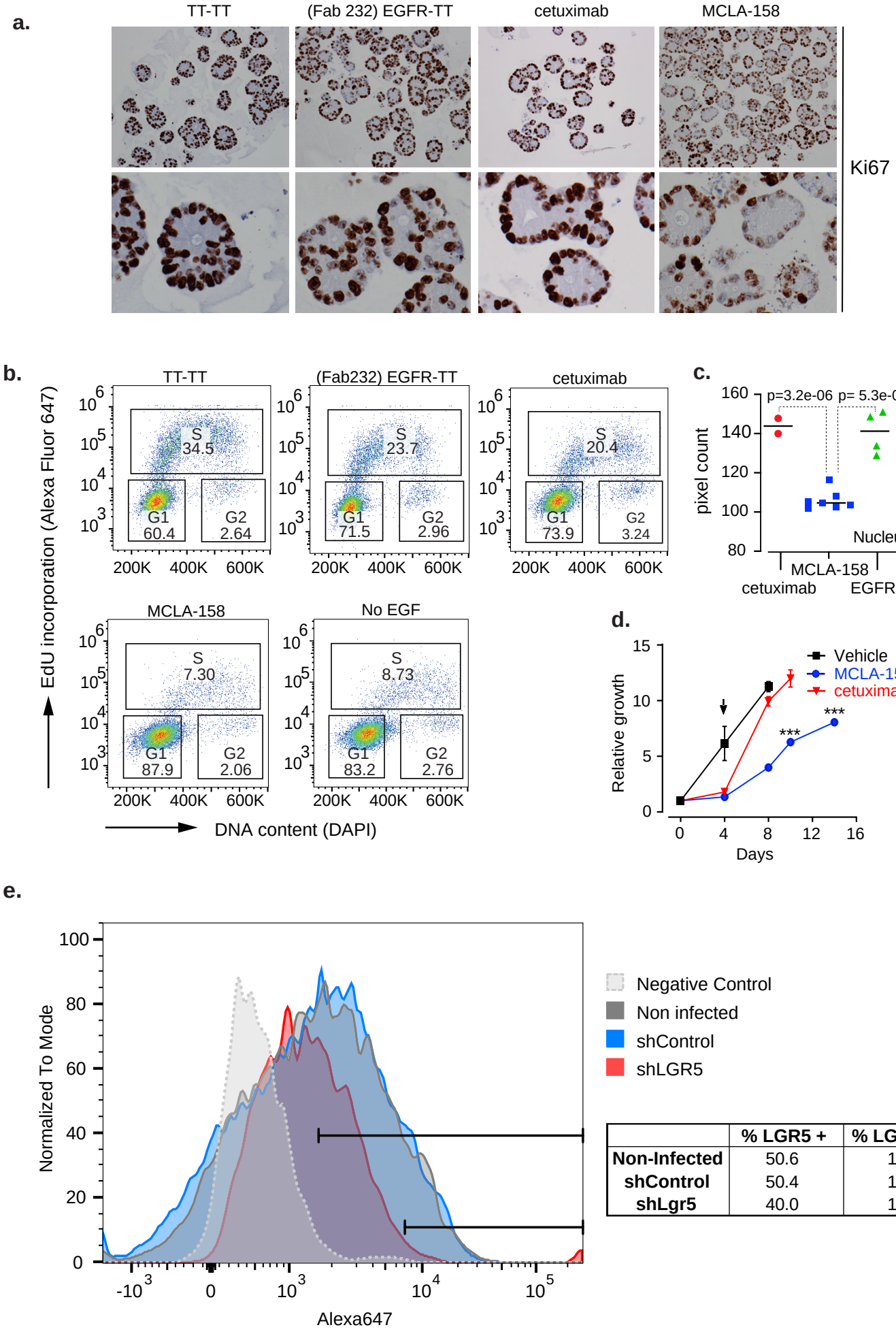

	% LGR5 +	% LGR5 High
Non-Infected	50.6	10.2
shControl	50.4	10.1
shLgr5	40.0	1.97

Extended Data Figure 4

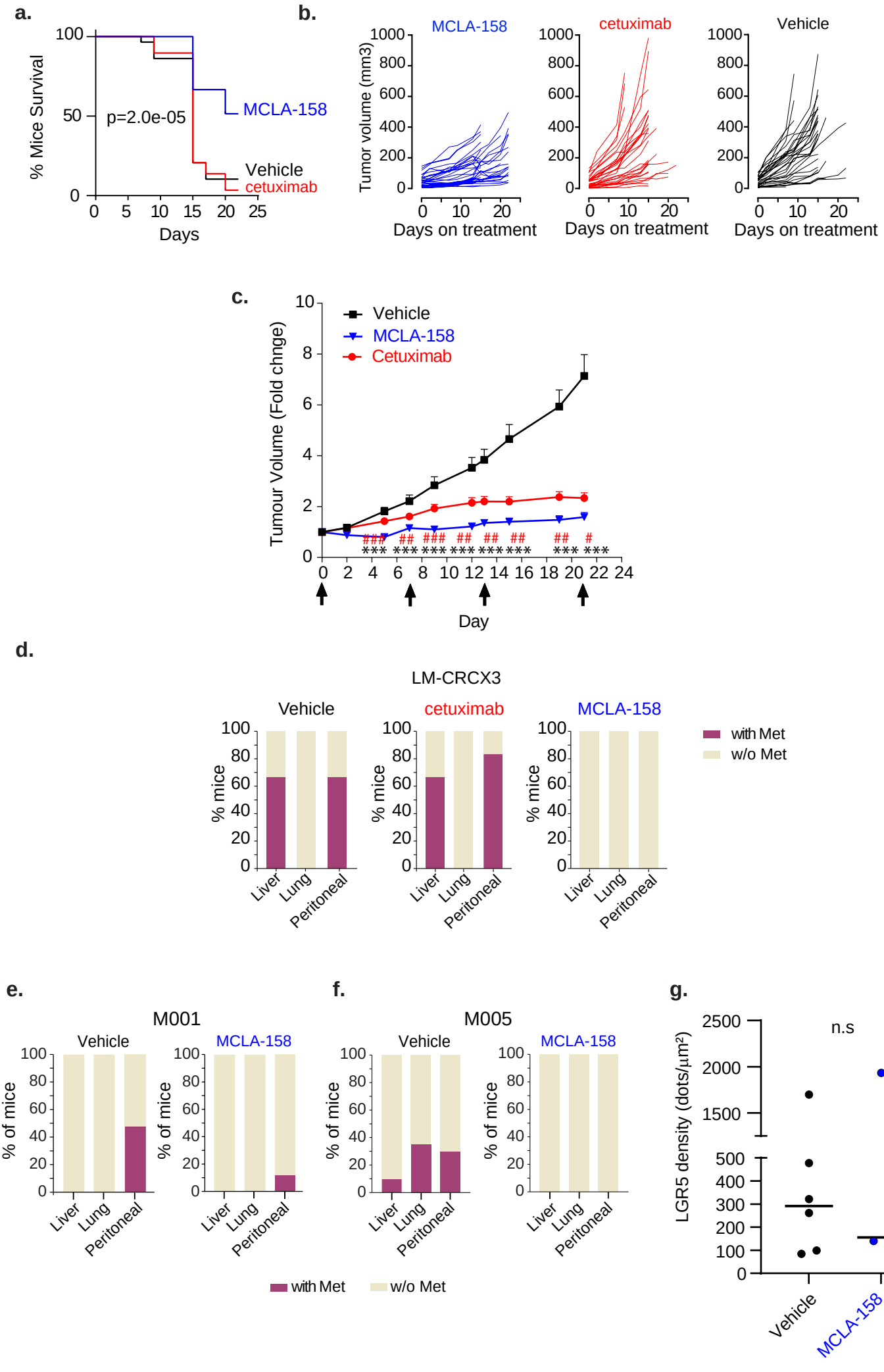

Extended Data Figure 5

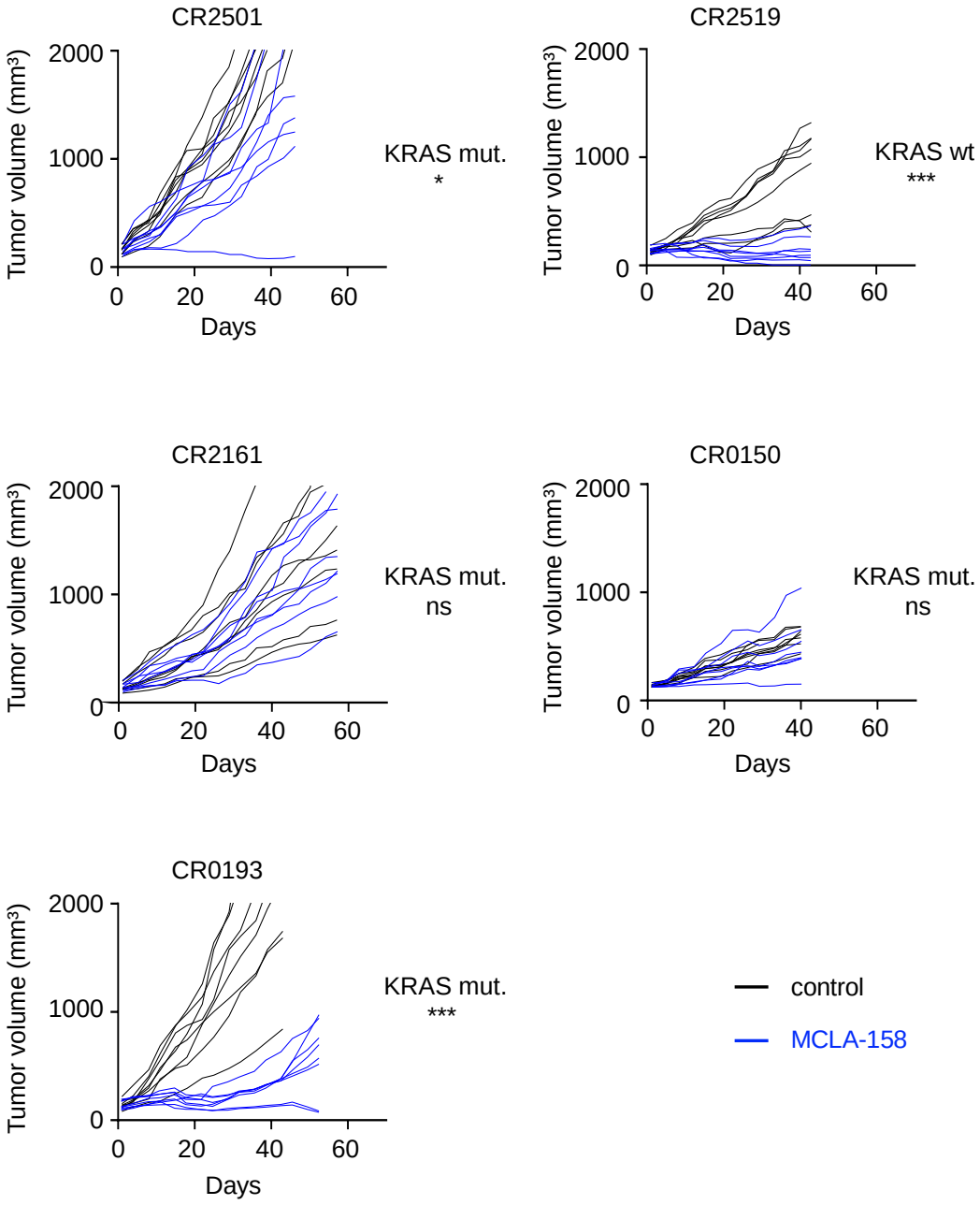

Extended Data Figure 6

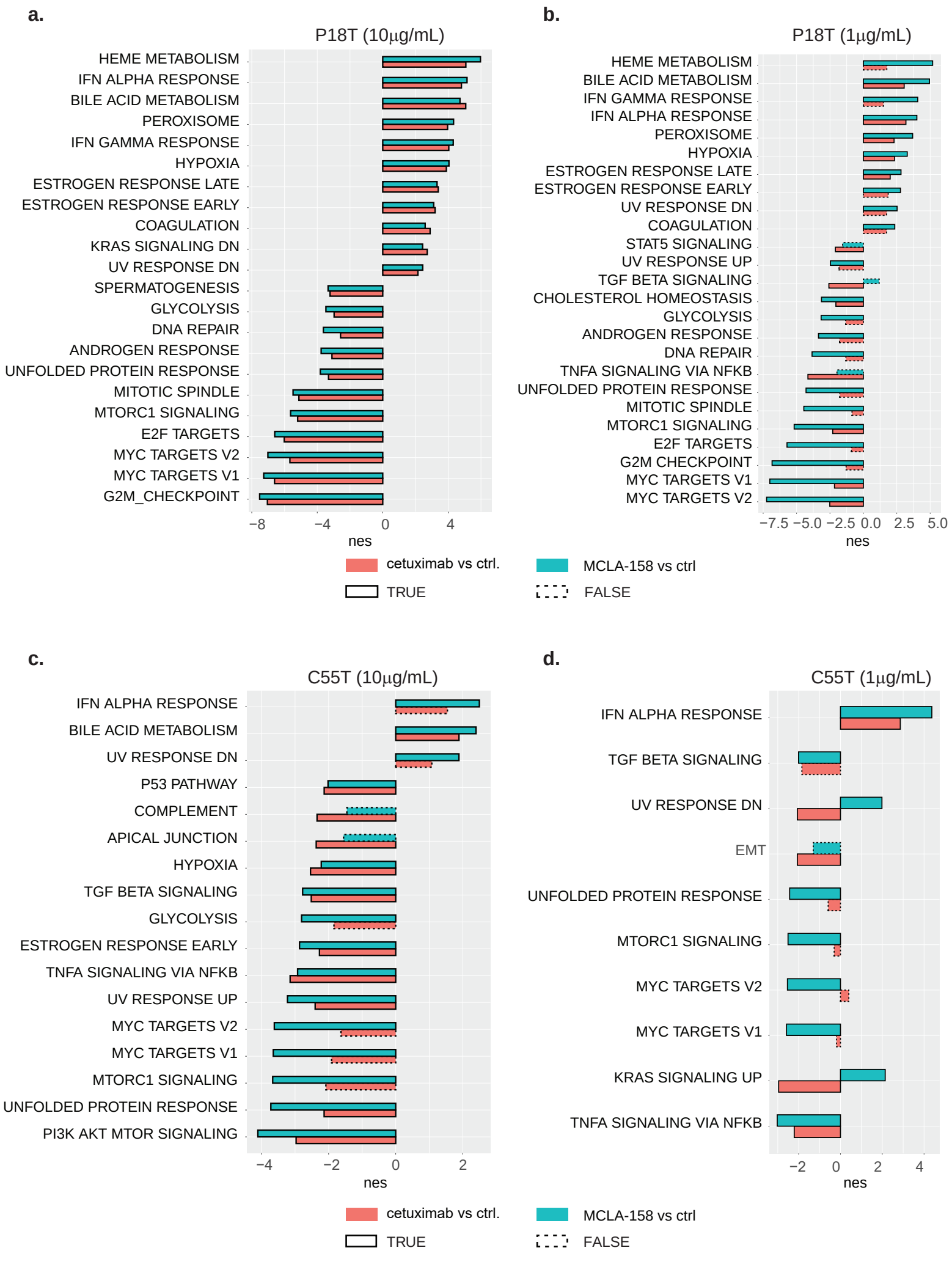

Extended Data Figure 7

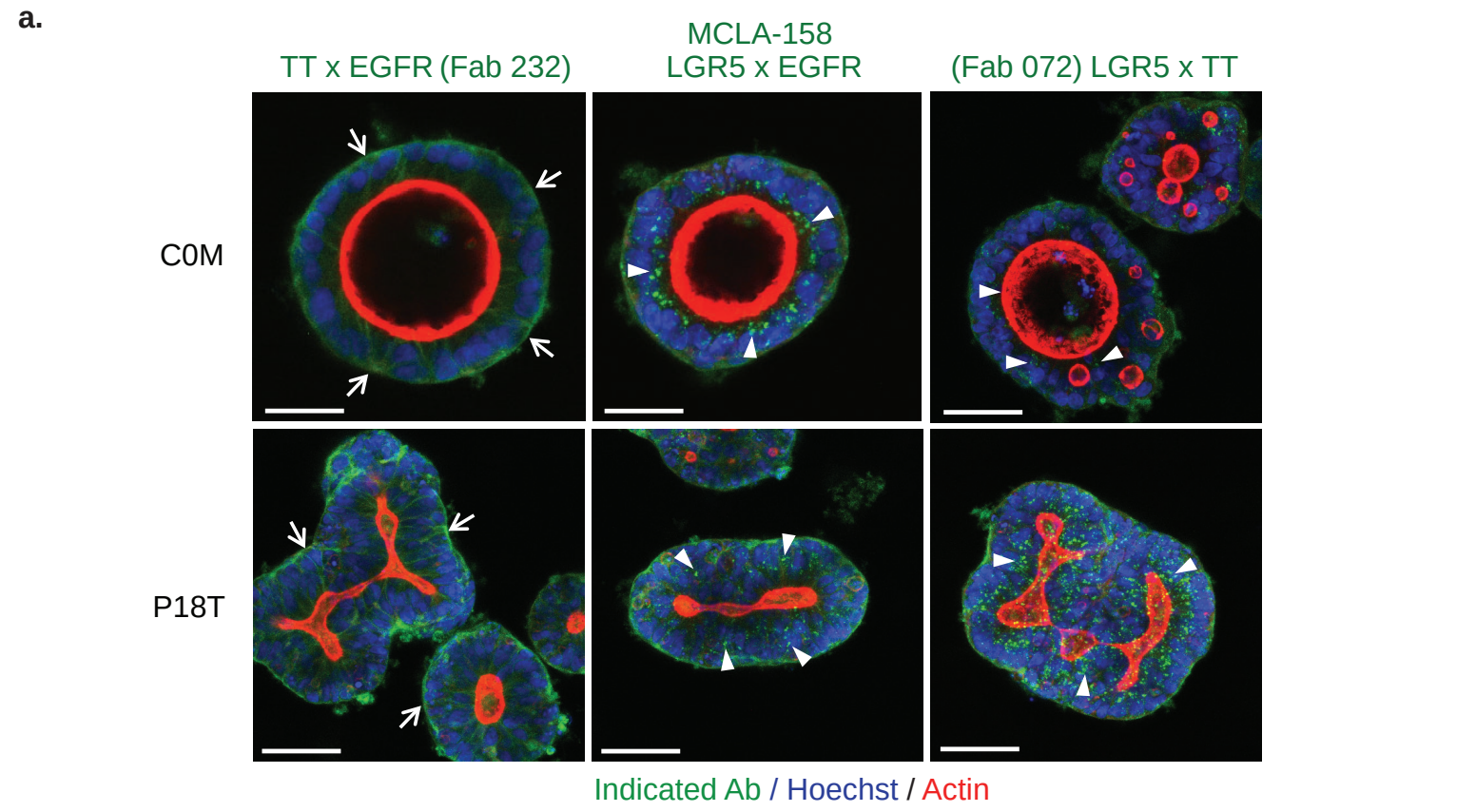

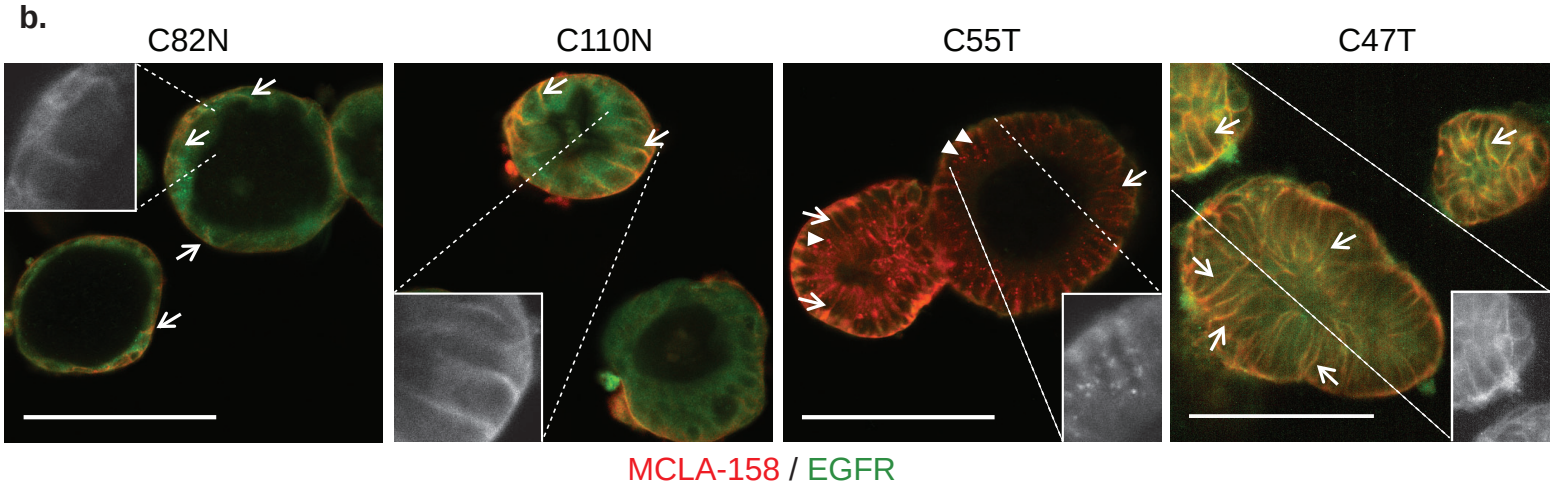

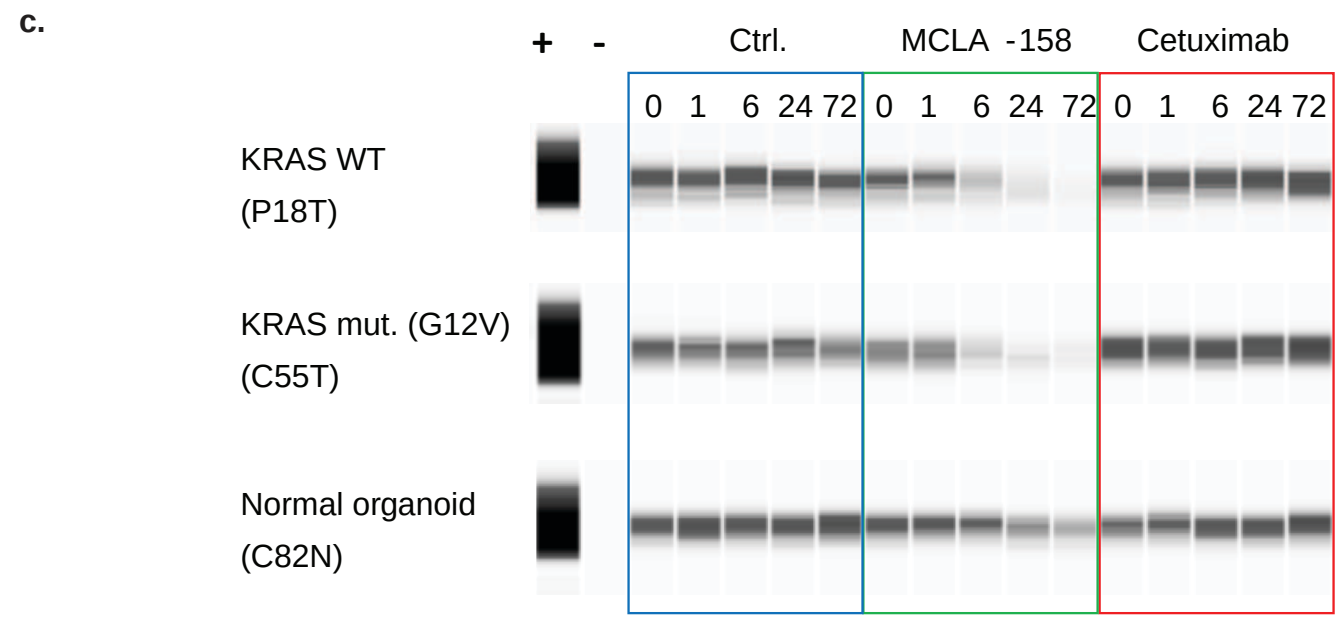

Supplementary Table 1. Features of FAB panels

FabNr	Target	Source	LGR4	LGR5	RNF43	ZNRF3	Stability	RSPO blocking
Fab001	LGR4	MeMo	0,253	0,07	0,106	0,099	69,1	No
Fab002	LGR4	MeMo	0,279	0,074	0,091	0,099	68,0	No
Fab003	LGR4	MeMo	0,228	0,078	0,105	0,099	68,1	No
Fab004	LGR4	MeMo	0,169	0,07	0,1	0,104	91,3	No
Fab005	LGR4	Synthetic	0,637	0,441	0,317	0,452	47	ND
Fab006	LGR4	Synthetic	0,769	0,197	0,326	0,437	10	ND
Fab007	LGR4	Synthetic	0,418	0,467	0,219	0,306	NA	ND
Fab008	LGR4	Synthetic	0,322	0,105	0,183	0,255	29	ND
Fab009	LGR4	Synthetic	0,757	0,113	0,172	0,253	11	ND
Fab010	LGR4	MeMo	0,164	0,104	0,149	0,157	76,7	No
Fab011	LGR4	Synthetic	1,128	0,211	0,342	0,393	NA	ND
Fab012	LGR4	Synthetic	0,783	0,089	0,14	0,172	NA	ND
Fab013	LGR4	Synthetic	0,785	0,097	0,249	0,213	20	ND
Fab014	LGR4	Synthetic	0,343	0,08	0,128	0,161	15	ND
Fab015	LGR4	Synthetic	0,62	0,069	0,125	0,138	29	ND
Fab016	LGR4	Synthetic	0,337	0,099	0,19	0,315	11	ND
Fab017	LGR4	Synthetic	1,118	0,114	0,217	0,237	NA	ND
Fab018	LGR4	Synthetic	0,352	0,104	0,159	0,207	NA	ND
Fab019	LGR4	Synthetic	0,711	0,198	0,245	0,351	8	ND
Fab020	LGR4	Synthetic	0,353	0,102	0,215	0,288	12	ND
Fab021	LGR4	Synthetic	0,83	0,105	0,204	0,214	32	ND
Fab022	LGR4	Synthetic	0,228	0,09	0,167	0,19	34	ND
Fab023	LGR4	Synthetic	0,652	0,089	0,176	0,193	22	ND
Fab024	LGR4	Synthetic	1,143	0,108	0,192	0,24	58	ND
Fab025	LGR4	Synthetic	0,77	0,105	0,204	0,228	7	ND
Fab026	LGR4	Synthetic	0,668	0,117	0,139	0,19	51	ND
Fab027	LGR4	Synthetic	0,836	0,196	0,196	0,276	NA	ND
Fab028	LGR4	Synthetic	0,582	0,188	0,587	0,306	57	ND
Fab029	LGR4	Synthetic	0,849	0,121	0,177	0,209	NA	ND
Fab030	LGR4	Synthetic	0,462	0,121	0,143	0,181	12	ND
Fab031	LGR4	Synthetic	0,669	0,094	0,113	0,122	35	ND
Fab032	LGR4	Synthetic	0,699	0,101	0,131	0,147	31	ND
Fab033	LGR4	Synthetic	1,042	0,142	0,173	0,2	NA	ND
Fab034	LGR4	Synthetic	0,866	0,143	0,183	0,221	NA	ND
Fab035	LGR4	Synthetic	0,817	0,149	0,185	0,227	19	ND
Fab036	LGR4	Synthetic	0,494	0,141	0,227	0,232	21	ND
Fab037	LGR4	MeMo	0,31	0,081	0,098	0,097	58,4	No
Fab038	LGR4	Synthetic	0,516	0,127	0,167	0,187	8	ND
Fab039	LGR4	Synthetic	0,818	0,148	0,203	0,218	NA	ND
Fab040	LGR4/5	Synthetic	0,233	0,796	0,142	0,247	16	ND
Fab041	LGR4/5	Synthetic	0,869	0,103	0,131	0,171	19	ND
Fab042	LGR5	MeMo	0,062	1,078	0,095	0,092	93,1	No
Fab043	LGR5	MeMo	0,072	1,613	0,188	0,17	84,5	No
Fab044	LGR5	MeMo	0,067	1,542	0,125	0,146	7,8	No
Fab045	LGR5	MeMo	0,069	1,612	0,143	0,164	53,5	No
Fab046	LGR5	MeMo	0,059	1,042	0,083	0,101	32,8	No
Fab047	LGR5	MeMo	0,057	0,935	0,097	0,098	49,0	No

Fab048	LGR5	MeMo	0,062	0,92	0,103	0,11	41,5	No
Fab049	LGR5	MeMo	0,059	1,152	0,094	0,093	6,1	Partial
Fab050	LGR5	MeMo	0,074	1,865	0,16	0,18	83,9	No
Fab051	LGR5	MeMo	0,075	1,621	0,22	0,197	93,3	No
Fab052	LGR5	MeMo	0,061	0,94	0,09	0,106	44,4	No
Fab053	LGR5	MeMo	0,058	1,033	0,087	0,098	27,7	No
Fab054	LGR5	MeMo	0,079	1,639	0,215	0,234	48,8	No
Fab055	LGR5	MeMo	0,062	1,559	0,35	0,118	61,0	No
Fab056	LGR5	MeMo	0,06	1,614	0,103	0,113	14,0	No
Fab057	LGR5	MeMo	0,062	0,894	0,099	0,115	69,3	No
Fab058	LGR5	MeMo	0,051	1,025	0,084	0,074	37,3	No
Fab059	LGR5	MeMo	0,06	1,118	0,094	0,095	37,2	Partial
Fab268	LGR5	MeMo	ND	2,027	ND	ND	100	No
Fab060	LGR5	MeMo	0,054	1,069	0,084	0,093	45,4	No
Fab061	LGR5	MeMo	0,065	1,667	0,119	0,124	84,2	No
Fab062	LGR5	MeMo	0,057	1,082	0,097	0,094	40,2	No
Fab063	LGR5	MeMo	0,06	1,151	0,096	0,099	12,2	No
Fab064	LGR5	MeMo	0,059	1,199	0,096	0,103	5,1	Partial
Fab065	LGR5	MeMo	0,057	1,296	0,085	0,097	21,9	No
Fab066	LGR5	MeMo	0,06	1,263	0,099	0,098	91,8	Partial
Fab067	LGR5	MeMo	0,061	1,254	0,099	0,106	11,4	No
Fab068	LGR5	MeMo	0,058	1,355	0,079	0,102	91,1	Partial
Fab069	LGR5	MeMo	0,065	1,265	0,099	0,114	76,4	Partial
Fab070	LGR5	MeMo	0,06	1,269	0,095	0,105	22,2	Partial
Fab071	LGR5	MeMo	0,061	1,131	0,097	0,111	29,0	Partial
Fab072	LGR5	MeMo	0,059	1,356	0,104	0,098	80,4	No
Fab073	LGR5	MeMo	0,062	1,217	0,105	0,111	84,1	No
Fab074	LGR5	MeMo	0,059	1,335	0,088	0,1	101,6	Partial
Fab075	LGR5	Synthetic	0,075	0,521	0,148	0,186	57	ND
Fab076	LGR5	Synthetic	0,079	0,307	0,172	0,206	11	ND
Fab077	LGR5	Synthetic	0,078	1,184	0,191	0,262	26	ND
Fab078	LGR5	Synthetic	0,069	0,389	0,145	0,311	43	ND
Fab079	LGR5	Synthetic	0,082	0,456	0,21	0,263	41	ND
Fab080	LGR5	Synthetic	0,069	0,483	0,159	0,179	15	ND
Fab081	LGR5	Synthetic	0,067	0,549	0,156	0,169	66	ND
Fab082	LGR5	Synthetic	0,073	0,658	0,142	0,174	52	ND
Fab083	LGR5	Synthetic	0,075	0,363	0,155	0,176	33	ND
Fab084	LGR5	Synthetic	0,07	0,215	0,142	0,186	20	ND
Fab085	LGR5	Synthetic	0,064	0,298	0,168	0,179	39	ND
Fab086	LGR5	Synthetic	0,072	0,839	0,153	0,175	83	ND
Fab087	LGR5	Synthetic	0,074	0,619	0,155	0,163	15	ND
Fab088	LGR5	Synthetic	0,063	0,502	0,17	0,19	23	ND
Fab089	LGR5	Synthetic	0,068	0,768	0,141	0,174	107	ND
Fab090	LGR5	Synthetic	0,075	0,407	0,149	0,182	67	ND
Fab091	LGR5	Synthetic	0,071	0,537	0,163	0,22	38	ND
Fab092	LGR5	Synthetic	0,076	0,478	0,157	0,188	28	ND
Fab093	LGR5	Synthetic	0,057	0,526	0,12	0,134	36	ND
Fab094	LGR5	Synthetic	0,081	0,216	0,146	0,146	55	ND
Fab095	LGR5	Synthetic	0,073	0,723	0,191	0,223	92	ND
Fab096	LGR5	Synthetic	0,068	0,261	0,145	0,19	13	ND

Fab097	LGR5	Synthetic	0,065	0,433	0,14	0,151	48	ND
Fab098	LGR5	Synthetic	0,068	0,392	0,149	0,17	25	ND
Fab099	LGR5	Synthetic	0,065	0,855	0,146	0,17	72	ND
Fab100	LGR5	Synthetic	0,067	0,596	0,129	0,154	55	ND
Fab101	LGR5	Synthetic	0,069	0,383	0,142	0,178	60	ND
Fab102	LGR5	Synthetic	0,068	0,596	0,167	0,192	99	ND
Fab103	LGR5	Synthetic	0,092	0,549	0,143	0,178	74	ND
Fab104	LGR5	Synthetic	0,083	0,235	0,135	0,182	23	ND
Fab105	LGR5	Synthetic	0,091	0,308	0,141	0,205	16	ND
Fab106	LGR5	Synthetic	0,094	0,526	0,141	0,17	7	ND
Fab107	LGR5	Synthetic	0,082	0,547	0,15	0,17	49	ND
Fab108	LGR5	Synthetic	0,092	0,592	0,137	0,164	81	ND
Fab109	RNF43	MeMo	0,061	0,064	1,408	0,099	76,4	No
Fab110	RNF43	MeMo	0,068	0,078	1,079	0,131	20,5	No
Fab111	RNF43	MeMo	0,063	0,067	0,164	0,107	69,1	No
Fab112	RNF43	MeMo	0,06	0,069	0,495	0,094	45,3	No
Fab113	RNF43	MeMo	0,056	0,062	1,487	0,091	85,8	Yes
Fab114	RNF43	MeMo	0,059	0,063	1,364	0,097	86,7	Partial
Fab115	RNF43	MeMo	0,069	0,08	1,43	0,132	59,2	Yes
Fab116	RNF43	MeMo	0,064	0,073	1,55	0,116	78,4	Partial
Fab117	RNF43	MeMo	0,056	0,063	1,437	0,11	86,9	Yes
Fab118	RNF43	MeMo	0,063	0,076	1,388	0,148	17,4	No
Fab119	RNF43	Synthetic	0,07	0,077	1,405	0,202	49	ND
Fab120	RNF43	Synthetic	0,066	0,074	1,213	0,139	32	ND
Fab121	RNF43	Synthetic	0,076	0,143	1,615	0,175	54	ND
Fab122	RNF43	Synthetic	0,116	0,146	0,986	0,244	25	ND
Fab123	RNF43	Synthetic	0,088	0,073	1,628	0,183	69	ND
Fab124	RNF43	Synthetic	0,084	0,083	1,243	0,187	4	ND
Fab125	RNF43	Synthetic	0,065	0,084	1,3	0,163	7	ND
Fab126	RNF43	Synthetic	0,08	0,102	1,274	0,215	65	ND
Fab127	RNF43	Synthetic	0,122	0,164	1,104	0,321	92	ND
Fab128	RNF43	Synthetic	0,222	0,31	1,553	0,483	13	ND
Fab129	RNF43	Synthetic	0,076	0,092	1,321	0,173	4	ND
Fab130	RNF43	Synthetic	0,085	0,077	1,047	0,185	42	ND
Fab131	RNF43	Synthetic	0,1	0,152	1,259	0,252	7	ND
Fab132	RNF43	Synthetic	0,07	0,078	1,284	0,21	84	ND
Fab133	RNF43	Synthetic	0,085	0,075	1,147	0,175	9	ND
Fab134	RNF43	Synthetic	0,078	0,088	1,25	0,157	57	ND
Fab135	RNF43	Synthetic	0,076	0,091	1,054	0,168	6	ND
Fab136	RNF43	Synthetic	0,085	0,111	1,244	0,191	19	ND
Fab137	RNF43	Synthetic	0,074	0,079	1,146	0,19	5	ND
Fab138	ZNRF3	MeMo	0,067	0,074	0,111	1,601	3,6	No
Fab139	ZNRF3	MeMo	0,068	0,08	0,123	1,549	3,8	No
Fab140	ZNRF3	MeMo	0,066	0,078	0,108	1,336	88,9	No
Fab141	ZNRF3	MeMo	0,076	0,086	0,135	1,643	3,6	No
Fab142	ZNRF3	MeMo	0,077	0,083	0,13	1,675	3,8	No
Fab143	ZNRF3	MeMo	0,118	0,151	0,243	0,804	80,0	No
Fab144	ZNRF3	MeMo	0,062	0,074	0,117	1,549	11,8	No
Fab145	ZNRF3	MeMo	0,062	0,071	0,114	1,511	10,7	No
Fab146	ZNRF3	MeMo	0,097	0,078	0,117	1,604	4,4	Partial

Fab147	ZNRF3	MeMo	0,066	0,082	0,118	1,702	7,8	No
Fab148	ZNRF3	MeMo	0,061	0,072	0,097	1,559	15,8	No
Fab149	ZNRF3	MeMo	0,063	0,075	0,11	1,47	16,3	No
Fab150	ZNRF3	MeMo	0,066	0,087	0,12	1,556	91,1	No
Fab151	ZNRF3	MeMo	0,069	0,077	0,126	1,619	95,7	No
Fab152	ZNRF3	MeMo	0,077	0,096	0,139	1,397	6,2	No
Fab153	ZNRF3	MeMo	0,063	0,073	0,111	1,109	75,0	No
Fab154	ZNRF3	MeMo	0,073	0,084	0,14	0,876	81,5	No
Fab155	ZNRF3	MeMo	0,075	0,092	0,143	1,238	65,1	No
Fab156	ZNRF3	MeMo	0,085	0,108	0,157	1,132	16,7	No
Fab157	ZNRF3	MeMo	0,078	0,092	0,146	1,412	17,8	No
Fab158	ZNRF3	MeMo	0,076	0,093	0,144	1,372	30,7	No
Fab159	ZNRF3	MeMo	0,077	0,088	0,15	0,803	92,2	No
Fab160	ZNRF3	MeMo	0,071	0,089	0,13	0,457	61,5	No
Fab161	ZNRF3	MeMo	0,077	0,093	0,151	1,406	23,3	No
Fab162	ZNRF3	MeMo	0,069	0,081	0,121	1,407	37,9	No
Fab163	ZNRF3	MeMo	0,065	0,073	0,105	1,147	95,7	No
Fab164	ZNRF3	MeMo	0,065	0,076	0,101	1,06	40,0	No
Fab165	ZNRF3	MeMo	0,07	0,082	0,122	1,367	76,3	No
Fab166	ZNRF3	MeMo	0,07	0,085	0,126	1,416	47,3	No
Fab167	ZNRF3	MeMo	0,069	0,079	0,123	1,556	19,0	No
Fab168	ZNRF3	MeMo	0,067	0,083	0,117	1,533	6,7	No
Fab169	ZNRF3	MeMo	0,126	0,169	0,237	0,913	65,2	No
Fab170	ZNRF3	MeMo	0,079	0,091	0,144	1,58	74,6	No
Fab171	ZNRF3	MeMo	0,068	0,075	0,118	1,745	24,5	No
Fab172	ZNRF3	MeMo	0,071	0,089	0,124	1,591	11,5	Yes
Fab173	ZNRF3	MeMo	0,074	0,084	0,135	1,477	7,3	No
Fab174	ZNRF3	MeMo	0,081	0,101	0,157	1,504	75,4	No
Fab175	ZNRF3	MeMo	0,07	0,088	0,121	1,599	13,0	No
Fab176	ZNRF3	MeMo	0,073	0,084	0,122	1,431	14,3	No
Fab177	ZNRF3	MeMo	0,068	0,076	0,108	1,412	38,6	No
Fab178	ZNRF3	MeMo	0,088	0,123	0,19	1,443	22,0	No
Fab179	ZNRF3	MeMo	0,067	0,081	0,124	1,321	73,3	No
Fab180	ZNRF3	MeMo	0,076	0,09	0,121	1,464	10,9	No
Fab181	ZNRF3	MeMo	0,074	0,092	0,136	1,407	56,0	No
Fab182	ZNRF3	MeMo	0,086	0,105	0,16	1,298	60,6	No
Fab183	ZNRF3	MeMo	0,07	0,084	0,12	1,17	97,9	No
Fab184	ZNRF3	Synthetic	0,083	0,099	0,173	1,422	76	ND
Fab185	ZNRF3	Synthetic	0,081	0,091	0,169	1,56	92	ND
Fab186	ZNRF3	Synthetic	0,081	0,095	0,175	1,535	71	ND
Fab187	ZNRF3	Synthetic	0,743	0,088	0,174	1,561	75	ND
Fab188	ZNRF3	Synthetic	0,164	0,204	0,306	1,129	3	ND
Fab189	ZNRF3	Synthetic	0,091	0,106	0,175	1,272	69	ND
Fab190	ZNRF3	Synthetic	0,75	0,09	0,181	1,086	40	ND
Fab191	ZNRF3	Synthetic	0,069	0,073	0,135	1,065	8	ND
Fab192	ZNRF3	Synthetic	0,081	0,108	0,144	1,661	90	ND
Fab193	ZNRF3	Synthetic	0,093	0,091	0,174	1,209	23	ND
Fab194	ZNRF3	Synthetic	0,077	0,085	0,149	1,35	76	ND
Fab195	ZNRF3	Synthetic	0,186	0,25	0,323	1,287	3	ND
Fab196	ZNRF3	Synthetic	0,096	0,122	0,187	1,309	77	ND

Fab197	ZNRF3	Synthetic	0,09	0,11	0,172	1,052	5	ND
Fab198	ZNRF3	Synthetic	0,067	0,074	0,127	1,129	40	ND
Fab199	ZNRF3	Synthetic	0,183	0,107	0,182	0,868	22	ND
Fab200	ZNRF3	Synthetic	0,084	0,088	0,155	0,825	41	ND
Fab201	ZNRF3	Synthetic	0,081	0,11	0,161	1,081	4	ND
Fab202	ZNRF3	Synthetic	0,089	0,096	0,158	1,696	95	ND
Fab203	ZNRF3	Synthetic	1,397	0,076	0,153	1,633	92	ND
Fab204	ZNRF3	Synthetic	0,085	0,093	0,144	1,332	94	ND
Fab205	ZNRF3	Synthetic	0,074	0,082	0,136	1,077	43	ND
Fab206	ZNRF3	Synthetic	0,067	0,082	0,136	1,928	77	ND
Fab207	ZNRF3	Synthetic	0,125	0,068	0,125	1,797	99	ND
Fab208	ZNRF3	Synthetic	0,111	0,143	0,21	1,088	5	ND
Fab209	ZNRF3	Synthetic	0,07	0,092	0,139	1,283	60	ND
Fab210	ZNRF3	Synthetic	0,097	0,137	0,236	0,656	17	ND
Fab211	ZNRF3	Synthetic	0,069	0,095	0,153	1,504	83	ND
Fab212	ZNRF3	Synthetic	0,118	0,115	0,175	0,979	96	ND
Fab213	ZNRF3	Synthetic	0,195	0,224	0,298	1,082	20	ND
Fab214	ZNRF3	Synthetic	0,126	0,146	0,233	1,121	12	ND
Fab215	ZNRF3	Synthetic	0,068	0,081	0,134	1,041	16	ND
Fab216	ZNRF3	Synthetic	0,178	0,234	0,328	1,421	4	ND
Fab217	ZNRF3	Synthetic	0,07	0,08	0,137	1,749	100	ND
Fab218	ZNRF3	Synthetic	0,116	0,109	0,187	1,125	7	ND
Fab219	ZNRF3	Synthetic	0,072	0,082	0,135	1,136	87	ND
Fab220	ZNRF3	Synthetic	0,078	0,093	0,165	1,242	51	ND
Fab221	ZNRF3	Synthetic	0,106	0,118	0,193	1,263	80	ND
Fab222	ZNRF3	Synthetic	0,572	0,079	0,175	1,162	10	ND
Fab223	ZNRF3	Synthetic	0,096	0,086	0,143	1,215	34	ND
Fab224	ZNRF3	Synthetic	0,106	0,128	0,229	0,858	9	ND
Fab225	ZNRF3	Synthetic	0,079	0,069	0,158	1,222	88	ND
Fab226	ZNRF3	Synthetic	0,096	0,138	0,167	1,141	10	ND
Fab227	ZNRF3	Synthetic	0,07	0,076	0,152	1,149	4	ND

Supplementary Table 3. Calculated KD for MCLA158 binding to EGFR and LGR5 using Scatchard assays

MCLA158	Cell Line	Apparent KD (nM)	KD EGFR (nM)	KD LGR5 (nM)
	CHO-EGFR	NA	0.22 +/- 0.086	NA
	CHO-LGR5	NA	NA	0.86 +/- 0.13
	DLD1	0.18 +/- 0.024	NA	NA

Main genetic alterations in driver genes in PDXs analyzed by whole exome sequencing

M001

Type	Locus	tumor_var_freq	Reference allele	Variant allele	Polyphen
stopgain SNV	APC:NM_000038:exon16:c.C3340T:p.R1114X,APC:NM_001127511:exon14:c.C3286T:p.R1096X,APC:	50%	C	T	0,732713
nonsynonymous SNV	KRAS:NM_033360:exon2:c.G35A:p.G12D,KRAS:NM_004985:exon2:c.G35A:p.G12D,	24%	C	T	0,657
stopgain SNV	TP53:NM_001126116:exon4:c.C520T:p.R174X,TP53:NM_001126117:exon4:c.C520T:p.R174X,TP53:N	50%	G	A	0,595512

M005

type	locus	tumor_var_freq	Reference allele	Variant allele	Polyphen
stopgain SNV	APC:NM_001127510:exon8:c.C706T:p.Q236X,APC:NM_000038:exon7:c.C706T:p.Q236X,	0,1944	C	T	0,735307
frameshift deletion	APC:NM_001127511:exon14:c.3750_3751del:p.1250_1251del,APC:NM_001127510:exon17:c.3804_	0,2759	AT	-	
nonsynonymous SNV	KRAS:NM_004985:exon2:c.G38A:p.G13D,KRAS:NM_033360:exon2:c.G38A:p.G13D,	0,3871	C	T	0,994
nonframeshift deletion	PIK3CA:NM_006218:exon2:c.334_336del:p.112_112del,	0,3846	TCC	-	
stopgain SNV	NF1:NM_000267:exon18:c.C2044T:p.Q682X,NF1:NM_001042492:exon18:c.C2044T:p.Q682X,	0,2727	C	T	0,735393
frameshift insertion	JAG1:NM_000214:exon12:c.1565_1566insT:p.C522fs,	0,0732	-	A	

LM-CRCX3

Type	Locus
nonsynonymous SNV	KRAS:NM_033360:exon2:c.G35A:p.G12D,KRAS:NM_004985:exon2:c.G35A:p.G12D,

Supplementary Table 4. MCLA158 versus Cetuximab at different EGF concentrations

	P18T			C1M			C55T		
ng/ml EGF	Cetuximab	MCLA158	IC50 ratio Cetuximab : MCLA158	Cetuximab	MCLA158	IC50 ratio Cetuximab : MCLA158	Cetuximab	MCLA158	IC50 ratio Cetuximab : MCLA158
0.5	0.8967	0.1596	5.6	0.01295	0.008192	1.6	0.4998	0.06784	7.4
5	15.29	2.62	5.8	2.591	0.08062	32.1	42.61	0.5124	83.2
50	>10000	96.9	103.2	158.8	0.8577	185.1	117.5	31.18	3.8

Supplementary Table 5 - % of LGR5+ cells in PDOs and MCLA-158 responses

PDO	% of LGR5+ cells by flow cytometry	Classification according to % LGR5+ cells [HIGH>average]	% of growth upon MCLA158 2μg/ML compared to control Ab	Response [YES<50% growth]
C55T	51,91	HIGH	27,08012949	YES
C57T	23,83	HIGH	34,07155262	YES
C25T	21,895	HIGH	23,89	YES
C0M	16,23	HIGH	12,0526654	YES
C31M	13,85	HIGH	37,78735575	YES
C27T	10,815	HIGH	55,04434163	NO
C37T	7,65	LOW	100	NO
C20T	6,34	LOW	100	NO
C17T	5,8	LOW	100	NO
C2T	5,35	LOW	100	NO
C42T	4,65	LOW	52,7611696	NO
C5T	3,21	LOW	38,09127514	YES
C28T	2,9	LOW	100	NO
C14T	2,66	LOW	100	NO
C7T	1,955	LOW	100	NO
C22T	1,635	LOW	100	NO
C43T	1,3	LOW	54,8527706	NO
C36T	0,89	LOW	24,0120043	YES
C26T	0,5	LOW	100	NO
C47	0	LOW	71	NO
Average	**9,17**			